

2022

Characterizing the Effects of Solvent and Analyte Properties on Ionization Efficiency by Novel Field-free and Field-enabled Ionization Techniques

Kinkini Udara Jayasundara
West Virginia University, kuj0001@mix.wvu.edu

Follow this and additional works at: <https://researchrepository.wvu.edu/etd>

 Part of the [Analytical Chemistry Commons](#)

Recommended Citation

Jayasundara, Kinkini Udara, "Characterizing the Effects of Solvent and Analyte Properties on Ionization Efficiency by Novel Field-free and Field-enabled Ionization Techniques" (2022). *Graduate Theses, Dissertations, and Problem Reports*. 11620.
<https://researchrepository.wvu.edu/etd/11620>

This Thesis is protected by copyright and/or related rights. It has been brought to you by the The Research Repository @ WVU with permission from the rights-holder(s). You are free to use this Thesis in any way that is permitted by the copyright and related rights legislation that applies to your use. For other uses you must obtain permission from the rights-holder(s) directly, unless additional rights are indicated by a Creative Commons license in the record and/ or on the work itself. This Thesis has been accepted for inclusion in WVU Graduate Theses, Dissertations, and Problem Reports collection by an authorized administrator of The Research Repository @ WVU. For more information, please contact researchrepository@mail.wvu.edu.

**Characterizing the Effects of Solvent and Analyte Properties on Ionization
Efficiency by Novel Field-free and Field-enabled Ionization Techniques**

Kinkini Udara Jayasundara

Dissertation submitted

to the Eberly College of Arts and Sciences

at West Virginia University

In partial fulfillment of the requirements for the degree of

Doctor of Philosophy

in Chemistry

Stephen J. Valentine, Ph.D. Chair

Peng Li, Ph.D.

Harry Finklea, Ph.D.

Carsten Milschmann, Ph.D.

Tatiana Trejos, Ph.D.

C.Eugene Bennett Dept. of Chemistry

Morgantown, West Virginia

2022

Keywords: Field-free ionization, mass spectrometry, solvent effects

Copyright 2022 Kinkini Udara Jayasundara

Abstract

Characterizing the Effects of Solvent and Analyte Properties on Ionization Efficiency by Novel Field-free and Field-enabled Ionization Techniques

Kinkini Udara Jayasundara

In recent years the mass spectrometry (MS) area of field and/or direct analysis has grown dramatically. As a result, field-portable and miniaturized mass spectrometers, introduced only a few years ago, are proliferating. A highly desired feature for field-portable MS, or in-field analysis, is the ability to use ionization techniques requiring very little sample preparation as well as an ability to generate the ions under ambient conditions. Recently, a new ambient ionization technique termed vibrating sharp-edge spray ionization (VSSI) has been introduced which overcomes the field-portable limitations of other spray-based methods including the requirements for auxiliary components (e.g., nebulizing gas and high voltage). As a new ambient ionization technique with significant potential for field-portable and direct analyses, it is important that the chemical and physical properties of the VSSI technique be elucidated to optimize ion production performance. Here, experimental and theoretical studies provide insight into the influence of analyte and solvent molecule properties on the production of ions. In Chapter 2, experiments employing protic solvents demonstrate that different analyte molecular properties are associated with increased ionization for VSSI methods compared with gold standard electrospray ionization (ESI) techniques; for VSSI methods correlations are observed for ion intensity and molecule proton affinity and polarity are observed which are absent for ESI. In Chapter 3, experiments employing acetonitrile as the solvent also reveal difference between VSSI and ESI techniques. For example, remarkably in positive ion mode, greater ion signals are observed for voltage-free VSSI compared with ESI. Additionally, analyte proton affinity exhibits an outsized relationship with ionization compared with protic solvents. In Chapter 4, molecular dynamics (MD) simulations of water droplets suggest that the energy of desorption of the ions can account for differences in voltage-free and field-enabled VSSI. Further MD studies provide some support of analyte polarity influencing ionization efficiency. Finally, Chapter 5 provides some direction for improving VSSI experiments and hardware to allow the clear elucidation of primary factors driving compound ionization.

*To my mother, Malinee Haputhanthri, and my father, Winee Jayasundara.
If it weren't for all their sacrifices,
love and support, I wouldn't be the person I have become today.*

Acknowledgments

I would like to express my sincere gratitude to my supervisor, Dr. Stephen Valentine, for his guidance, kindness, patience, and generosity throughout the years of work in his lab. It was an ample opportunity for me to work under a great scientist like you. Thank you for sharing your broad knowledge with me, and the things I learned from you will benefit me as a scientist in the future. Most importantly, you taught me how to be a scientist with great qualities.

Also, I would like to thank my committee members; Dr. Peng Li, Dr. Harry Finklea, Dr. Carsten Milsmann, and Dr. Tatiana Trejos. Your feedback, advice, and academic insights have been valuable for my research projects. Also, I would like to thank Dr. Blake Mertz, Dr. Chitrak Gupta, and Dr. Sadegh Faramarzi for their generous help in overcoming the challenges associated with molecular dynamics simulation work at the beginning.

I would like to express my sincere gratitude to two institutes, the University of Colombo, and West Virginia University, for all the opportunities they offered me to become a scientist.

Working with my past and present lab mates, Ahmad, Sandra, Daud, Tony, Madison, Samira, Jewel, and Sultan, was my pleasure. Thank you all for your kind support. And I would express my sincere thanks to Chong Li from Li's group for helping me with cVSSI experiments. Also, I am grateful for all my friends outside the research lab, especially Lihini, Sachini, Mario, Randika, Susith, and Uthpala.

I am forever grateful for my family. My parents showed me that dedication, persistence, and hard work could help to overcome difficult work. I owe everything to both of you. To my eldest brother Kushan, your love, support, and generosity helped me spend my time in graduate school without difficulty. And my second eldest brother, Krishan, thank you for your logical advices and motivation when I needed it.

Finally, a big thank you to my amazing husband, Kalana De Silva, who is so proud of everything I do and always encourages me to achieve more. I appreciate your great support for everything, and I am so blessed and lucky to have such a wonderful man in my life!

Table of Contents

1.	Introduction.....	1
1.1.	Mass spectrometry	1
1.2.	Electrospray Ionization	3
1.3.	Ionization mechanisms: CRM and IEM	5
1.4.	Ambient ionization.....	10
1.5.	Capillary Vibrating Sharp-edge Spray Ionization (cVSSI)	11
1.6.	Molecular Dynamics (MD) simulations	16
1.7.	Research Description	20
1.8.	References.....	21
2	Physicochemical property correlations with ionization efficiency in capillary Vibrating Sharp-edge Spray Ionization (cVSSI).....	26
2.1	Introduction.....	26
2.2	Experimental	29
2.2.1	Ionization device fabrication.....	29
2.2.2	Reagents and sample preparation.....	31
2.2.3	Mass spectrometry data collection.....	34
2.2.4	Data analysis	34
2.3	Results and Discussion	36
2.3.1	Linear ion trap experiments: ion intensities from compounds in methanol solvent.	36
2.3.2	Linear ion trap experiments: ion intensities for compounds from aqueous samples.	40
2.3.3	Linear ion trap experiments: evaluating physicochemical property associations with ion intensity.....	43
2.3.4	Orbitrap experiments: physicochemical property associations.....	51
2.3.5	Ionization mechanism considerations.	54
2.4	Continued studies: motivation and future work.....	58
2.5	Conclusions.....	60
2.6	Acknowledgments.....	61
2.7	References.....	62
3	Associating Molecular Physicochemical Properties with Ionization Efficiency for Compounds in Aprotic, Polar Solvent Using Field-free and Field-enabled cVSSI Techniques ..	68
3.1	Introduction.....	68
3.2	Experimental	72
3.2.1	Ionization device fabrication.....	72
3.2.2	Reagents and Sample Preparation.....	73
3.2.4	Data Analysis.	78
3.3	Results and Discussion	80

3.3.1	Relative ion intensities for compounds in neat acetonitrile using positive ion mode.	80
3.3.2	Relative ion intensities for compounds in acetonitrile(ACN):water (95:5) solutions using positive ion mode.	84
3.3.3	Relative ion intensities for compounds in neat acetonitrile using negative ion mode.	87
3.3.4	Relative ion intensities for compounds in acetonitrile (ACN):water (95:5) solutionnegative ion mode.	90
3.3.5	Associating molecular physicochemical property with ion intensity in positive ion mode studies.	93
3.3.6	Associating molecular physicochemical property with ion intensity in negative ion mode studies.	94
3.3.7	Ionization process considerations.	95
3.3.8	Ion signal enhancement in field-free cVSSI in positive ion mode.	101
3.4	Conclusions	102
3.5	References	104
4	Insights into Ion release from cVSSI droplets obtained with Molecular Dynamics Simulations	109
4.1	Introduction	109
4.2	Experimental	114
4.2.1	Sample Preparation.	114
4.2.2	cVSSI-Mass Spectrometry Data Collection.	116
4.2.3	Molecular Dynamics (MD) simulations.	116
4.2.4	Data analysis.	119
4.3	Results and Discussion	123
4.3.1	Comparing ion intensities for acetaminophen and dopamine.	123
4.3.2	Using estimated diffusion coefficient to assess ion surface activity	125
4.3.3	Modeling desorption energy for [M+H] ⁺ ions.	127
4.3.4	Associating analyte log P with ion release for field-enabled cVSSI and cESI conditions.	130
4.4	Conclusions	133
4.5	References	135
5.	Future Directions	139
5.1.	Improving the ionization efficiency of cVSSI with nonpolar aprotic solvent compositions	139
5.2.	Investigating the acetonitrile solvent effect on ionization efficiency with molecular dynamics (MD) simulations.	141
5.3.	Microwave-assisted heating for efficient droplet evaporation in field-free ionization Mass Spectrometry	143
5.4	References	145

List of Figures

Figure 1-1 Schematic diagram of a general mass spectrometer.	3
Figure 1-2 .Schematic diagram of the Electrospray Ionization process.	5
Figure 1-3 Shown are a sole precursor droplet, droplet drying (solvent evaporation), and the release of the analyte ion via desorption (right side) and complete drying (left side)	8
Figure 1-4 Schematic diagram of the free energy change associated with the ion releasing into the gas phase from the droplet.	9
Figure 1-5. Schematic diagram of droplet formation in cVSSI at different stages of a droplet's life time.-	13
Figure 1-6 Schematic diagram of droplet formation in cVSSI at different stages of droplet's life time.	13
Figure 1-7 Schematic diagram of an ESI-like droplet charging process and voltage-free charging process.....	15
Figure 1-8 Simplified flow chart showing the steps of a general MD simulation process.	19
Figure 1-9. A simplified flow chart showing the steps of a general MD simulation process. ...	19
Figure 2- 1Illustration of the cVSSI device and droplet production used in the current studies..	30
Figure 2- 2 Plot of relative ion intensities for the voltage-free cVSSI (solid circles), field-enabled cVSSI (solid triangles), and ESI (open triangles) experiments using the methanol samples. The blunt-tip emitters were used to collect the data.	38
Figure 2- 3 Plot of relative ion intensities for the voltage-free cVSSI (solid circles), field-enabled cVSSI (solid triangles), and ESI (open triangles) experiments using the water samples. The blunt-tip emitters were used to collect the data.	40
Figure 2- 4 Plots of individual correlations between separate physicochemical property and ion intensity for the voltage-free cVSSI analysis of methanol samples using blunt-tip emitters.	45
Figure 2- 5 Plots of individual correlations between separate physicochemical property and ion intensity for the voltage-free cVSSI analysis of water samples using blunt-tip emitters.	49
Figure 2- 6 Plots of individual correlations between separate physicochemical property and ion intensity for the voltage-field enabled cVSSI analysis of water samples using blunt-tip emitters.....	50
Figure 3- 1 Bar diagram log of the ion signal intensities of each analyte molecule in 95% acetonitrile under positive mode Field-free cVSSI, Field-enabled cVSSI, ESI.	82
Figure 3- 2 Bar diagram log of the ion signal intensities of each analyte molecule in 95% acetonitrile under positive mode Field-free cVSSI, Field-enabled cVSSI,ESI.	85
Figure 3- 3. Bar diagram log of the ion signal intensities of each analyte molecule in 95% acetonitrile under positive mode Field-free cVSSI, Field-enabled cVSSI, ESI. Blue bars represent Field-free cVSSI, orange bars represent Field-enabled cVSSI and grey bars represent relative error of one standard deviation about the mean.	88

Figure 3- 4. Bar diagram log of the ion signal intensities of each analyte molecule in 95% acetonitrile under positive mode Field-free cVSSI, Field-enabled cVSSI, ESI. Blue bars represent Field-free cVSSI, orange bars represent Field-enabled cVSSI and grey bars represent Field-enabled cVSSI and grey bars represent relative error of one standard deviation about the mean.	91
Figure 4- 1 Snapshots from a MD simulation trajectory of a droplet containing an acetaminophen ion (green) and a dopamine ion (blue) in 4H ₃ O ⁺ , 2 OH ⁻ , 4 Na ⁺ (field-free cVSSI system).	117
Figure 4- 2 Free energy profile of a dopamine ion obtained from the field-enabled cVSSI droplet system (see text for details).....	121
Figure 4- 3 Plot of the average time for analyte desorption into the gas phase from a field-enabled cVSSI type nanodroplet versus log P of the analyte molecule.	122
Figure 4- 4 Plot of the average time for analyte desorption into the gas phase from a cESI cVSSI type nanodroplet versus log P of the analyte molecule.	122
Figure 4- 5 spectral intensities for [M+H] ⁺ acetaminophen and dopamine ions produced from water samples under field-free cVSSI conditions and different field-enabled cVSSI conditions.	123
Figure 5- 1 Schematic diagram of the instrumental platform to apply microwave assisted heating into the spray plume.....	144

List of Tables

Table 2- 1 Structures and physicochemical property values for the compounds used in the ionization experiments.	32
Table 2- 2 Molecule-specific ion intensities for the methanol experiments employing blunt-tip emitters.	37
Table 2- 3 Molecule-specific ion intensities for the methanol experiments employing blunt-tip emitters.	41
Table 2- 4 Beta coefficients and the associated significance values for the LTQ experiments.	46
Table 2- 5 Molecule-specific ion intensities for the aqueous experiments employing pulled-tip emitters.	52
Table 2- 6 Molecule-specific ion intensities for the methanol experiments employing pulled-tip emitters.	53
Table 2- 7 Beta coefficients and the associated significance values for the Q-Exactive experiments	54
Table 3- 1 Structures and physicochemical property values for the compounds used in the positive mode ionization experiment.	74
Table 3- 2 Structures and physicochemical property values for the compounds used in the negative mode ionization experiment.	76
Table 3- 3 Beta coefficients and the associated significance values for the positive mode.	79
Table 3- 4 Beta coefficients and the associated significance values for the negative mode.	79
Table 3- 5 Molecule-specific ion intensities for the neat acetonitrile in positive mode analysis .	83
Table 3- 6. Molecule-specific ion intensities for the 95% acetonitrile in positive mode analysis.	86
Table 3- 7 Molecule-specific ion intensities for the neat acetonitrile in negative mode analysis.	89
Table 3- 8 Molecule-specific ion intensities for the 95% acetonitrile in negative mode analysis.	92
Table 4- 1 Chemical structures of Acetaminophen and Dopamine.	114
Table 4- 2 Structures and physicochemical property values for the compounds used in the ionization event studies as examined by MD simulations.	115
Table 4- 3 Diffusion coefficients for acetaminophen and dopamine ions in field-free and field-enabled cVSSI droplet systems.	120
Table 4- 4 Free energy of desorption of acetaminophen and dopamine ions for field-free cVSSI and field-enabled cVSSI droplet systems.	121

1. Introduction

1.1. Mass spectrometry

Mass spectrometry (MS) is a versatile analytical technique used in many laboratories where it is utilized for measuring the mass-to-charge ratio (m/z) of ions in the gas phase. Using these m/z measurements, structural information can be deduced for a variety of compounds ranging from small metabolites to large biological compounds.^{1 2 3 4 5} These include molecular species such as proteins, nucleic acids, lipids and carbohydrates. Moreover, MS can be performed in different operational modes such that different types of ions can be observed. These include the analysis of the intact molecular species (precursor ions) or portions of the organic molecules (fragment ions). The mass information from such analyses can be used to elucidate the covalent framework of different compounds as well as makeup of large, non-covalent complexes.

A schematic diagram of a typical mass spectrometer instrument is shown in Figure 1.1. It consists of a vacuum system (vacuum chamber(s) and pumps), an ion source, a mass analyzer, and a detector. The ion source generates gas-phase ions from different samples including solution-phase analyte molecules. These ions are ultimately focused into the vacuum chamber housing the mass analyzer. Typically, the pressure in this portion of the instrument is maintained at $\sim 10^{-6}$ to 10^{-9} Torr depending on the type of mass analyzer utilized. This low-pressure region is required to avoid ion-neutral collisions with background gas that would otherwise occur under normal atmospheric conditions and create a relatively small mean free path ($\sim 1 \mu\text{m}$). A large mean free path is required as ultimately the m/z measurement correlates with an ion's trajectory in a vacuum under the influence of an electric field(s). Thus, in the mass analyzer, the ions produced in the source are distinguished according to their m/z . Additionally, different mass analyzer consist of electric (and/or magnetic) fields that influence the trajectories of these ions ultimately leading to

their sorting by their m/z ratios. Finally, with the use of a suitable ion detector, the sorted ions will be associated with m/z values using the integration of the data collection software and a mass spectrum will be produced.⁶ Each mass spectrum displays m/z values on the x -axis and ion intensity or ion counts as the y -axis value.

As mentioned above, ionization of the analyte in MS experiments occurs at the ion source (Figure 1.1). A broadly used area of ionization for MS is that occurring under atmospheric conditions. In such ion sources processes such as compound protonation, deprotonation, electron ejection, charge transfer, and adduction of small ions such as Na^+ or NH_4^+ can be operational. One of the first ion sources used extensively in the early development of MS was Electron Ionization (EI). In EI, the solution phase sample is transferred into the gas phase via processes such as heating and the gas-phase neutral compounds are bombarded with electrons emanating from a heated filament and focused into an energetic beam. With sufficiently energetic collisions, the ejection of an electron from the analyte molecule is an outcome and a radical cation of the analyte molecule is produced. The ion energetics of this process are such that EI can cause extensive ion fragmentation (severing of chemical bonds) which is not preferred for large biomolecules. Over the decades, softer ionization techniques were pursued such as chemical ionization (CI)⁷ and fast atom bombardment (FAB)⁸ in part to develop techniques that would not result in extensive fragmentation of larger compound ions such as those produced for peptides. It can be argued that the most successful (and impactful) developments of soft ionization techniques occurred in the late 1980s with the introduction of electrospray ionization (ESI) and matrix-assisted laser desorption ionization (MALDI). Both techniques do not produce extensive fragmentation and thus, fully intact macromolecules can be ionized.^{9 10 11 12} That said, as with all progress in measurement

science, it is crucial to continue the development of such techniques in order to produce a higher amount of charged analyte ions to obtain robust and sensitive MS measurements.

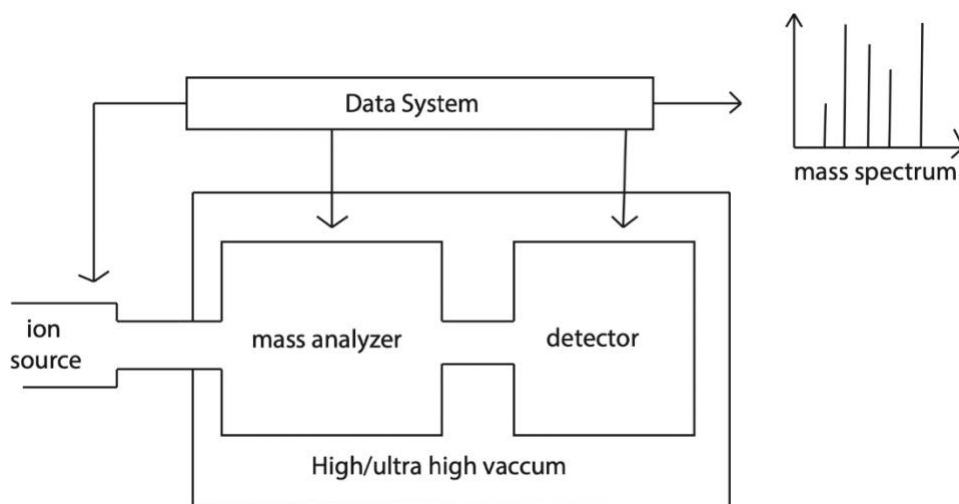


Figure 1-1 Schematic diagram of a general mass spectrometer.
The inset shows the data output (mass spectrum).

1.2. Electrospray Ionization

ESI has become a standard ionization method for analyzing small molecules and larger biomolecules. In traditional ESI, the first step in the ionization process is the production of a microdroplet spray of a solution containing an analyte(s) molecule(s). This is generally accomplished by infusing a sample solution through a capillary tip where a high electric voltage ($\sim 2\text{--}3\text{ kV}$) is applied as shown in Figure 1.2. The electric field creates an electrophoretic charge separation at the meniscus (the solution at the capillary tip). Eventually this charge buildup leads to a deformation of the meniscus and the formation of the Taylor cone which disintegrates at the distal end to micrometer-sized, charged droplets. Due to a series of solvent evaporation events, the charge density on the droplet surface increases and eventually the cohesive surface tension forces

and the Coulombic repulsive forces reach a critical point. This is called the Rayleigh limit.¹³ At this point, the total number of charges the droplets contain (Z_R) can be determined according to:

$$Z_R e = 8\pi\sqrt{\varepsilon_o\gamma R^3} \quad \text{equation 1.1}$$

Where e is the elementary charge, ε_o is the permittivity of free space, γ is the surface tension of the solvent and R is the radius of the droplet. When the droplet reaches the Rayleigh limit, it becomes unstable leading to a series of Coulombically-driven fission events resulting in the micrometer-sized parent droplets create several much smaller progeny droplets¹⁴. After a fission event, the charge density of the parent droplet becomes lower than that at the Rayleigh limit. However, after another series of evaporation events, the charge density on the droplet again reaches the Rayleigh limit resulting in further droplet fissioning. While this process is occurring, the analyte ion present in a droplet may release into the gas phase. The theoretical models which have been introduced to describe this ESI process has shown that ~20 progeny droplets conduct ~2% of the mass and 15% of the charge away from the precursor droplet.

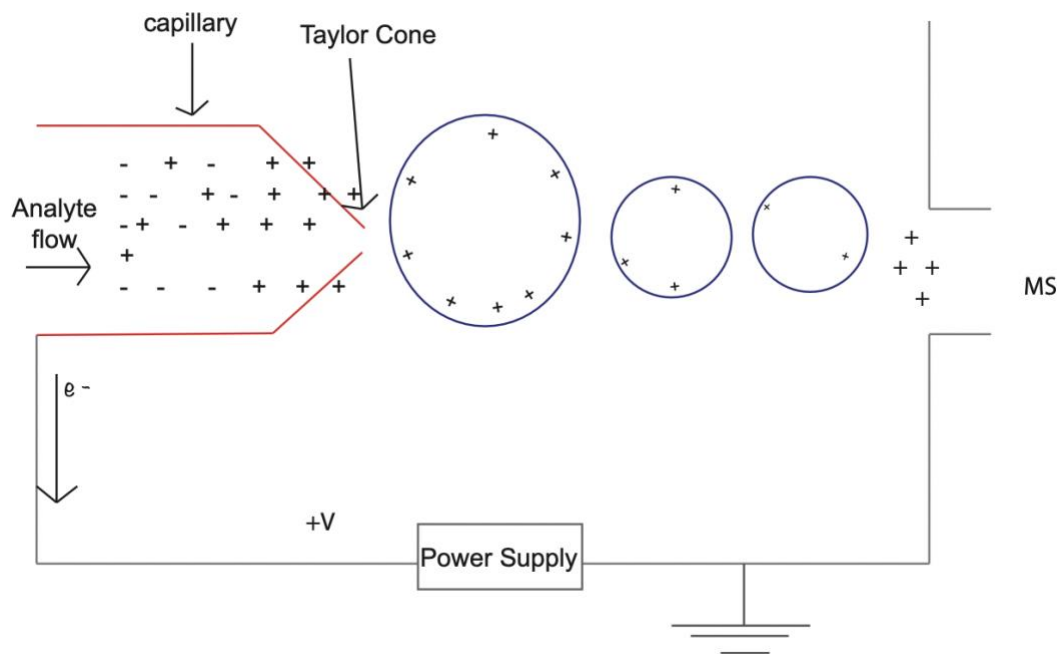


Figure 1-2 .Schematic diagram of the Electrospray Ionization process.

1.3. Ionization mechanisms: CRM and IEM

Shortly after the introduction of ESI as a method for biomolecular ion generation, two different mechanisms were proposed to describe the process of ion production at the end of the droplet lifetime. These two mechanisms are based on a number of theoretical and experimental studies. Much of the information comes from early ESI-MS studies. The two models are referred to as the ion evaporation model (IEM)¹⁵ and the charged residue model (CRM)¹⁶. Both IEM and CRM processes undergo solvent evaporation and Coulombic fission events but eventually these two mechanisms diverge into distinct pathways. Figure 1.3 shows a simplified diagram of both processes. In the IEM, an analyte ion is released into the gaseous environment by overcoming the activation barrier associated with desorbing from the surface of a charged droplet. In the CRM,

the droplet is evaporated to dryness, a portion of the remaining charge may be transferred to the ion, and then the ion is released into the gas phase. Because the mechanism for analyte ion transfer into the gas phase at the latter stages of ESI remains a matter of debate, there are some new models apart from the IEM and CRM mechanisms. The combined charged residue-field emission model proposed by Hogan and coworkers is a mechanism that seeks to resolve the difference between IEM and CRM.¹⁷ Additionally, a new mechanism of ion evaporation of macromolecules introduced by Consta and Malevanets is different from the conventional CRM and the IEM.¹⁸ The Konermann group proposed a chain ejection model (CEM) where they describe the effect of protons “hopping” from the droplet surface to transfer onto emerging portions of unfolded proteins being expelled into the gas phase.¹⁹ Though others have proposed mechanisms that are somewhat controversial and there is ongoing debate in the field of mass spectrometry, it is considered that the CRM and IEM are the most established models to describe the ionization mechanism.

According to the IEM model, the precursor droplet undergoes successive columbic fission events and evaporation before an ion emission can occur²⁰. Smaller droplets that contain small analytes are proposed to go through this process when the electric field at the droplet surface approaches the Rayleigh limit. When this occurs, the stability of the droplet is regained by ejecting the solvated analytes and/or electrolyte ions. According to Thomson’s IEM model, the detachment of a solvated analyte ion from the parent droplet is a process which requires an activation energy as shown in Figure 1.4. The free energy minimum of the profile corresponds to an initial configuration where the analyte ion is in the droplet. The free energy maximum or the transition state (TS), represents a disconnected state between the precursor droplet and the detached solvated analyte ion. This TS energy barrier is overcome when the ion is approximately a distance x from the surface of the droplet as shown in Figure 1.4 The above-mentioned free energy barrier is a

result of two competing electrostatic factors namely, the attractive force is a result of the image charge effect ²¹ of the detached analyte ion and the repulsive force arising from the detached analyte ion and like charges on the droplet surface. According to early explanations of the IEM, it is assumed that the transition state represents the final (detached) state more than the initial configuration and it is known as a ‘late transition’ state ¹⁵ . Hence, according to Born’s model the free energy barrier can be estimated as a free energy change required to move a solvated ion from the bulk neutral solvent to an infinite distance from the droplet center.

An estimation of the activation energy (ΔG^*) can be used to determine the rate constant of charge detachment by the transition state theory expression ^{15 22 23}. In equation 1.2, ΔG^* is the height of the activation energy barrier, h is plank's constant, T is the temperature, and k_B is the Boltzmann constant.

$$k = \frac{k_B T}{h} \exp\left(\frac{-\Delta G^*}{k_B T}\right) \quad \text{Equation 1.2}$$

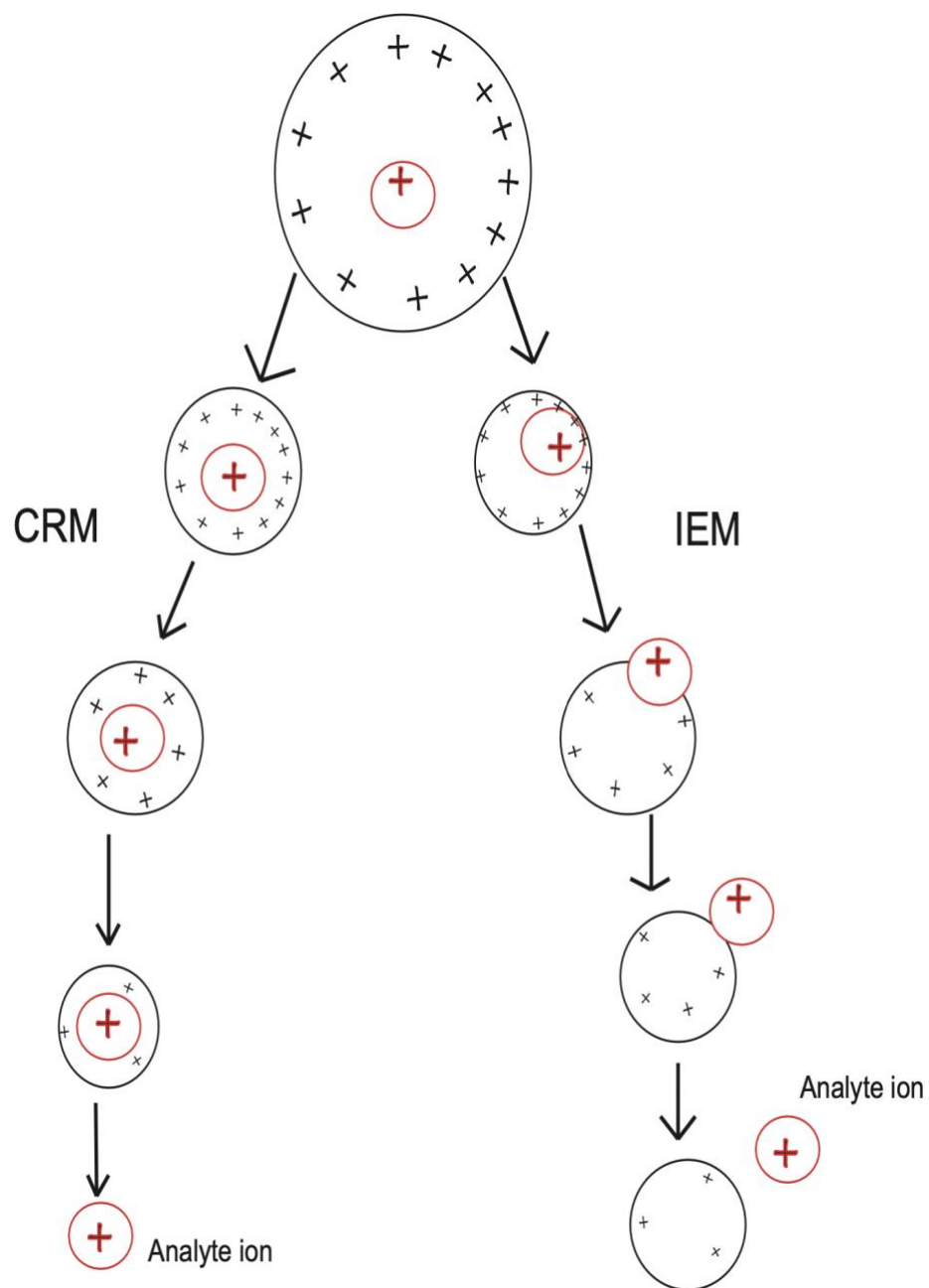


Figure 1-3 Shown are a sole precursor droplet, droplet drying (solvent evaporation), and the release of the analyte ion via desorption (right side) and complete drying (left side)

The red circle with the charge represents the analyte ion and the black circle represents the final droplet.

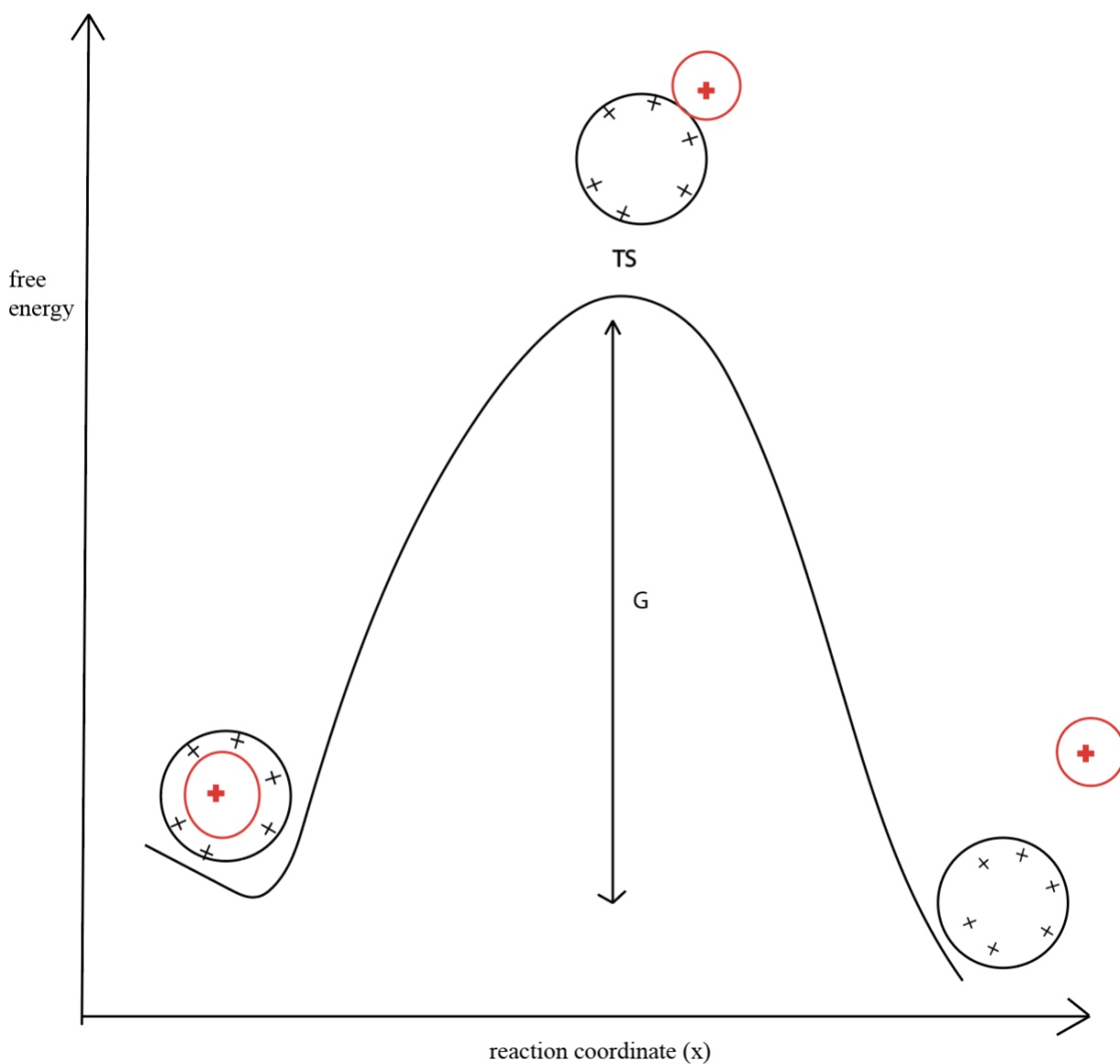


Figure 1-4 Schematic diagram of the free energy change associated with the ion releasing into the gas phase from the droplet.

Here, TS represents the transition state and ΔG^* is the activation energy barrier. The red circle represents the analyte ion and the black circle represents the final droplet.

1.4. Ambient ionization

After the introduction of ESI and MALDI, scientists began to consider other techniques to generate gas phase ions for MS under ambient conditions (i.e., atmospheric pressure, near ambient temperature) with minimal or no sample preparation and pre-ionization separations.²⁴ In part this developmental period was influenced by a desire to extend the utility of mass spectrometry to direct or in-situ analyses as well as for field work.^{25 26 27}

The first alternative sources to be designated as an ambient ionization source was desorption electrospray ionization (DESI) which was introduced in 2004.²⁸ It is an effective technique derived from traditional ESI methods; here, a spray of charged droplets from a pneumatically assisted electrospray needle is directed towards a surface containing the sample of interest which is placed directly in front of the mass spectrometer inlet (ambient environment). This results in an extraction of the analyte into droplets emerging from the surface via recoiling or sputtering. The droplets are charged and thus undergo traditional ESI processes such as the IEM, CRM, or CEM mentioned above to produce gas-phase ions from molecules residing on the surface. Shortly later another ionization technique was introduced and named direct analysis in real time (DART). DART operates based upon the desorption of condensed- or solid-phase analytes with the aid of a hot gas carrying active species generated from a plasma discharge. The ionization process of DART initiates with penning ionization of gaseous species such as N₂. A series of reactions produce various reagent ions (water cluster ions) which interact with the neutral analyte in the gas phase to produce the ions of interest. Such interactions include those listed above (e.g., protonation and deprotonation). Since the introduction of DESI and DART, there has been a rapid proliferation of ambient ionization methods over the past decade which can be categorized according to various operating principles such as electric discharge and plasma generation,^{29 30 31} electrospray variants,^{32 33} thermal desorption,³⁰ acoustic nebulization,^{34 35 24 36} and inlet-assisted³⁷

^{38 39}, as well as the method of sample introduction (e.g spray-based, plasma-based, vacuum-based, and laser-based) to the mass spectrometer.

It should be noted that one of the desires for ambient ionization is to allow for its usage with field-portable MS. That said, most of the reported methods mentioned above require dedicated and specialized instrumentation or auxiliary components (pressurized gas, solvents, laser, power supplies, etc.). These limitations are problematic when it comes to designing a field – portable mass spectrometer. That said, some research has been directed towards simplifying the ambient ionization source such as the zero-voltage paper spray ionization (zPSI) method introduced by Wang *et al.* in 2010 to address some of these limitations ⁴⁰. zPSI adds to a growing repertoire of voltage-free ionization methods such as sonic spray ionization (SSI) ⁴¹, EASI ⁴², zero-voltage paper spray ionization ⁴³, ultrasonic ionization ⁴⁴ and solvent assisted inlet ionization ³⁹. All of these techniques are currently available in the field of mass spectrometry and yet there is ample room for further development of ambient ionization techniques. This is especially true with regard to increasing the portability of the technique as well as the sensitivity while decreasing the overall cost of the approach.

1.5. Capillary Vibrating Sharp-edge Spray Ionization (cVSSI)

As part of the renewed ionization source development work, in 2018, Li and coworkers introduced a new, spray-based ionization technique termed vibrating sharp-edge spray ionization (VSSI) ⁴⁵. The new approach only required a vibrating substrate containing a sharp edge. The first demonstration consisted of placing a liquid pool at the edge of a microscope slide and subsequently vibrating the slide (~100 kHz at ~10 V_{pp}). This was shown to produce a plume of micrometer-sized droplets which only emanated from the sharp tip of the slide. Ionization from

the plume was demonstrated to produce ESI-like ions.⁴⁵ Subsequent studies showed that the sharp edge employed in droplet production could be a fused-silica capillary segment through which sample was infused; this was termed capillary VSSI (cVSSI)⁴⁶. The demonstration of direct infusion enabled the coupling of VSSI with condensed-phase separation techniques. More recently, the coupling of a voltage applied to the infused solution with cVSSI (field-enabled cVSSI) using a pulled-tip capillary was shown to provide enhancements of ~10 to 100 fold in ion signal levels compared with ESI for native MS analyses performed in negative ion mode; more modest improvements (typically 5 fold) were observed for positive ion mode⁴⁷. Conceptually, field-free cVSSI may be similar to sonic spray ionization, SAIL, surface acoustic wave nebulization ionization, and field-free paper spray ionization in that a plume of similarly charged droplets is directed into a mass spectrometer inlet results in ion production. Unique to the VSSI and cVSSI approaches is the method of droplet production which requires the vibrating sharp edge.

Overall, the process that underlies the above ionization methods including cVSSI, is desolvation of the micro or nano droplets which consist of the analyte of interest. Thus, the final stages of the cVSSI process may be similar to an ESI mechanism (e.g., IEM or CRM), but this remains to be determined. Notably, the mechanism proposed by Cooks and co-workers for zPSI may ultimately be applied to cVSSI as demonstrated in Figure 1.5⁴³. In order to improve cVSSI techniques and applications an improved understanding of the late-stage ionization process is required. This work seeks to fill lay the foundation for such required experimental and theoretical studies. A goal is to begin to address how physicochemical properties of analyte molecules as well as the solvent molecules contribute to the overall ionization efficiency. Admittedly to begin to describe the process, the precise makeup of the end-stage droplets is highly critical. However, the exact mechanism by which the vibrating sharp edge creates the spray of solvent is still an active

area of investigation. Thus, here, a first principles treatment of droplet composition is utilized to begin to compare and contrast the experimental and theoretical results for cVSSI with those of ESI.

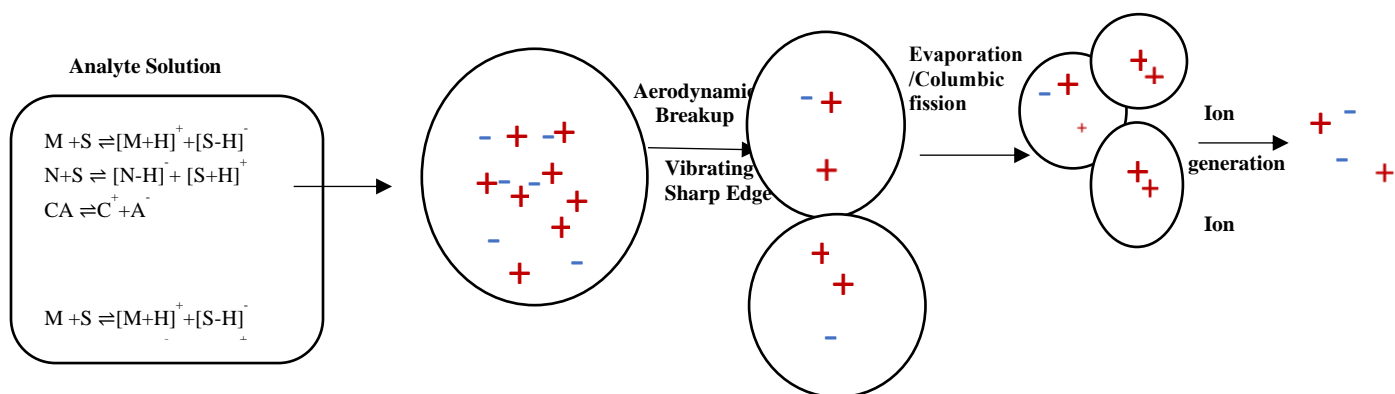
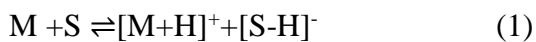
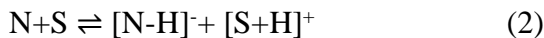


Figure 1-6 Schematic diagram of droplet formation in cVSSI at different stages of droplet's life time.

When an analyte solution is introduced to the microscope slide (VSSI) or capillary emitter (cVSSI), the analyte may be ionized in the solution phase. If the analyte is a basic compound (M) it will be dissolved in solvent (S), and depending on pH to some extent, the analyte can be protonated by the solvent, according to following equation,



If the analyte is an acidic compound (N), depending on the solution pH, it may exchange protons with the solvent to produce the following ion pairs:



For any present ionic molecules such as salts or buffer components (CA), these species will dissociate into the equilibrium ionic forms:



Hence, the droplets which are formed due to the streaming effect and aerodynamic breakup in VSSI and cVSSI may consist of droplets with a net positive or negative charge while containing ion pairs as shown in Figure 1.5.

In ESI, the droplet composition may be entirely different than that suggested for VSSI. Therefore, it is important to examine both ESI and cVSSI at the final stages of progeny droplets with a closer view. For example, the counter ions present in the infused solution for ESI are mostly neutralized by the supplied voltage. Thus, the droplets formed by the capillary tip primarily consist of either cations or anions (Figure 1.7 A) ⁴⁸. This is mainly because of the high voltage applied in the ESI method. If a positive voltage is applied, due to the oxidation process, anions are neutralized and cations survive through migration to the meniscus. When a negative voltage is applied, anions will survive as the cations are neutralized. This phenomenon is known as “neutralizing the counter ion” principle ⁴⁹.

In contrast, in field-free VSSI and cVSSI, rather than neutralizing counter ions, anions and cations are separated to a lesser degree (Figure 1.7 B), which is suggested to be common to the voltage-free ionization techniques.^{43 50 51} This can occur due to mechanical forces, shockwaves or abrupt heat provided to the analyte solution according to the operation of each ionization technique. In VSSI techniques, this occurs due to the streaming occurring right at the sharp edge of the device. Here, aerodynamic breakup is expected to provide a distribution of droplets centered at zero net charge. However, many positively and negatively charged droplets are produced within this distribution. This may occur due to aerodynamic breakup charging as proposed by Jarrold and coworkers.⁵² This is also somewhat similar to a mechanism explained by the electric double layer as described by Chapman. When the solvent films are torn apart extensively by pneumatic forces, the uniform distribution of cations and anions is disrupted and an unequal distribution of

ions occurs in the progeny droplets. This phenomenon is known as “separating the ions”⁴⁹. This could lead to droplets of the form shown in Figure 1B.

A final consideration is given to field-enabled cVSSI. Here, it is acknowledged that it may produce ions by a different process due to differences in overall droplet makeup. That is, the aerodynamic breakup of the droplet may occur before fuller charge separation as experienced by electrophoretic migration of charge carriers thereby producing droplets having a net charge that is intermediate to those produce by field-free cVSSI and ESI (Figure 1.7).

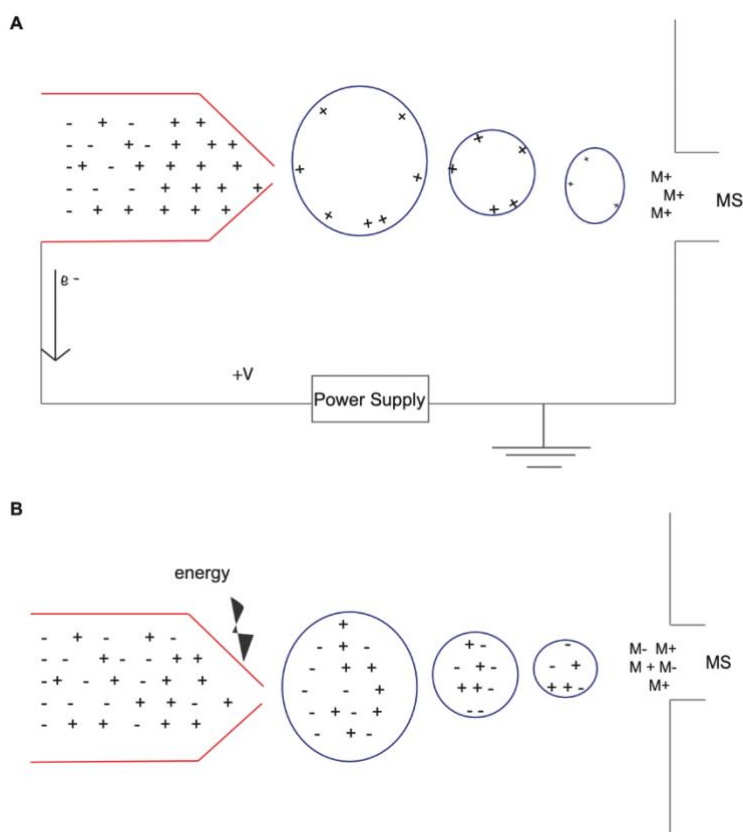


Figure 1-7 Schematic diagram of an ESI-like droplet charging process and voltage-free charging process. Panel shows a cartoon representation of electrophoretic charge migration imposed by the application of voltage during ESI. Panel B shows an input of energy and aerodynamic breakup producing limited charge separation as may be expected for field-free cVSSI.

1.6. Molecular Dynamics (MD) simulations

Several groups have studied ionization processes using molecular dynamics (MD) simulations. Russel and coworkers studied the structural evolution of proteins in drying nanodroplets. Here a droplet model which consisted of Cl^- and H_3O^+ as counter ions was utilized⁵³. Consta et al. also published similar work for PEG analyte molecules in a droplet containing Na^+ and Cl^- ions as counter ions⁵⁴. Furthermore, the Konermann group has presented simulation studies for different proteins in an aqueous environment containing Na^+ and Cl^- ions⁵⁵. All of the above-reported work mainly focused on the impact of the counter ions on analyte structure. A major limitation of such work is that the analyte ion's behavior in the droplet with different degrees of charges and its effect on mass spectrometry signals was not considered to be effective. Work performed by the Vertes group focused on the analyte ion's chemistry inside the droplet while accounting for the diffusion coefficient and the enthalpy of evaporation in only a cation environment⁵⁶. In this work, it was indicated that the further introduction of counter ions and macromolecular ions with different hydrophobicity would lead to a promising path of investigation for the segregation of analyte ions into a charged droplet and eventually into the gas phase.

With advanced development in computer science, researchers have increasingly adopted molecular simulations as an alternative method for verifying experimental measurements and making theoretical predictions. Several powerful techniques such as X-ray crystallography spectroscopy, cryo-electron microscopy, and nuclear magnetic resonance spectroscopy that provide detailed conformational information in both the liquid and solid phases but, for the study of the release of an analyte ion from a nanodroplet to the gaseous environment, these are in effective tools. Molecular dynamics (MD) simulations may play a role for such studies by while possibly providing atomic-level structural detail during the process. Additionally, even though MS-associated tools such as ion mobility spectrometry⁵⁷, optical techniques, and dissociation

studies can be used to investigate the transfer of analyte ions from the solution phase to the gas phase, this information is still not sufficient to completely understand the chemistry occurring inside the solvent droplet⁵⁸.

MD adopts Newtonian mechanics to model the temporal movement of atoms within a system. In MD, there are potential functions that account for covalent and non-covalent interactions. The covalent interactions like bond bending, stretching, and rotation of chemical bonds can be modeled by harmonic potentials. In the case of non-covalent interactions like electrostatic forces, a Coulomb potential can be employed, and for van der Waals forces, a Lennard-Jones (LJ) potential can be used. Additional algorithms are often also employed for non-covalent interactions.⁵⁹

In MD each atom is considered as a classical particle and the force on the particle is modeled using Newton's second Law (equation 1.3), where the particle index is i , the time is t , the mass of the particle m and the potential energy function U ³;

$$\vec{F}_i = m_i \frac{\Delta^2 \vec{r}_i}{\Delta t^2} = \frac{\partial U(\vec{r}_i \dots \vec{r}_N)}{\partial \vec{r}_i} \quad ; \text{equation (1.3)}$$

The potential energy (U) of an atom is calculated by interactions with all other atoms in the system using the force field which considers atomic charges, Lennard-Jones parameters and torsional parameters. According to equation 1.3, any particle in motion without any external force will continue in its uniform trajectory, and for every interaction between particles there is an equal and opposite reaction as encountered in Newtonian mechanics. From this description, it is clear that MD simulation models a system of particles which are at the atomic level. Hence, the trajectory of all particles in the system will give a series of microscopic states. From this

microscopic data, one may be able to elucidate macroscopic properties such as structure, as well as thermodynamic (temperature, pressure, density) and other properties like diffusion and activation energy by applying statistical mechanics.

Figure 1.8 shows the general steps of a MD simulation. As an initial step of a MD simulation, the parameters of the system which control all aspects of the simulation run (temperature, time step, parameters for the particles, number of particles, etc.) are input from an external file (normally termed a configuration file). Then, the initial coordinates of all the atoms in the system (the PDB file) are read into the memory of the program. Next the forces are calculated between all the atoms in a pair-wise fashion. Eventually, newly calculated forces are used to obtain the new positions of the atoms. When the atomic positions are updated, new velocities, kinetic energy and linear angular momentum can be computed. The current/instantaneous positions of the atoms are written to an external file for future analysis as well as resetting the initial positions, to be used for the next time step. The above steps require approximately 1 femtosecond. After resetting the new positions, the process reaches a conditional statement, where a check is imposed on whether or not the time limit of the simulation has been reached. If the time limit has been reached, the simulation run will be terminated; if it has not been reached, the simulations will recur in an iterative manner until reaching the time limit.

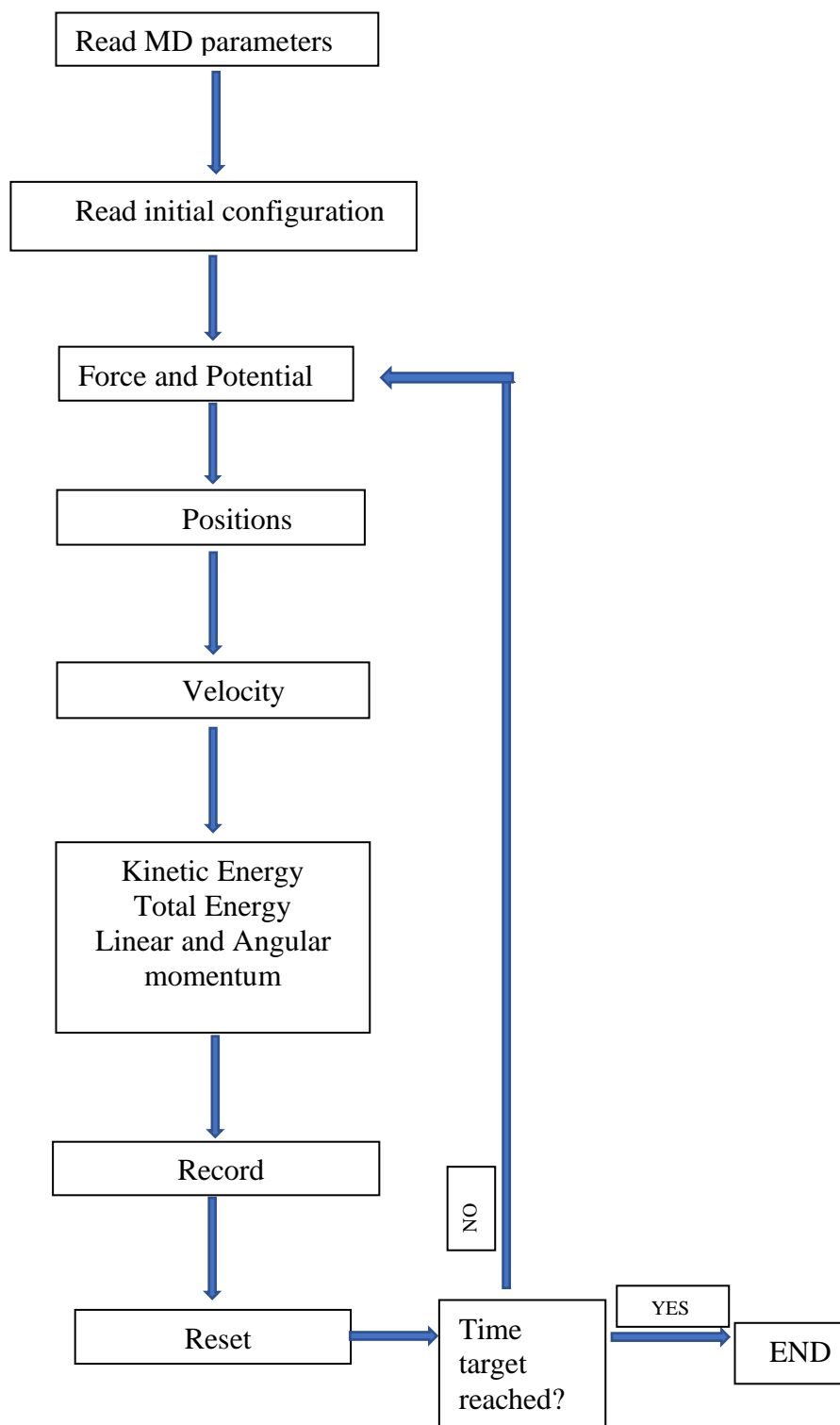


Figure 1-8 Simplified flow chart showing the steps of a general MD simulation process.

1.7. Research Description

Having described the new ionization technique of cVSSI and the type of droplet that may be produced by the new approach as well as the MD simulations tools available for its study, it is useful to briefly review the contents of this dissertation. The work will focus on elucidating factors that contribute to the ionization of different molecular species. These efforts focus on studying the influence of physicochemical properties of the solvent and analyte compounds. For the analytes, the influence of the property parameters log of the partition coefficient ($\log P$), log of the base dissociation constant (pK_b), and proton affinity (PA) are examined. For the solvent systems the effect of solvent polarity and whether or not protic conditions exist are considered.

Chapter 2 of this work describes the relative influence of $\log P$, pK_b , and PA on the ionization efficiency of different compounds undergoing ionization by field-free and field-enabled cVSSI as well as ESI. The samples are sprayed from solutions of the protic, polar solvents of methanol and water. Chapter 3 of this work then presents the same experiments with the exceptions that a polar, aprotic solvent (acetonitrile) is used as well as experiments are conducted in both positive and negative ion mode. Chapter 4 uses the droplet makeup considerations outlined above and applies them in MD simulations. A goal of this approach is to better understand the influence of $\log P$ on ionization efficiency; $\log P$ is implicated as playing a major role in ionization efficiency for field-enabled cVSSI with both protic, polar and aprotic, polar solvent systems (Chapter 2 and Chapter 3). Notably, the mechanism proposed by Cooks and coworkers suggests that the surface activity of the analytes in the droplets plays a major role in zero-potential ionization techniques.⁴³ Chapter 5 discusses future work that may help to further develop VSSI techniques of highly sensitive MS measurements.

Overall, the work reported here lays the foundation for understanding important factors associated with ionization by an already highly efficient ionization technique. With such

knowledge it may be possible to further the advantages of cVSSI relative to other ionization techniques. The importance of such advancements cannot be overstated. Currently, a portion of ‘omics experiments are transitioning to single cell analyses.^{60 61} Such work has the potential to greatly expand the knowledge of factors affecting human health.

1.8 References

- (1) Fenn, J. B.; Mann, M.; Meng, C. K.; Wong, S. F.; Whitehouse, C. M. Electrospray Ionization for Mass-Spectrometry of Large Biomolecules. *Science* **1989**, 246 (4926), 64-71. DOI: DOI 10.1126/science.2675315.
- (2) Mann, M. Electrospray - Its Potential and Limitations as an Ionization Method for Biomolecules. *Organic Mass Spectrometry* **1990**, 25 (11), 575-587. DOI: DOI 10.1002/oms.1210251104.
- (3) Smith, R. D.; Loo, J. A.; Loo, R. R. O.; Busman, M.; Udseth, H. R. Principles and practice of electrospray ionization—mass spectrometry for large polypeptides and proteins. *Mass Spectrometry Reviews* **1991**, 10 (5), 359-452. DOI: 10.1002/mas.1280100504.
- (4) Smith, R. D.; Loo, J. A.; Edmonds, C. G.; Barinaga, C. J.; Udseth, H. R. New developments in biochemical mass spectrometry: electrospray ionization. *Anal Chem* **1990**, 62 (9), 882-899. DOI: 10.1021/ac00208a002.
- (5) Covey, T. R.; Bonner, R. F.; Shushan, B. I.; Henion, J. The determination of protein, oligonucleotide and peptide molecular weights by ion-spray mass spectrometry. *Rapid Commun Mass Spectrom* **1988**, 2 (11), 249-256. DOI: 10.1002/rcm.1290021111.
- (6) El-Aneed, A.; Cohen, A.; Banoub, J. H. Mass Spectrometry, Review of the Basics: Electrospray, MALDI, and Commonly Used Mass Analyzers. *Applied Spectroscopy Reviews* **2009**, 44, 210 - 230.
- (7) Harrison, A. G. Chemical Ionization Mass Spectrometry. 2 ed.; Routledge: New York, 1992; pp 91-100.
- (8) Barber, M.; Bordoli, R. S.; Elliott, G. J.; Sedgwick, R. D.; Tyler, A. N. Fast atom bombardment mass spectrometry. *Analytical Chemistry* **1982**, 54 (4), 645-657.
- (9) Fenn, J. B. Electrospray Wings for Molecular Elephants (Nobel Lecture). *Angewandte Chemie International Edition* **2003**, 42 (33), 3871-3894. DOI: <https://doi.org/10.1002/anie.200300605>.
- (10) Tanaka, K. The origin of macromolecule ionization by laser irradiation (Nobel lecture). *Angew Chem Int Ed Engl* **2003**, 42 (33), 3860-3870. DOI: 10.1002/anie.200300585 [doi].
- (11) Bruins, A. P. Mechanistic aspects of electrospray ionization. *Journal of Chromatography A* **1998**, 794, 345-357.
- (12) Karas, M.; Bachmann, D.; Hillenkamp, F. Influence of the Wavelength in High-Irradiance Ultraviolet-Laser Desorption Mass-Spectrometry of Organic-Molecules. *Analytical Chemistry* **1985**, 57 (14), 2935-2939. DOI: DOI 10.1021/ac00291a042.

- (13) Rayleigh, L. XX. On the equilibrium of liquid conducting masses charged with electricity. *The London, Edinburgh, and Dublin Philosophical Magazine and Journal of Science* **1882**, *14* (87), 184-186. DOI: 10.1080/14786448208628425.
- (14) Konermann, L. A simple model for the disintegration of highly charged solvent droplets during electrospray ionization. *Journal of the American Society for Mass Spectrometry* **2009**, *20* (3), 496-506. DOI: 10.1016/j.jasms.2008.11.007.
- (15) Iribarne, J. V. On the evaporation of small ions from charged droplets. *The Journal of Chemical Physics* **1976**, *64* (6). DOI: 10.1063/1.432536.
- (16) Dole, M.; Mack, L. L.; Hines, R. L. MOLECULAR BEAMS OF MACROIONS. *Journal of Chemical Physics* **1968**, *49* (5), 2240-&, Article. DOI: 10.1063/1.1670391.
- (17) Hogan, C. J., Jr.; Carroll, J. A.; Rohrs, H. W.; Biswas, P.; Gross, M. L. Combined charged residue-field emission model of macromolecular electrospray ionization. *Anal Chem* **2009**, *81* (1), 369-377. DOI: 10.1021/ac8016532.
- (18) Consta, S.; Malevanets, A. Manifestations of Charge Induced Instability in Droplets Effected by Charged Macromolecules. *Physical Review Letters* **2012**, *109* (14), 148301. DOI: 10.1103/PhysRevLett.109.148301.
- (19) Konermann, L.; Rodriguez, A. D.; Liu, J. On the Formation of Highly Charged Gaseous Ions from Unfolded Proteins by Electrospray Ionization. *Analytical Chemistry* **2012**, *84* (15), 6798-6804. DOI: 10.1021/ac301298g.
- (20) Kebarle, P. A brief overview of the present status of the mechanisms involved in electrospray mass spectrometry. *Journal of Mass Spectrometry* **2000**, *35* (7), 804-817, Article. DOI: 10.1002/1096-9888(200007)35:7<804::aid-jms22>3.0.co;2-q.
- (21) Onsager, L.; Samaras, N. N. T. The Surface Tension of Debye-Hückel Electrolytes. *J. Chem. Phys.* **1934**, *2*, 528-536.
- (22) Kebarle, P.; Peschke, M. On the mechanisms by which the charged droplets produced by electrospray lead to gas phase ions. *Analytica Chimica Acta* **2000**, *406* (1), 11-35, Article. DOI: 10.1016/S0003-2670(99)00598-x.
- (23) Kebarle, P.; Tang, L. From ions in solution to ions in the gas phase - the mechanism of electrospray mass spectrometry. *Analytical Chemistry* **1993**, *65* (22), 972A-986A. DOI: 10.1021/ac00070a001.
- (24) Huang, M. Z.; Cheng, S. C.; Cho, Y. T.; Shiea, J. Ambient ionization mass spectrometry: a tutorial. *Anal Chim Acta* **2011**, *702* (1), 1-15, Review. DOI: S0003-2670(11)00844-0 [pii] 10.1016/j.aca.2011.06.017 [doi].
- (25) Ma, X.; Ouyang, Z. Ambient ionization and miniature mass spectrometry system for chemical and biological analysis. *TrAC Trends in Analytical Chemistry* **2016**, *85*, 10-19. DOI: <https://doi.org/10.1016/j.trac.2016.04.009>.
- (26) Rankin-Turner, S.; Reynolds, J. C.; Turner, M. A.; Heaney, L. M. Applications of ambient ionization mass spectrometry in 2021: An annual review. *Analytical Science Advances* **2022**, *3* (3-4), 67-89. DOI: <https://doi.org/10.1002/ansa.202100067>.
- (27) Feider, C. L.; Krieger, A.; DeHoog, R. J.; Eberlin, L. S. Ambient Ionization Mass Spectrometry: Recent Developments and Applications. *Analytical Chemistry* **2019**, *91* (7), 4266-4290. DOI: 10.1021/acs.analchem.9b00807.
- (28) Haddad, R.; Sparrapan, R.; Eberlin, M. N. Desorption sonic spray ionization for (high) voltage-free ambient mass spectrometry. *Rapid Commun Mass Spectrom* **2006**, *20* (19), 2901-2905. DOI: 10.1002/rcm.2680.

- (29) Harper, J. D.; Charipar, N. A.; Mulligan, C. C.; Zhang, X.; Cooks, R. G.; Ouyang, Z. Low-Temperature Plasma Probe for Ambient Desorption Ionization. *Analytical Chemistry* **2008**, *80* (23), 9097-9104. DOI: 10.1021/ac801641a.
- (30) Gross, J. Direct analysis in real time—A critical review on DART-MS. *Analytical and bioanalytical chemistry* **2013**, *406*. DOI: 10.1007/s00216-013-7316-0.
- (31) Cody, R. B.; Laramée, J. A.; Durst, H. D. Versatile new ion source for the analysis of materials in open air under ambient conditions. *Anal Chem* **2005**, *77* (8), 2297-2302. DOI: 10.1021/ac050162j.
- (32) Takats, Z.; Wiseman, J. M.; Gologan, B.; Cooks, R. G. Mass spectrometry sampling under ambient conditions with desorption electrospray ionization. *Science* **2004**, *306* (5695), 471-473. DOI: 10.1126/science.1104404.
- (33) Liu, J.; Wang, H.; Manicke, N. E.; Lin, J. M.; Cooks, R. G.; Ouyang, Z. Development, characterization, and application of paper spray ionization. *Anal Chem* **2010**, *82* (6), 2463-2471, Evaluation Study
Research Support, Non-U.S. Gov't
Research Support, U.S. Gov't, Non-P.H.S. DOI: 10.1021/ac902854g [doi].
- (34) Heron, S. R.; Wilson, R.; Shaffer, S. A.; Goodlett, D. R.; Cooper, J. M. Surface acoustic wave nebulization of peptides as a microfluidic interface for mass spectrometry. *Anal Chem* **2010**, *82* (10), 3985-3989, Research Support, N.I.H., Extramural
Research Support, Non-U.S. Gov't. DOI: 10.1021/ac100372c [doi].
- (35) Huang, Y.; Yoon, S. H.; Heron, S. R.; Masselon, C. D.; Edgar, J. S.; Tureček, F.; Goodlett, D. R. Surface Acoustic Wave Nebulization Produces Ions with Lower Internal Energy than Electrospray Ionization. *J. Am. Soc. Mass Spectrom.* **2012**, *23* (6), 1062-1070. DOI: 10.1007/s13361-012-0352-8.
- (36) Chen, H.; Gamez, G.; Zenobi, R. What can we learn from ambient ionization techniques? *J. Am. Soc. Mass Spectrom.* **2009**, *20* (11), 1947-1963. DOI: 10.1016/j.jasms.2009.07.025.
- (37) Hiraoka, K.; Saito, S.; Katsuragawa, J.; Kudaka, I. A new liquid chromatography mass spectrometry interface: Laser spray. *Rapid Communications in Mass Spectrometry* **1998**, *12* (17), 1170-1174, Article. DOI: 10.1002/(SICI)1097-0231(19980915)12:17<1170::AID-RCM297>3.0.CO;2-O.
- (38) Laiko, V. V.; Baldwin, M. A.; Burlingame, A. L. Atmospheric pressure matrix-assisted laser desorption/ionization mass spectrometry. *Anal Chem* **2000**, *72* (4), 652-657. DOI: 10.1021/ac990998k.
- (39) Pagnotti, V. S.; Chubaty, N. D.; McEwen, C. N. Solvent assisted inlet ionization: an ultrasensitive new liquid introduction ionization method for mass spectrometry. *Anal Chem* **2011**, *83* (11), 3981-3985. DOI: 10.1021/ac200556z.
- (40) Li, A.; Wang, H.; Ouyang, Z.; Cooks, R. G. Paper spray ionization of polar analytes using non-polar solvents. *Chemical Communications* **2011**, *47* (10), 2811-2813, 10.1039/C0CC05513A. DOI: 10.1039/C0CC05513A.
- (41) Hirabayashi, A.; Sakairi, M.; Koizumi, H. Sonic spray mass spectrometry. *Anal Chem* **1995**, *67* (17), 2878-2882. DOI: 10.1021/ac00113a023.
- (42) Alberici, R. M.; Vendramini, P. H.; Eberlin, M. N. Easy ambient sonic-spray ionization mass spectrometry for tissue imaging. *Analytical Methods* **2017**, *9* (34), 5029-5036, 10.1039/C7AY00858A. DOI: 10.1039/C7AY00858A.

- (43) Wlekinski, M.; Li, Y.; Bag, S.; Sarkar, D.; Narayanan, R.; Pradeep, T.; Cooks, R. G. Zero Volt Paper Spray Ionization and Its Mechanism. *Anal Chem* **2015**, 87 (13), 6786-6793. DOI: 10.1021/acs.analchem.5b01225.
- (44) Chen, T.; Lin, J.; Chen, J.; Chen, Y. Ultrasonication-Assisted Spray Ionization Mass Spectrometry for the Analysis of Biomolecules in Solution. *Journal of the American Society For Mass Spectrometry* **2010**, 21 (9), 1547-1553, Article. DOI: 10.1016/j.jasms.2010.04.021.
- (45) Li, X.; Attanayake, K.; Valentine, S. J.; Li, P. Vibrating Sharp-edge Spray Ionization (VSSI) for voltage-free direct analysis of samples using mass spectrometry. *Rapid Commun Mass Spectrom* **2018**. DOI: 10.1002/rcm.8232.
- (46) Ranganathan, N.; Li, C.; Suder, T.; Karanji, A. K.; Li, X.; He, Z.; Valentine, S. J.; Li, P. Capillary Vibrating Sharp-Edge Spray Ionization (cVSSI) for Voltage-Free Liquid Chromatography-Mass Spectrometry. *J Am Soc Mass Spectrom* **2019**, 30 (5), 824-831. DOI: 10.1007/s13361-019-02147-0.
- (47) Li, C.; Attanayake, K.; Valentine, S. J.; Li, P. Facile Improvement of Negative Ion Mode Electrospray Ionization Using Capillary Vibrating Sharp-Edge Spray Ionization. *Anal Chem* **2020**, 92 (3), 2492-2502. DOI: 10.1021/acs.analchem.9b03983.
- (48) Kebarle, P.; Verkerk, U. H. ELECTROSPRAY: FROM IONS IN SOLUTION TO IONS IN THE GAS PHASE, WHAT WE KNOW NOW. *Mass Spectrometry Reviews* **2009**, 28 (6), 898-917, Review. DOI: 10.1002/mas.20247.
- (49) Teunissen, S. F.; Eberlin, M. N. Transferring Ions from Solution to the Gas Phase: The Two Basic Principles. *J. Am. Soc. Mass Spectrom.* **2017**, 28, 2255-2261.
- (50) Teunissen, S. F.; Eberlin, M. N. Transferring Ions from Solution to the Gas Phase: The Two Basic Principles. *Journal of The American Society for Mass Spectrometry* **2017**, 28 (11), 2255-2261. DOI: 10.1007/s13361-017-1779-8.
- (51) Yao, Y.-N.; Wu, L.; Di, D.; Yuan, Z.-C.; Hu, B. Vibrating tip spray ionization mass spectrometry for direct sample analysis. *Journal of Mass Spectrometry* **2019**, 54. DOI: 10.1002/jms.4429.
- (52) Zilch, L. W.; Maze, J. T.; Smith, J. W.; Ewing, G. E.; Jarrold, M. F. Charge separation in the aerodynamic breakup of micrometer-sized water droplets. *J Phys Chem A* **2008**, 112 (51), 13352-13363. DOI: 10.1021/jp806995h.
- (53) Conant, C. R.; Fuller, D. R.; Zhang, Z.; Woodall, D. W.; Russell, D. H.; Clemmer, D. E. Substance P in the Gas Phase: Conformational Changes and Dissociations Induced by Collisional Activation in a Drift Tube. *J. Am. Soc. Mass Spectrom.* **2019**, 30 (6), 932-945. DOI: 10.1007/s13361-019-02160-3 PubMed.
- (54) Consta, S.; Chung, J. K. Charge-induced conformational changes of PEG-(Na⁺)_n in a vacuum and aqueous nanodroplets. *The Journal of Physical Chemistry B* **2011**, 115 (35), 10447-10455.
- (55) Konermann, L.; Ahadi, E.; Rodriguez, A. D.; Vahidi, S. Unraveling the Mechanism of Electrospray Ionization. *Analytical Chemistry* **2013**, 85 (1), 2-9, Article. DOI: 10.1021/ac302789c.
- (56) Znamenskiy, V.; Marginean, I.; Vertes, A. Solvated Ion Evaporation from Charged Water Nanodroplets. *The Journal of Physical Chemistry A* **2003**, 107 (38), 7406-7412. DOI: 10.1021/jp034561z.
- (57) Kanu, A. B.; Dwivedi, P.; Tam, M.; Matz, L.; Hill Jr., H. H. Ion mobility-mass spectrometry. *J. Mass Spectrom.* **2008**, 43 (1), 1-22. DOI: <https://doi.org/10.1002/jms.1383>.

- (58) Konermann, L.; Metwally, H.; McAllister, R. G.; Popa, V. How to run molecular dynamics simulations on electrospray droplets and gas phase proteins: Basic guidelines and selected applications. *Methods* **2018**, *144*, 104-112. DOI: <https://doi.org/10.1016/j.ymeth.2018.04.010>.
- (59) Verlet, L. Computer "Experiments" on Classical Fluids. I. Thermodynamical Properties of Lennard-Jones Molecules. *Physical Review* **1967**, *159*, 98-103.
- (60) Couvillion, S. P.; Zhu, Y.; Nagy, G.; Adkins, J. N.; Ansong, C.; Renslow, R. S.; Piehowski, P. D.; Ibrahim, Y. M.; Kelly, R. T.; Metz, T. O. New mass spectrometry technologies contributing towards comprehensive and high throughput omics analyses of single cells. *Analyst* **2019**, *144* (3), 794-807, 10.1039/C8AN01574K. DOI: 10.1039/C8AN01574K.
- (61) Wang, D.; Bodovitz, S. Single cell analysis: the new frontier in 'omics'. *Trends in Biotechnology* **2010**, *28* (6), 281-290. DOI: <https://doi.org/10.1016/j.tibtech.2010.03.002>.

2 Physicochemical property correlations with ionization efficiency in capillary Vibrating Sharp-edge Spray Ionization (cVSSI)

Reprinted with permission from the American Society for Mass Spectrometry: Physicochemical property correlations with ionization efficiency in capillary Vibrating Sharp-edge Spray Ionization (cVSSI). **Kinkini Udara Jayasundara**, Chong Li, Anthony DeBastiani, Daud Sharif, Peng Li, Stephen J. Valentine. J. Am. Soc. Mass Spectrom.(2021), 32 (1), 84-94.

2.1 Introduction

The introduction of the soft ionization techniques electrospray ionization (ESI) and matrix-assisted laser desorption ionization (MALDI) in the 1980s opened the door to the world of biomolecule mass spectrometry (MS)¹⁻³. Even with the MS instrumentation of the day, it became possible to accurately measure the masses of large biomolecular species with a high degree of accuracy^{1, 4-7}. In the immediately ensuing years, different variations on these ionization themes were developed such as atmospheric pressure MALDI⁸, micro and nano-spray ionization^{9, 10}, desorption electrospray ionization¹¹, sonic spray ionization (SSI)¹², electrosonic spray ionization¹³, and paper spray ionization¹⁴. Furthermore, combinations of the two methods were also developed to include electrospray laser desorption ionization¹⁵, and matrix-assisted laser desorption electrospray ionization¹⁶ and laser ablation electrospray ionization¹⁷. Indeed, gauging the impact of ESI and MALDI on the scientific world is a difficult task. Since their inception, these techniques have spawned whole fields of study including (but not limited to) bottom-up and top-down quantitative proteomics¹⁸⁻²⁶, structural proteomics²⁷⁻³³, molecular imaging in biological samples³⁴⁻³⁸, and microbe characterization/identification³⁹⁻⁴².

The development of Laser Spray Ionization within the last decade initiated a new round of rapid ionization technique development^{43, 44}. Seminal studies would shortly later reveal that ions could be produced from MALDI matrices using only the presence of a vacuum⁴⁵. More remarkably still, further studies showed that ion formation from solid and liquid matrices as well

as ablated material required only heat and the inlet of a mass spectrometer^{46, 47}. Later it was also shown that even the heated transfer tube was not required to produce ions from some matrices⁴⁸. This foundational work has most recently led to the demonstration of high-sensitivity measurements and the introduction of a commercial source employing solvent-assisted inlet ionization (SAII), matrix-assisted inlet ionization (MAII), and ESI methods⁴⁹.

As part of the renewed ionization source development work, in 2018, Li and coworkers introduced a new, spray-based ionization technique termed Vibrating Sharp-edge Spray Ionization (VSSI)⁵⁰. The new approach only required a vibrating substrate containing a sharp edge. Placing a liquid pool at the edge of a microscope slide and subsequently vibrating the slide (~100 kHz) was shown to produce a plume of micrometer-sized droplets which only emanated from the sharp tip of the slide. Ionization from the plume was demonstrated to produce ESI-like ions. Subsequent studies showed that the sharp edge employed in droplet production could be a capillary through which sample was infused; this was termed capillary VSSI (cVSSI)⁵¹. The demonstration of direct infusion enabled the coupling of VSSI with condensed-phase separation techniques. More recently, the coupling of a voltage applied to the solution with cVSSI (field-enabled cVSSI) using a pulled-tip capillary was shown to provide enhancements of ~10 to 100 fold in ion signal levels compared with ESI for native MS analyses performed in negative ion mode; more modest improvements (typically 5 fold) were observed for positive ion mode⁵². Conceptually, field-free cVSSI is similar to sonic spray ionization, SAII, surface acoustic wave nebulization ionization, and field-free paper spray ionization in that a plume of droplets directed into a mass spectrometer results in ion production. Unique to the VSSI and cVSSI approaches is the method of droplet production which requires the vibrating sharp edge.

Over the years, much development for spray-based ionization techniques has been directed towards improving ionization efficiency. Examples include the use of heated transfer tubes and bath gases to aid ion desolvation^{53, 54}, the use of precise sample application to the transducer in SAWN⁵⁵, the use of microchips and microfluidic-chips in sonic spray ionization^{56, 57}, the use of heated ion transfer tubes in SAI⁴⁶, and the use of carbon nanotube (CNT)-impregnated paper surface in field-free PSI^{58, 59}. More recently, and from a different perspective, significant interest has been given to the role of the physicochemical properties of different analytes in the ionization process. For ESI, most studies have indicated that log of the base dissociation constant (pK_b) has the strongest correlation with the formation of small-molecule ions^{60, 61}. However, some studies have suggested that different solvent conditions such as pH could cause other factors such as polarity and volatility to be associated with the process^{62, 63}. Remarkably, to some degree, differences in the degree of correlation by different molecular properties were found to be instrument dependent indicating the challenge associated with quantifying molecular property effects.

Here we present the first efforts to associate the effects of different molecular physicochemical properties with ion intensities for field-free and field-enabled cVSSI. The results are compared to those obtained for ESI using the same flow rates and emitter tips. For these experiments, the molecular properties were described by pK_b , log of the partition coefficient ($\log P$), and gas-phase proton affinity (PA). In an attempt to hold all other variables constant, the same emitter tip type (blunt-tip and pulled-tip), the same applied voltages (field-enabled cVSSI and ESI) and the same emitter tip distance to the MS inlet are used for conducting the separate analyses. Similarly, all mass spectrometer settings are maintained between the separate experiments. In total, experiments were conducted for analytes in aqueous and non-aqueous (methanol) samples to

determine whether or not molecular properties could exhibit different correlations for samples relying on different solution charge carriers. In general, from multiple regression analysis, differences in physicochemical factors associated with ion intensities were observed for all six systems (field-free and field-enabled cVSSI and ESI \times 2 solvent systems). These differences are discussed below in light of previous findings from ESI experiments and brief consideration is given to relationship to ionization mechanism.

2.2 Experimental

2.2.1 Ionization device fabrication

5-cm-long, blunt-tip capillary emitters were obtained using pre-cut fused silica (100 μ m ID \times 360 μ m OD). Pulled-tip capillary emitters were obtained using a laser puller (Sutter Instrument Co, Model P-2000, Novato CA, USA) and the same fused silica. Multiple devices were constructed (see below) using the blunt- and pulled-tip emitters. All pulled-tip diameters were examined by microscope and only those having diameters of \sim 25 to 30 μ m were used for these studies. Droplet size distributions were obtained using representative blunt- and pulled-tip emitters where cVSSI was employed to create a droplet plume and droplets were captured on an oil surface. Under voltage free conditions, aqueous droplet diameters were determined to be 23.7 ± 12.5 and 17.5 ± 5.6 μ m for the blunt- and pulled-tip emitters, respectively.

cVSSI and ESI sources were constructed as described previously⁵². Briefly, the blunt- or pulled-tip emitter was attached to the edge of a cVSSI device in the orientation shown in Figure 2-1. The cVSSI devices consists of a piezoelectric transducer (Murata) which was attached to a microscope slide (VWR). This was accomplished with epoxy-based superglue (Devcon).

To couple direct infusion of the samples with the emitter tips, 30-gauge PTFE tubing is placed over the blunt end of the blunt- or pulled-tip capillary. Near the tubing-emitter interface, a small (typically ~10 cm long) platinum wire is pushed through the PTFE tubing and glued in place. For the field-free and field-enabled cVSSI experiments, an amplified (2×, Mini-Circuits) square waveform (Tektronix) was applied to the piezoelectric transducer in the range of ~94-95 kHz while infusing the sample at flow rates of 10 μL / min (blunt-tip experiments) and 5 μL / min (pulled-tip experiments).

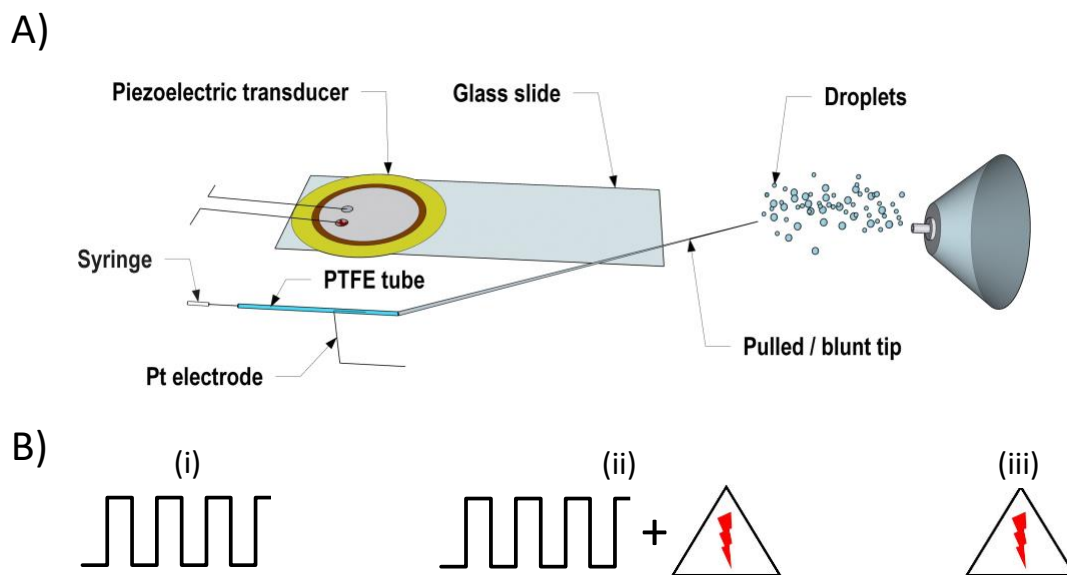


Figure 2- 1 Illustration of the cVSSI device and droplet production used in the current studies. A). Component parts are labeled. Component parts are not drawn to scale to provide greater detail. B) Operational modes of the cVSSI device representing (i) voltage-- free cVSSI, (ii) field-enabled cVSSI, and (iii) ESI. For (i) and (ii), the waveform is applied to the leads on the piezoelectric transducer. For (ii) and (iii), the DC voltage is applied to the platinum wire. DC voltages and waveform characteristics are provided in the Methods section

2.2.2 Reagents and sample preparation

For the experiments described here, 18 compounds were used and represent a similar group of molecules as analyzed by ESI in a previous study ⁶⁰. The compounds thymine, p-nitroaniline, benzamide, diphenylamine, 4-methoxybenzamide, cytosine, adenine, N-ethylaniline, 4-methoxyaniline, 2-2 bipyridine, methyltriazinaminec, benzylamine, triethanolamine, triethylamine, N-methylbenzylamine, quinuclidine, N,N-dimethylbenzylamine, phenylethylamine were purchased from Thermo Fisher Scientific (Pittsburgh, PA USA) and used without further purification. Table 2-1 shows the structures of the compounds and provides molecular weights, $\log P$, pK_b , and PA values. pK_b values were obtained from chemicalize.org by ChemAxon, Budapest, Hungary [<https://chemicalize.com>]. The majority of the PA values were obtained from the NIST Chemistry WebBook [<http://webbook.nist.gov/chemistry>] and the PA values of 4 compounds which were not included in NIST data base were calculated using the Gaussian 09 software suite⁶⁴.

For the aqueous samples, p-nitroaniline (#2), benzamide (#3), and diphenylamine (#4) did not dissolve completely in the aqueous buffer and so these compounds were not included in the comparisons. For all experiments, ammonium acetate (100 mM) was utilized to limit the amount of droplet protonating species (H_3O^+ or $MeOH_2^+$) for both of the solvent systems. Prior to analysis by MS, all samples were diluted to 0.01 mg / mL with the appropriate buffered solvent. Stock solutions of each compound were made by dissolving 1 mg of each compound in 1 mL of solvent. Two different solvent systems were investigated namely methanol and water.

Table 2- 1 Structures and physicochemical property values for the compounds used in the ionization experiments.

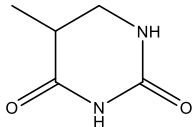
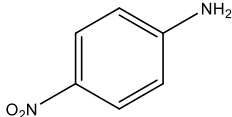
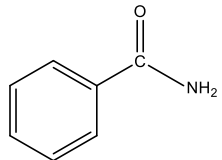
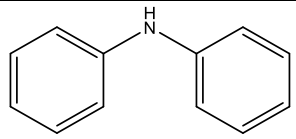
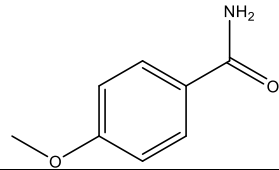
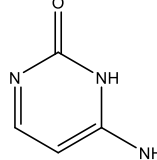
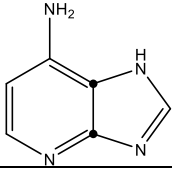
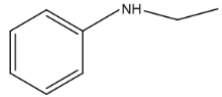
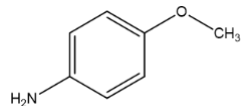
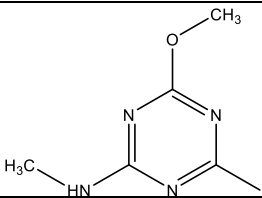
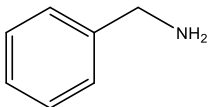
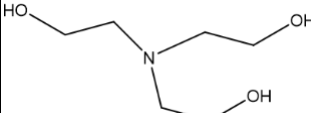
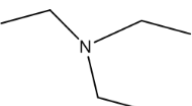
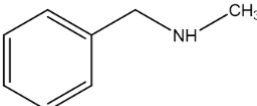
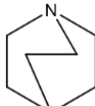
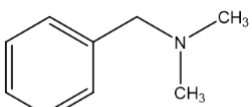
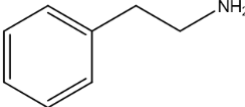
#	Compound	Structure	pK _b		logP	PA (kJ/mol)	MW
			Water	MeOH			
1	Thymine		15.61	17.51	-1.00	880.0	126.11
2	p-Nitroaniline		11.9	13.8	1.37	866	138.12
3	Benzamide		14.36	16.26	0.74	892.1	121.05
4	Diphenylamine		13.2	15.1	2.97	916.5	169.22
5	4-Methoxybenzamide		14.21	16.11	0.81	900.3	151.16
6	Cytosine		9.2	11.1	-2.29	949.9	111.10
7	Adenine		10.3	12.2	-0.03	942.8	135.13
8	N-ethylaniline		9.1	11	2.13	924.8	123.15
10	4-Methoxyaniline		8.9	10.8	0.74	900.3	123.5

Table 2-1. continued

#	Compound	Structure	pK _b		logP	PA (KJ/mol)	MW
			Water	MeOH			
12	Methyltriazinaminec		9.2	11.1	-1.34	882.7	154.17
13	Benzylamine		4.7	6.6	1.09	922.7	107.15
14	Triethanolamine		5.6	7.5	-0.74	1000.4	149.19
15	Triethylamine		3.8	5.7	1.66	981.8	101.19
16	N-methylbenzylamine		4.6	6.5	1.60	980.4	121.18
17	Quinuclidine		3.1	5	1.38	983.3	111.18
18	N,N-dimethylbenzylamine		5.1	7	1.98	968.4	135.21
19	Phenylethylamine		4.2	6.1	1.49	936.2	121.18

2.2.3 Mass spectrometry data collection

Experiments were conducted on two separate mass spectrometers as prior research has suggested that different physicochemical properties are more effective in ionization by ESI for different instruments⁶². The first set of experiments utilized a linear ion trap (LTQ-XL, ThermoFisher) and employed cVSSI devices with blunt-tip emitters. The second set of experiments were carried out on an orbitrap mass spectrometer (Q-Exactive, ThermoFisher) using cVSSI devices with pulled tip emitters. Replicate datasets for the methanol and aqueous samples were conducted on both mass spectrometers. Droplet production was initiated on the infused samples by voltage-free cVSSI, field-enabled cVSSI, or ESI. For voltage-free and field-enabled cVSSI experiments, the glass slide was vibrated as described above. For the latter two methods, voltages of 4 kV and 2 kV were utilized for the blunt- and pulled-tip emitters, respectively; the higher voltage was required to initiate ion production from the more diffuse charge and higher flow rate. The voltage was applied to the platinum wire just prior to the emitter tip (see Figure 1). Experiments were conducted in positive ion mode on both mass spectrometers. The ion transfer tube temperatures for both mass spectrometers were maintained at 275 °C for all experiments. Unit resolution was employed on the linear ion trap instrument and the precursor ion resolving power was set at 7×10^4 on the orbitrap mass spectrometer. Data were collected for 30 seconds over a m/z range of 50 to 300.

2.2.4 Data analysis

Peak intensities were obtained using the xCalibur software suite (ThermoFisher). For all comparisons signal intensities were obtained from total ion signals for each compound. In orbitrap experiments, for two compounds, neutral loss of ammonia was observed. For these compounds,

the fragment ions were included in the summation of the ion intensities. This was done because the separate experiments on the LTQ XL mass spectrometer using the same transfer tube temperature did not show ion fragmentation for these compounds in either water or methanol. Thus, it is believed that the fragments should be counted as part of the total ion intensities. Additionally it is noted that ion fragmentation has been treated in this manner in the past for ESI studies ⁶².

For single parameter correlations, linear regression was performed using the Excel software suite (Microsoft, Redmond CA) for the data (peak intensity versus property) from the separate analyses. R-squared values were compared for the separate regression analyses. Because the R-squared values were relatively small, separate Spearman's rank correlation analyses were performed using the Excel software suite (Microsoft, Redmond CA) for a subset of the data to serve as a cross check of the linear regression analysis.

Peak intensities and molecular physicochemical properties for each analyte were input into the regression software (IBM SPSS Statistics 25). Multiple regression analysis was performed using the three descriptor columns as the independent variables and the peak intensities as the dependent variable. Beta coefficient values from the multiple regression analysis were used to indicate the relative degree of influence each molecular characteristic has on the degree of ionization (ion intensity). The coefficients and their associated significance are listed in Tables 2-4 (blunt-tip emitters) and 5 (pulled-tip emitters) for the different experiments.

2.3 Results and Discussion

2.3.1 Linear ion trap experiments: ion intensities from compounds in methanol solvent.

When voltage-free cVSSI is employed using the linear ion trap mass spectrometer, ion production for the 18 different compounds is observed to occur over an ~ 2.7 (i.e., $10^{2.7}$) decade range in intensity. The compound exhibiting the greatest ionization efficiency is quinuclidine with an average ion intensity value of 1833. The lowest ionizing species is thymine with an average ion intensity value of 3. Table 2-2 lists the intensities of all of the compounds in methanol for the voltage-free study. Figure 2-2 shows the relative intensity values for each of the compounds for these same experiments. Notably, the numbering of the compounds in Figure 2 is the same as that used in the work by Cech *et al.*⁶⁰, where the compounds were numbered according to increased ion intensity as observed by ESI. Figure 2-2 shows that, in general, the relative ion intensities for the voltage-free cVSSI experiments are somewhat similar to those reported earlier for these compounds in that the higher-numbered compounds typically have higher intensities. Notable exceptions are 4-Methoxyaniline (#10), triethylamine (#15), and N,N-dimethylbenzylamine (#18). Additionally, Figure 2-2 reveals differences in the compounds in that large fluctuations in ion intensities are observed for species numbered above compound #10; this introduces some differences between these results and those reported previously. The relating of such fluctuations to physicochemical properties of the compounds is the subject of the multiple regression analysis discussed below.

Table 2- 2 Molecule-specific ion intensities for the methanol experiments employing blunt-tip emitters.

#	Compound	MeOH solvent system					
		cVSSI		cVSSI+4KV		ESI	
		[M+H] ⁺	S.D.	[M+H] ⁺	S.D.	[M+H] ⁺	S.D.
1	Thymine	3.11E+00	8.93E-01	1.66E+04	2.48E+03	9.25E+03	2.30E+03
2	p-Nitroaniline	1.01E+02	1.93E+01	3.10E+04	9.93E+03	7.66E+04	4.08E+03
3	Benzamide	1.05E+02	1.84E+01	4.86E+05	2.00E+04	5.17E+05	1.50E+04
4	Diphenylamine	1.11E+02	9.54E+00	2.04E+05	4.67E+04	3.48E+05	4.73E+03
5	4-Methoxybenzamide	2.26E+02	1.90E+01	5.64E+05	2.30E+05	3.76E+05	1.91E+04
6	Cytosine	2.39E+02	1.40E+01	4.68E+04	2.88E+04	1.57E+05	8.89E+03
7	Adenine	1.51E+02	1.95E+01	1.95E+05	8.08E+03	2.26E+05	2.78E+04
8	N-ethylaniline	2.86E+02	3.09E+01	3.53E+05	6.00E+04	5.68E+05	2.08E+04
10	4-Methoxyaniline	4.85E+01	4.62E+00	5.74E+05	1.69E+05	2.11E+05	1.40E+04
11	2-2 bipyridine	1.36E+03	2.36E+02	3.60E+05	4.90E+04	5.24E+05	1.15E+05
12	Methyltriazinaminec	7.56E+02	1.25E+02	9.68E+05	1.06E+05	1.39E+06	3.79E+04
13	Benzylamine	4.66E+02	1.04E+02	4.21E+05	4.30E+04	1.14E+06	8.00E+04
14	Triethanolamine	1.11E+03	5.51E+01	8.58E+05	2.05E+05	1.37E+06	5.00E+04
15	Triethylamine	9.53E+01	3.44E+01	7.65E+04	1.09E+04	1.44E+05	7.00E+03
16	N-methylbenzylamine	8.62E+02	8.06E+01	1.29E+06	70945.99	2.77E+06	7.21E+04
17	Quinuclidine	1.83E+03	2.37E+02	2.41E+05	4.41E+04	1.04E+06	4.05E+04
18	N,N-dimethylbenzylamine	2.61E+02	3.74E+01	1.24E+06	95043.85	6.91E+05	3.48E+04
19	Phenylethylamine	1.11E+03	2.19E+02	3.58E+05	5.55E+04	1.46E+06	1.89E+05

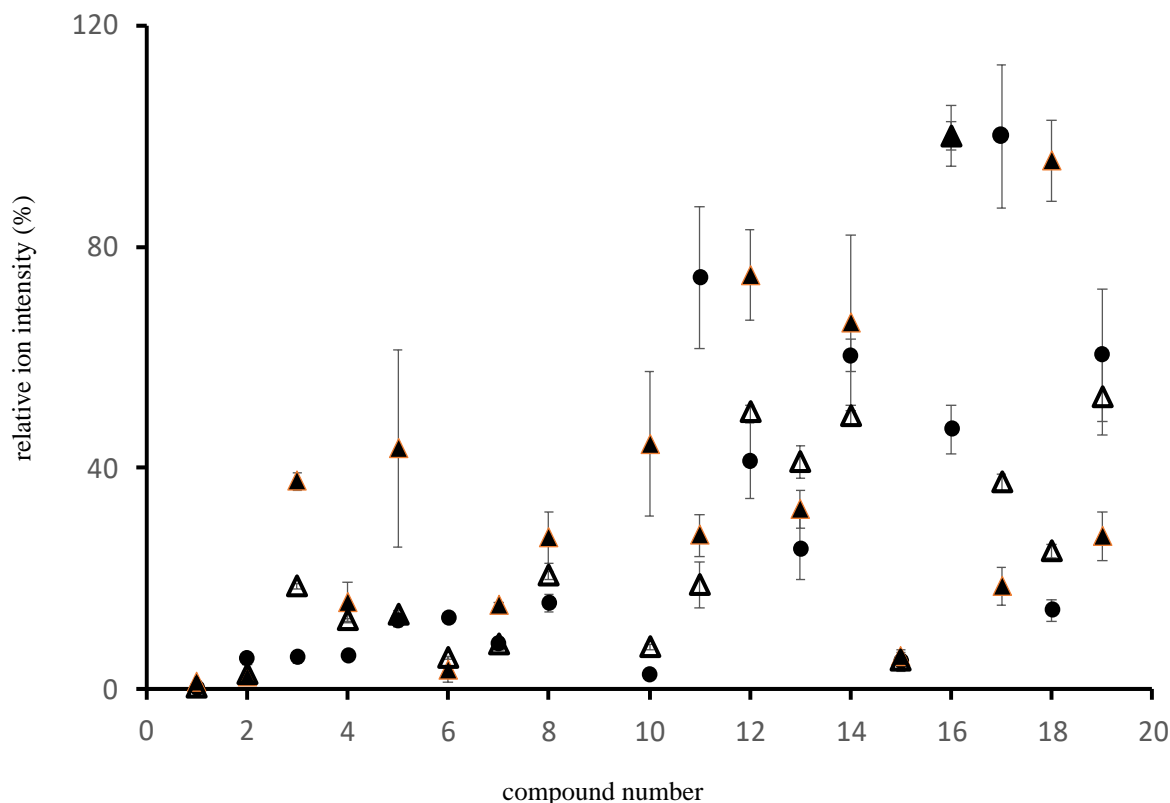


Figure 2- 2 Plot of relative ion intensities for the voltage-free cVSSI (solid circles), field-enabled cVSSI (solid triangles), and ESI (open triangles) experiments using the methanol samples. The blunt-tip emitters were used to collect the data.

The next experiments examined the effects on ionization upon applying a voltage to the infused solvent while vibrating the cVSSI device (field-enabled cVSSI). One motivating factor for studying field-enabled cVSSI has been the tremendous advantage observed in ionizing biomolecules from aqueous environments compared with ESI alone; 10 to 100 fold enhancements in signal levels have been reported for a variety of molecules when using field-enabled cVSSI⁵². Upon applying voltage to the cVSSI device, the intensities of all compounds increase (see Table 2-2). The range of ion intensities narrows somewhat compared with the voltage-free experiments (~2.7 to ~2 decades). N-methylbenzylamine (#16) exhibits the greatest ionization efficiency with an ion intensity value of 1.3×10^6 . The lowest ionizing species is again thymine with an ion

intensity value of 1.7×10^4 . In general, the ion intensities also increase with increasing compound number as shown in Figure 2-2. That said, there are notable differences between the voltage-free and field-enabled cVSSI experiments. For example, although N-methylbenzylamine (#16) is ionized relatively well by field-enabled cVSSI, it exhibits a relatively low ion signal level (<50%) in the voltage-free cVSSI experiments. Another dramatic difference is the observed increase in ionization of 4-methoxyaniline (#10) upon application of voltage to the cVSSI device (see Figure 2-2). Two more examples in which a dramatic increase in relative ion signal level is observed are benzamide (#3) and 4-methoxybenzamide (#5).

The ion intensities of the same compounds have also been recorded upon removal of the vibration of the cVSSI device. Here, charged droplets are produced by the application of the high voltage alone. For these ESI experiments, differences and similarities are observed with the other two ionization techniques. For example, Figure 2-2 shows that for the ions phenylethylamine (#19), N,N-dimethylbenzylamine (#18), triethylamine (#15), methyltriazinaminec (#12), 4-methoxyaniline (#10), and 4-methoxybenzamide (#5), the relative ion signal levels of ESI are closer in value to those obtained from voltage-free cVSSI. In contrast, the ESI ion signal levels for quinuclidine (#17), N-methylbenzylamine (#16), 2-2 bipyridine (#11), cytosine (#6), and diphenylamine (#4) are more similar to those recorded for the same compounds examined by field-enabled cVSSI. Notably, the relative ion signal level was the same for all three techniques for triethylamine (#15) in methanol solution

2.3.2 Linear ion trap experiments: ion intensities for compounds from aqueous samples.

To investigate whether or not changes in relative ion intensity levels could be affected significantly by the solvent environment for the different experimental modes of ion production, the same studies have been conducted for samples in which the compounds were dissolved in buffered water. The intensities of ions produced from the aqueous samples for the voltage-free cVSSI, field-enabled cVSSI, and ESI experiments are listed in Table 2-3. Additionally, the relative ion signal intensities are shown for the three different experiments in Figure 2-3.

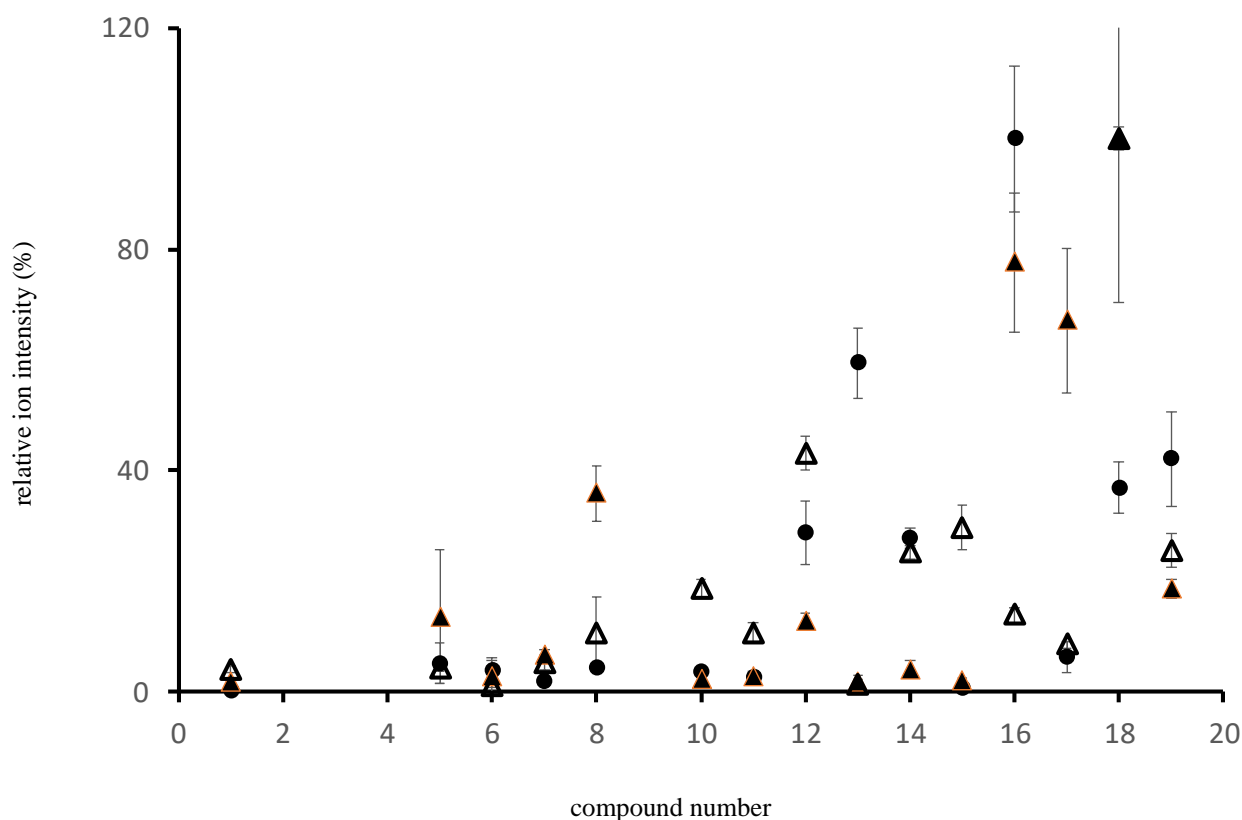


Figure 2- 3 Plot of relative ion intensities for the voltage-free cVSSI (solid circles), field-enabled cVSSI (solid triangles), and ESI (open triangles) experiments using the water samples. The blunt-tip emitters were used to collect the data.

Table 2- 3 Molecule-specific ion intensities for the methanol experiments employing blunt-tip emitters.

#	Compound	Water solvent system					
		cVSSI		cVSSI+4KV		ESI	
		[M+H] ⁺	S.D.	[M+H] ⁺	S.D.	[M+H] ⁺	S.D.
1	Thymine	3.70E+00	3.10E+00	8.97E+03	2.20E+03	1.56E+04	2.46E+03
5	4-Methoxybenzamide	1.28E+02	9.25E+01	6.65E+04	5.88E+04	1.67E+04	1.78E+03
6	Cytosine	9.77E+01	5.65E+01	1.39E+04	1.33E+04	4.51E+03	8.87E+02
7	Adenine	4.47E+01	2.06E+01	3.23E+04	5.37E+03	2.05E+04	5.14E+03
8	N-ethylaniline	1.05E+02	1.53E+01	1.75E+05	2.44E+04	4.07E+04	2.56E+04
10	4-Methoxyaniline	8.88E+01	1.14E+01	1.08E+04	7.01E+03	7.21E+04	6.38E+03
11	2-2 bipyridine	6.40E+01	8.02E+00	1.33E+04	4.44E+03	4.13E+04	6.89E+03
12	Methyltriazinaminec	7.08E+02	1.40E+02	6.25E+04	7.57E+03	1.67E+05	1.19E+04
13	Benzylamine	1.46E+03	1.59E+02	8.81E+03	6.00E+03	5.03E+03	3.40E+03
14	Triethanolamine	6.84E+02	4.47E+01	1.97E+04	7.79E+03	9.77E+04	4.93E+03
15	Triethylamine	1.71E+01	6.07E+00	9.65E+03	3.12E+03	1.15E+05	1.57E+04
16	N-methylbenzylamine	2.46E+03	3.24E+02	3.79E+05	6.11E+04	5.39E+04	5.23E+03
17	Quinuclidine	1.56E+02	6.98E+01	3.27E+05	6.37E+04	3.31E+04	2.31E+03
18	N,N-dimethylbenzylamine	9.09E+02	1.13E+02	4.88E+05	1.44E+05	3.87E+05	7.77E+03
19	Phenylethylamine	1.04E+03	2.10E+02	9.10E+04	8.35E+03	9.88E+04	1.16E+04

Upon sample nebulization by vibration alone, as with the methanol samples, the ion intensity levels exhibit nearly a 2.8 decade range in values for the various compounds (see Table 2-3). The highest and lowest ionizing compounds are N-methylbenzylamine and thymine, respectively. Figure 2-3 shows that, in general, relative ion intensities increase with increasing compound number as was observed for the methanol samples. Notable differences in relative ion signal levels are evident for the voltage-free cVSSI experiments when comparing the two different sample types. For example, consider the relative intensities of N-methylbenzylamine (#16) and quinuclidine (#17). For the water samples (Figure 2-3), the relative values of the respective compounds are 100% and ~9%. For the methanol samples (Figure 1), the relative ion signal levels are reversed (47% and 100%, respectively). Similar to the methanol studies, 4-methoxyaniline (#10) and triethylamine (#15) exhibit some of the lowest relative ion intensity levels (Figure 2-3).

When high voltage is applied to the cVSSI device, the intensity levels of all ions increase as was also observed for the methanol samples (Table 2-3). The range of ion intensity values (~1.7 decades) narrows with the application of voltage to these aqueous samples as was observed for the methanol samples. As with all other experiments described to this point, a general trend is an increase in relative ion signal level with increasing compound number as shown in Figure 2-3. However, there are notable differences among the data obtained for the field-enabled cVSSI for the methanol and aqueous samples. One example is that the relative ion intensity levels for 4-Methoxyaniline (#10) and 2-2 bipyridine (#11) decrease by ~20% and ~10%, respectively, for the aqueous samples (Figure 2-3). Conversely, for quinuclidine(#17), the relative ion signal is about 4 times higher for the aqueous sample. In comparison to the voltage-free cVSSI of the aqueous samples, the relatively ion signal levels for the field-enabled cVSSI change the most for thymine

(#1) and triethanolamine (#14) where an ~12 fold increase and an ~7 fold decrease are observed, respectively.

Upon removal of the glass slide vibration, ESI also produces ions with varying intensities (i.e., a range of ~1.9 decades) as shown in Table 2-3. In general, Figure 2-3 shows that, for ESI of aqueous samples, the relative ion intensities increase with increasing compound number as observed for all other experiments. Compared to ESI from methanol (Figure 2-2), the relative ion signal level for N-methylbenzylamine (#16) changes from 100% to ~14% for the methanol and aqueous samples, respectively. In opposition to this, the respective relative ion signal levels for N,N-dimethylbenzylamine (#18) are ~25% and 100%. The ESI data for the aqueous samples also shows differences when compared with the voltage-free and field-enabled cVSSI data (Figure 2-3). In comparison to voltage-free cVSSI experiments for aqueous samples, the relative ion intensities for thymine (#1) and N-methylbenzylamine (#16) increase and decrease by factors of ~26 and 7, respectively. In comparison to the field-enabled cVSSI, the compounds exhibiting the largest change in relative ion intensity are 4-methoxyaniline (#10) and quinuclidine (#17) which exhibit an increase and decrease by ~8 fold each for the ESI experiments.

2.3.3 Linear ion trap experiments: evaluating physicochemical property associations with ion intensity.

To determine whether or not ion intensities correlate with specific compound properties, linear regression can be employed and R^2 values can be compared. Figure 2-4 shows the correlations of ion intensity with pK_b , $\log P$, and PA of the compounds. The data for Figure 2-4 are obtained from experiments in which compounds are ionized from methanol solutions using voltage-free cVSSI. From the R^2 values, the strongest correlation, based on R^2 values, is with PA

($R^2 = 0.3239$) The second largest correlator with a similar value ($R^2 = 0.2873$) is pK_b and $\log P$ is not observed to correlate appreciably ($R^2 = 0.0014$) with ion intensity. Because the R^2 values are low, separate Spearman's Rank Correlation analyses were performed for the data represented in Figure 2-4 to provide a cross check of the individual correlations. Spearman's rank coefficients were observed to resemble the R^2 values from the linear regression; coefficients of 0.577, -0.501, and 0.124 for PA , pK_b , and $\log P$, respectively were obtained. Here we note that previous experiments employing ESI have shown that the strongest correlator with these compounds was pK_b . In that regard, it might be argued that voltage-free cVSSI produces ions in a manner similar to ESI. However, notably the stronger correlation with PA is different than that observed previously for ESI possibly suggesting differences in ionization process(es) of these compounds by voltage-free cVSSI (see discussion below).

To better compare all associations with ion intensity, multiple regression analysis has been conducted for each separate experiment. The beta coefficients (relative effect) for each of the three molecular properties and their respective significance (p-value) are presented in Table 2-4. From the multiple regression analysis of the voltage-free cVSSI results for methanol samples, the beta coefficients for pK_b , $\log P$, and PA are -0.391, -0.024, and 0.325, respectively. The significance assigned to the respective coefficients are 0.021, 0.838, and 0.058. These beta coefficients and their respective significance values are mostly reflective of the R^2 values that are obtained from the linear regression analyses of the individual physical characteristics (Figure 2-4). In the independent comparisons, the compound PA shows the highest correlation followed by the pK_b and the $\log P$ having respective R^2 values of 0.324, 0.287, and 0.001. Here, it is again noted that the primary correlation of ion intensity and pK_b for voltage-free cVSSI is similar to what has been obtained for these compounds in the prior study using ESI ⁶⁰. A difference is that a secondary

correlation with *PA* is observed for the voltage-free cVSSI that is just outside the $p < 0.05$ significance threshold.

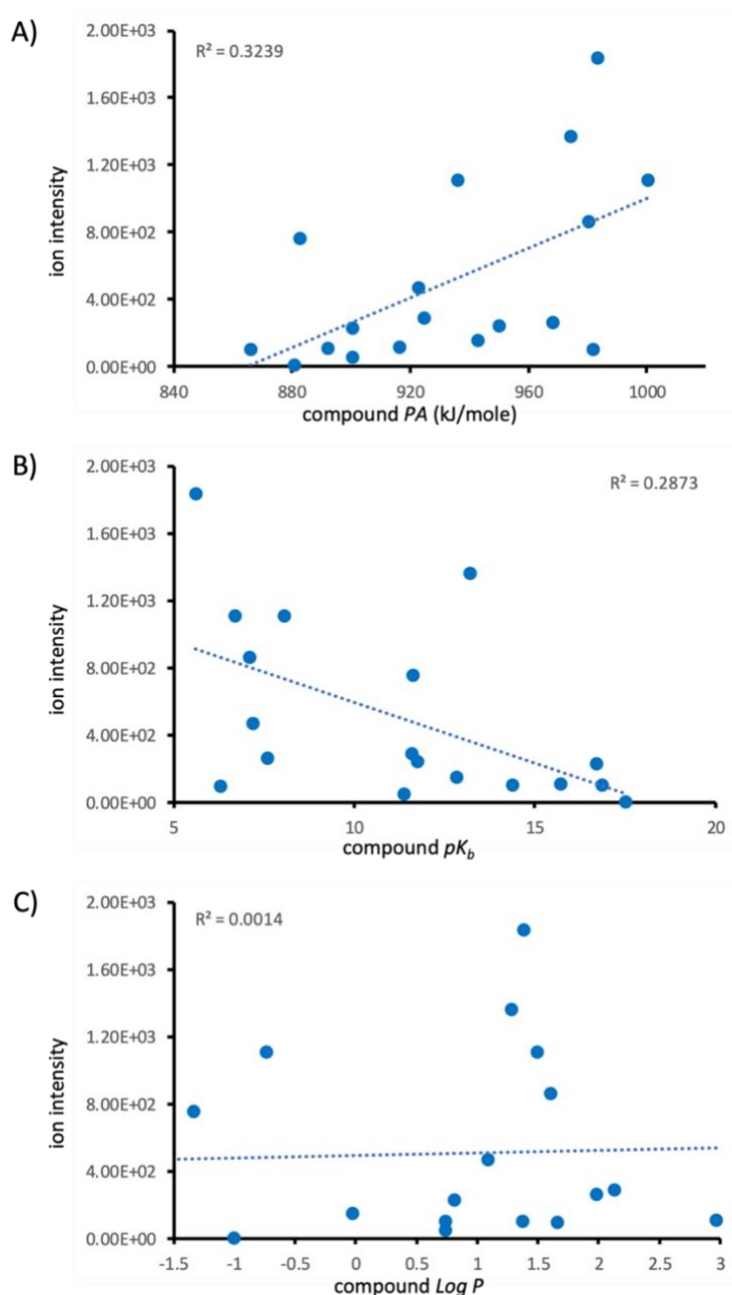


Figure 2- 4 Plots of individual correlations between separate physicochemical property and ion intensity for the voltage-free cVSSI analysis of methanol samples using blunt-tip emitters.

The compounds are numbered according to the method used in Table 1. Shown are the plots of ion intensity versus A) *PA*, B) pK_b , and C) $\log P$. Linear least-squares best-fit lines are provided as dotted lines and the R^2 value for each is shown in the respective plot.

When voltage is applied to the emitter tip of the cVSSI device used in the methanol studies, the correlation with pK_b is not as strong resulting in a beta coefficient value of -0.279 and a significance of 0.187. The beta coefficient for $\log P$ is -0.224 with a significance of 0.138 suggesting a slightly stronger correlation albeit well outside the $p < 0.05$ significance limit. The least correlated physicochemical parameter is the PA with a beta coefficient of -0.937 and a significance of 0.354. When the vibration of the slide is removed and ESI alone is performed, the only significant (0.000) correlator with ion intensity is pK_b with a beta coefficient value of -0.770. This is followed by PA with a beta coefficient value of -0.259 and a significance of 0.130. The respective values for $\log P$ are -0.125 and 0.303. Notably, the result showing a significant association with pK_b is again consistent with the results obtained in previous ESI studies of the same compounds⁶⁰.

Table 2- 4 Beta coefficients and the associated significance values for the LTQ experiments.

Property ^a	MeOH solvent system			Water solvent system		
	cVSSI ^b	cVSSI+4KV	ESI	cVSSI	cVSSI+4KV	ESI
pK_b	-0.391(0.021)^c	-0.279(0.187)	-0.774(0.000)	-0.932(0.000)	-0.101(0.639)	-0.665(0.005)
Log P	-0.024(0.838)	-0.224(0.138)	-0.125(0.303)	-0.223(0.122)	0.365(0.025)	0.246(0.131)
PA	0.315(0.058)	-0.937(0.354)	-0.259(0.130)	-0.562(0.004)	0.139(0.495)	-0.330(0.121)

^aPhysicochemical property for the different compounds. The compound-specific values are listed in Table 1 in the Supporting Information section.

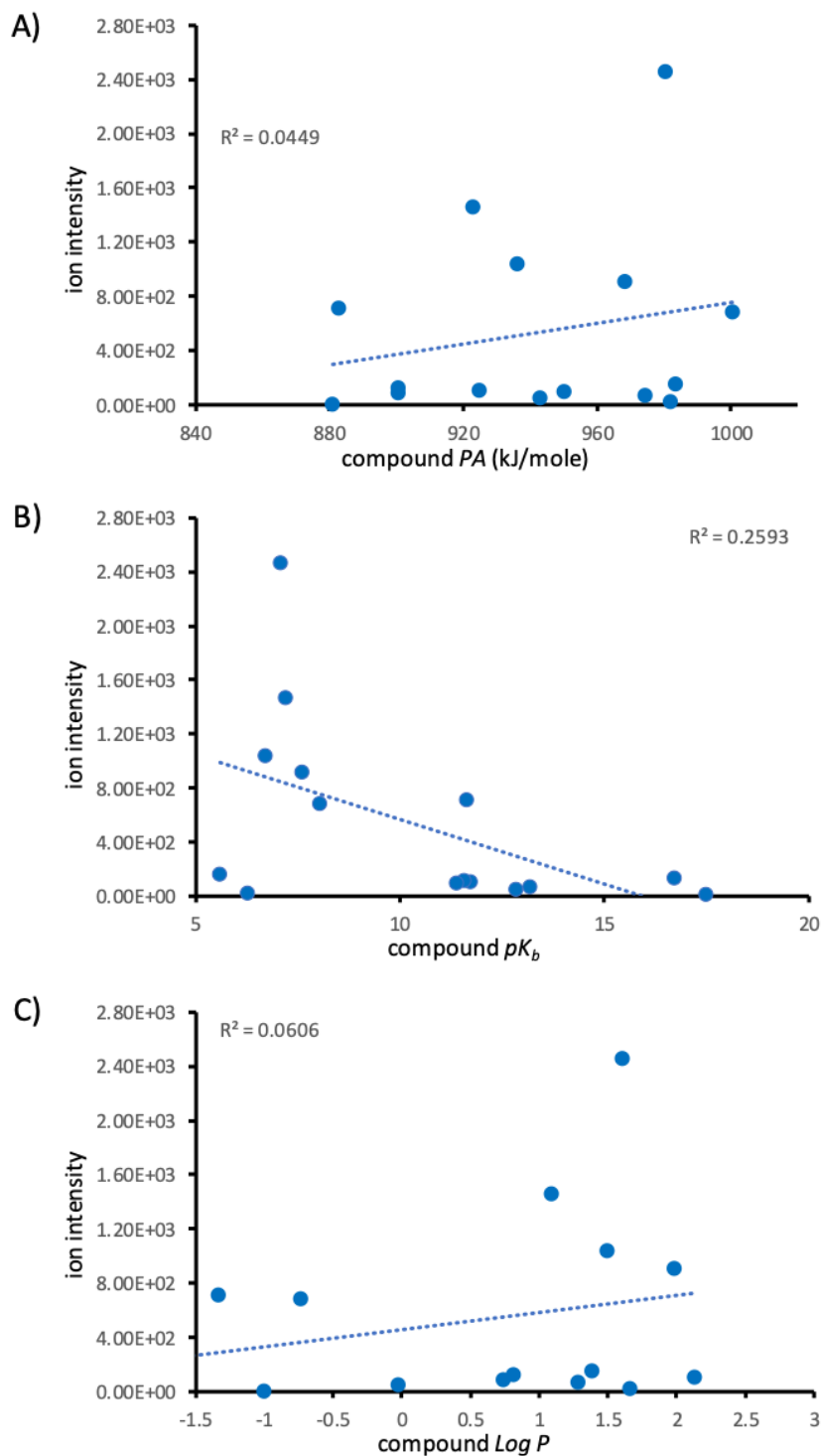
^bIonization mode. cVSSI, cVSSI+2kV, and ESI correspond to the voltage-free cVSSI, field-enabled cVSSI, and ESI experiments, respectively. See the Experimental section for more details.

^cBeta coefficients and associated significance values (given parenthetically) for the separate regression analyses. Bolded values represent the most significant results for each experiment. The sign of the coefficient indicates the nature of the correlation (positive versus negative correlation).

The multiple regression analysis for the aqueous samples show a marked similarity to those obtained for methanol as presented in Table 2-4. That is, for the voltage-free cVSSI, the most significant correlators are pK_b and PA . When voltage is applied to the solution to enact field-enabled cVSSI, $\log P$ provides the most significant association. Finally, the ordering of significance for ESI of the water solutions is pK_b , PA , and $\log P$ where only pK_b meets the $p < 0.5$ confidence limit.

It is instructive to consider the individual correlations in light of the beta coefficient and significance values obtained from the multiple regression analyses. For example, for the water analyses, using voltage-free cVSSI, the strongest individual correlation is observed for pK_b exhibiting a R^2 value of 0.26 as shown in Figure 2-5. The individual correlations with PA and $\log P$ are markedly lower with R^2 values of 0.04 and 0.06, respectively. Therefore, it is somewhat perplexing that PA is indicated to be a significant correlator by the multiple regression analysis (Table 2-4). It is noted that the difference in R^2 values and beta coefficients is that the latter attempts to mathematically assign a relative association while accounting for the contributions of the other factors while the former only considers the single variable correlation. That said, for the field-enabled cVSSI analysis of the water samples, the individual correlations are $\log P$ ($R^2 = 0.26$) $> pK_b$ ($R^2 = 0.19$) $> PA$ ($R^2 = 0.14$) as shown in Figure 2-6. This ordering is consistent with the respective beta coefficient significance values of 0.025, 0.495, and 0.639 (Table 2-4). From this analysis it is evident that care should be taken when interpreting results either from the multiple regression or the individual correlation analyses. In cases such as this where a single beta coefficient value significance is well outside the $p < 0.05$ threshold and yet the R^2 value is similar to the highest correlating factor, the difference is likely due to the fact that most of the individual correlation is assigned by the multiple regression analysis to the property with the highest beta

coefficient value; that is, there is a fairly large overlap between the two properties and their correlation with ion intensity. That said, in general, the results agree when beta coefficient significance values are extremely low or high ($p < 0.05$ or $p > 0.12$) where the former predicts the strongest individual correlation and the latter often predicts little to no individual correlation.



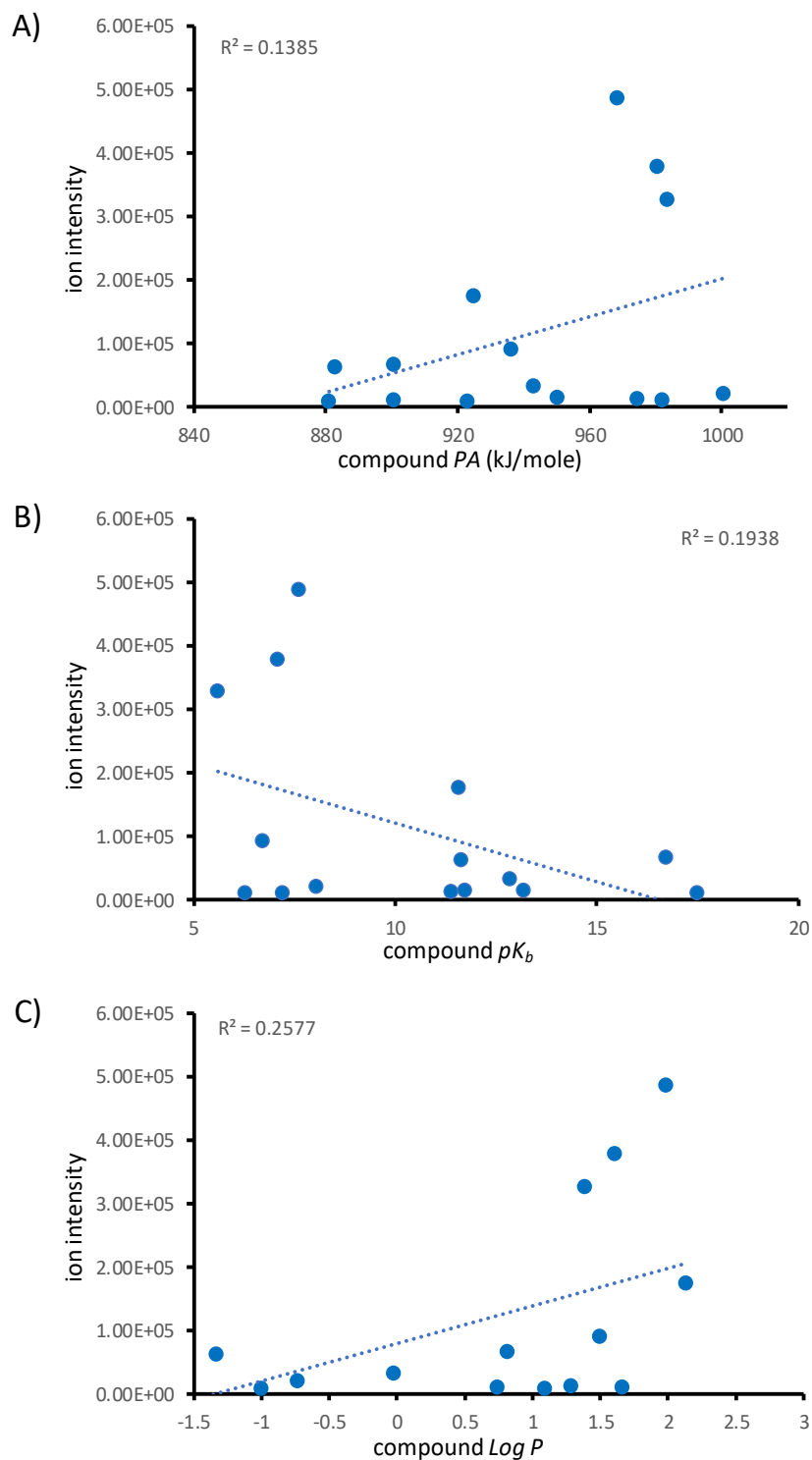


Figure 2- 6 Plots of individual correlations between separate physicochemical property and ion intensity for the voltage-field enabled cVSSI analysis of water samples using blunt-tip emitters. The compounds are numbered according to the method used in Table 1. Shown are the plots of ion intensity versus A) PA, B) pK_b , and C) $\log P$. Linear least-squares best-fit lines are provided as dotted lines and the R^2 value for each is shown in the respective plot.

2.3.4 Orbitrap experiments: physicochemical property associations.

Because the orbitrap mass spectrometer has a larger inlet aperture, it can better sample a diffuse droplet plume produced by voltage-free cVSSI. This enables the use of pulled-tip emitters which were employed for the orbitrap studies (see Experimental section). Molecule-specific ion intensities for the aqueous and methanol experiments employing pulled tip emitters in Orbitrap experiments show in Table 2-5 and 2-6 respectively. Table 2-7 shows the beta coefficient values for each of the physicochemical molecular properties as well as their corresponding significance as obtained from the multiple regression analysis for data obtained on the orbitrap mass spectrometer. For the methanol analyses, the most significant associations with ionization are found to be pK_b , pK_b , and $\log P$ for the voltage-free cVSSI, field-enabled cVSSI, and ESI methods, respectively. Here none meet the threshold of $p < 0.05$; only the voltage-free cVSSI exhibits an approaching significance ($p = 0.058$) for pK_b . This highest significance attributed to pK_b is similar to what was observed for the voltage-free cVSSI analyses of the methanol samples performed on the linear ion trap mass spectrometer (Table 2-4).

Results from multiple regression analyses for the data collected for aqueous samples using the orbitrap mass spectrometer show better agreement with the same data obtained from the linear ion trap mass spectrometer. For example, the most significant correlators with ion intensities are the same for both sets of analyses. Here the factors providing the most significant association for the voltage-free cVSSI, field-enabled cVSSI, and ESI are pK_b , $\log P$, and pK_b , respectively (see Table 2-7). This ordering is identical for the strongest correlating factors from the linear ion trap analyses (see Table 2-4). A notable difference is that, for the ion trap data, the multiple regression analysis also suggests an association for PA in voltage-free cVSSI experiments. That said, the individual correlation is very weak for PA as mentioned above and shown in Figure 2-5.

Table 2- 5 Molecule-specific ion intensities for the aqueous experiments employing pulled-tip emitters.

#	Compound	Water solvent system					
		cVSSI		cVSSI+2KV		ESI	
		[M+H] ⁺	S.D.	[M+H] ⁺	S.D.	[M+H] ⁺	S.D.
1	Thymine	3.68E+04	4.74E+04	6.31E+08	2.25E+07	4.23E+08	2.38E+07
5	4-Methoxybenzamide	1.08E+05	2.64E+04	2.27E+09	4.25E+08	3.13E+07	2.54E+07
6	Cytosine	5.06E+04	8.73E+03	3.08E+08	3.68E+07	3.68E+08	1.68E+07
7	Adenine	6.79E+04	1.06E+04	7.78E+08	5.64E+07	8.79E+08	1.91E+08
8	N-ethylaniline	1.61E+05	8.97E+04	1.37E+09	2.23E+08	1.42E+09	1.65E+08
10	4-Methoxyaniline	2.65E+04	4.48E+03	1.43E+09	1.33E+08	1.00E+09	1.30E+08
11	2-2 bipyridine	4.29E+05	2.37E+05	1.76E+09	6.24E+07	1.58E+09	3.68E+08
12	Methyltriazinaminec	2.12E+05	6.64E+04	2.08E+09	1.55E+08	2.45E+09	6.93E+07
13	Benzylamine	6.19E+05	2.44E+04	1.34E+09	2.00E+08	9.65E+08	1.43E+07
14	Triethanolamine	1.40E+05	4.40E+04	1.15E+09	4.04E+07	1.59E+09	1.15E+07
15	Triethylamine	1.58E+05	8.32E+04	6.68E+08	1.35E+08	4.62E+08	4.53E+07
16	N-methylbenzylamine	7.45E+05	4.24E+05	2.68E+09	3.61E+07	2.65E+09	2.31E+07
17	Quinuclidine	1.13E+06	6.11E+05	2.31E+09	2.52E+07	1.56E+09	2.62E+08
18	N,N-dimethylbenzylamine	6.16E+04	1.53E+04	1.33E+09	8.14E+07	1.54E+09	2.00E+07
19	Phenylethylamine	3.67E+05	7.16E+04	2.66E+09	1.39E+08	2.27E+09	5.47E+08

Table 2- 6 Molecule-specific ion intensities for the methanol experiments employing pulled-tip emitters.

#	Compound	MeOH solvent system					
		cVSSI		cVSSI+2KV		ESI	
		[M+H] ⁺	S.D.	[M+H] ⁺	S.D.	[M+H] ⁺	S.D.
1	Thymine	3.07E+06	1.22E+06	7.68E+08	3.18E+07	7.76E+08	1.98E+07
2	p-Nitroaniline	3.32E+06	3.54E+04	2.38E+09	3.54E+08	2.04E+09	4.95E+07
3	Benzamide	3.94E+06	2.40E+05	3.09E+09	5.66E+07	3.22E+09	1.41E+07
4	Diphenylamine	7.97E+05	5.73E+04	1.53E+09	0.00E+00	1.32E+09	1.48E+08
5	4-Methoxybenzamide	9.99E+06	1.00E+06	3.53E+09	-	4.36E+09	1.06E+08
6	Cytosine	3.10E+06	2.62E+06	1.22E+09	7.07E+06	1.17E+09	2.12E+07
7	Adenine	1.45E+06	1.41E+04	6.22E+08	1.34E+07	7.82E+08	4.95E+06
8	N-ethylaniline	1.03E+06	1.13E+06	2.81E+09	1.13E+08	1.96E+09	3.25E+08
10	4-Methoxyaniline	2.85E+05	2.72E+05	5.56E+08	-	1.03E+09	1.41E+07
11	2-2 bipyridine	1.74E+06	6.36E+04	2.37E+09	8.49E+07	2.20E+09	7.78E+07
12	Methyltriazinaminec	8.73E+06	2.33E+06	6.07E+09	4.95E+07	6.15E+09	5.66E+07
13	Benzylamine	8.56E+06	4.76E+05	2.76E+09	7.07E+06	2.49E+09	3.06E+07
14	Triethanolamine	8.39E+06	2.75E+06	4.34E+09	2.92E+08	4.71E+09	9.90E+07
15	Triethylamine	1.14E+06	1.34E+05	8.66E+08	3.10E+07	6.08E+08	9.07E+06
16	N-methylbenzylamine	2.43E+07	6.43E+05	3.52E+09	7.23E+07	3.05E+09	3.51E+07
17	Quinuclidine	3.54E+07	4.06E+06	4.50E+09	7.20E+08	4.50E+09	8.19E+07
18	N,N-dimethylbenzylamine	3.11E+05	2.27E+05	2.00E+09	2.08E+07	1.35E+09	2.61E+08
19	Phenylethylamine	1.07E+07	1.04E+06	1.49E+09	2.83E+07	2.57E+09	1.17E+08

Table 2- 7 Beta coefficients and the associated significance values for the Q-Exactive experiments

Property ^a	MeOH solvent system			Water solvent system		
	cVSSI ^b	cVSSI+2KV	ESI	cVSSI	cVSSI+2KV	ESI
Pk _b	-0.443(0.058)^c	-0.403(0.119)	-0.334 (0.183)	-0.435(0.043)	-0.235(0.303)	-0.688(0.002)
Log P	-0.029(0.844)	-0.206(0.216)	-0.257(0.123)	0.110(0.467)	0.348(0.035)	-0.0278(0.856)
PA	0.027(0.904)	-0.132(0.595)	-0.196(0.422)	0.028(0.888)	-0.181(0.397)	-0.229(0.242)

The compound-specific values are listed in Table 1 in the Supporting Information section.

^bIonization mode. cVSSI, cVSSI+2kV, and ESI correspond to the voltage-free cVSSI, field-enabled cVSSI, and ESI experiments, respectively. See the Experimental section for more details.

^cBeta coefficients and associated significance values (given parenthetically) for the separate regression analyses. Bolded values represent the most significant results for each experiment. The sign of the coefficient indicates the nature of the correlation (positive versus negative correlation).

2.3.5 Ionization mechanism considerations.

Previous studies have suggested a strong pK_b correlation with ion intensity for these and similar small molecules^{61, 65, 66}. That said, very extensive studies using a large number of compounds has suggested that despite this observed correlation, other factors such as $\log P$ and volatility can also correlate with ionization efficiency depending on factors as varied as solvent pH and the type of mass spectrometer employed for the analysis^{62, 67}. Because the same ionization device types are employed here, perhaps it is not entirely surprising that such a high degree of agreement is obtained for the analyses conducted on the linear ion trap and orbitrap instruments. That said, the observation that the voltage-free cVSSI and field-enabled cVSSI each exhibit different significant associations (compared with each other and with ESI) could indicate differences in the types of droplets produced and ultimately the process responsible for ionization.

Admittedly, the number of molecules studied here is limited and so possible explanations for the observation of the different associations are highly tentative. That said, it is instructive to consider potential explanations for these observations with the acknowledgment that further substantiation of such explanations will require much more extensive experimentation.

It is generally accepted⁶⁸⁻⁷² that ESI of small molecules results in ion production via the ion evaporation mechanism (IEM) first proposed by Iribarne and Thomson⁷³. In summary, ion evaporation occurs as the field produced by the surface charge density of the droplets becomes sufficiently large to overcome forces associated with ion solvation. It has been proposed that this field-induced emission process is highly suited to the ionization of molecules of low pK_b ^{60, 73}. Essentially Coulombic interactions would cause the location of the protonated species to be near the surface of the droplet whereupon further solvent evaporation would produce a field at the surface that is sufficiently large to eject the preformed ion into the gas phase. Indeed, molecular dynamics simulations of the ESI droplet have shown that this Coulomb-driven positioning of ions at the surface can occur very rapidly⁷⁴⁻⁷⁶. Thus, it is not surprising that, for the ESI experiments on the two mass spectrometers, the strongest association with ion intensity is pK_b (see Table 2-4 and Table 2-7). Additionally, this is consistent with what has been observed on other instruments using small-molecule analytes^{60, 62, 66, 77}.

The molecular property associations for the field-free cVSSI are difficult to ascribe to physical processes in part because of the differences observed between the two instruments. For the orbitrap instrument, as with ESI, pK_b is the only significant association for field-free cVSSI (see Table 2-7). For the linear ion trap studies pK_b and PA were both calculated to associate with ion intensity for both water and methanol samples. To present a possible explanation for such a difference it may be necessary to consider another field-free, spray-based ionization process. It

has often been proposed⁷⁷⁻⁷⁹ that ion production from sonic spray ionization (SSI)¹² occurs via the charge residue model (CRM)⁸⁰. This proposal stems from the concept of the statistical charging mechanism responsible for generating the net droplet charge. It has even been suggested that only CRM is operative in SSI due to the comparatively low charge density of the SSI droplets⁷⁸. For field-free cVSSI, it can be argued that charged droplets are produced in a similar manner. Therefore, ions could be formed via the CRM and thus the change in calculated association (i.e., the inclusion of *PA* along with *pK_b* in Table 2-4) results from a change in ionization mechanism. Because, for CRM, analytes remain in the droplet until complete solvent evaporation, ion production could be governed ultimately by the relative proton affinities of the remaining species (solvent versus analyte). Such a solvent-mediated process has been proposed for dictating protein charge state relatively early on⁸¹.

Having described the possibility of ion production via CRM and a potential link to the *PA* association, it is necessary to discuss caveats to the explanation. The first problem is that the *PA* association is only observed for the linear ion trap instrument. As mentioned above, others have noted differences in correlations for ESI performed on different instruments⁶². One explanation for such differences could be related to instrument location (e.g., field and pressure regimes) where the bulk of ion production occurs even to include proposed processes such as IEM in the final stages of CRM⁷⁰. Notably, droplet sizes produced by cVSSI are slightly different (see Experimental section) for the two instruments due to the necessity to produce a denser plume for the linear ion trap which could also affect the location of ion production. The second problem is the negative beta coefficient value for water samples suggesting a negative correlation with *PA*. Comparatively, the single variable correlation with *PA* (Figure 2-4) is one of the weakest observed. The combination of a weak correlation and the limitation that only 3 parameters are tested by the

multiple regression analysis could result in a computational artifact. This could also explain the lack of supporting data for a PA association from the orbitrap instrument. That said, the fact that the ordering of compound ionization is sufficiently different from ESI in the linear ion trap data such that a difference in beta coefficients is obtained as well as the fact that the CRM has been proposed for other field-free ionization techniques suggests that further investigation of ion formation by field-free cVSSI is warranted.

Perhaps the most remarkable (and best supported by separate datasets here) observation is the fact that pK_b decreases in association with ionization for field-enabled cVSSI and $\log P$ increases. It does so in every case (both solvent systems and both mass spectrometers) which serves as supporting evidence for the importance of molecular hydrophobicity in field-enabled cVSSI. The effect is observed more dramatically for the water samples where $\log P$ becomes the only association of statistical significance; simultaneously, pK_b shows essentially no significance on both instruments for the aqueous samples. In ESI, the surface activity of molecules has long been argued to benefit their ionization as more polar species are argued to prefer the core of the droplets whereas more hydrophobic species would locate at the surface^{71, 82-84}. Indeed, a number of models have been developed to account for surface activity⁸⁵⁻⁸⁷ in the ionization of different molecules. The increased ionization of surface-active molecules in ESI would arise from their localization in the droplet as the ions would be more prone to be ejected in the ion-producing progeny droplets as well as their overall decreased solvation energies^{71, 72}. Above we presented the process whereby a preformed ion could be expelled from an ESI droplet readily due to rapid surface positioning by Coulomb forces and expulsion by the same. For field-enabled cVSSI, experiments have shown that very efficient ionization occurs at voltages well below the onset of a Taylor cone and microdroplet production by Coulomb forces⁵². Additionally, these experiments have shown that

field-enabled cVSSI dissipates charge at the emitter tip and thus overcomes the corona discharge problem in negative ion mode analyses. Thus, it can be argued that field-enabled cVSSI produces droplets of net charge that are higher than field-free cVSSI (because of increased ion signal level observations) and yet smaller than ESI (because of charge dissipation and voltage onset observations). The lower charge density could decrease the effect of rapid positioning of the preformed ion at the droplet surface (and thus enrichment to some degree) due to Coulomb repulsion. Additionally, the decreased surface field would affect field-induced ion evaporation events. In this environment, surface activity could provide somewhat more of an advantage to ionization leading to the log P associations obtained for field-enabled cVSSI.

One interesting observation of the log P prominence in field-enabled cVSSI is the sign of the beta coefficients. For water, the beta coefficients are significant, and their sign is positive for both instruments. This can be argued as being somewhat expected as the increased hydrophobicity of the molecules should result in greater surface association and thus ionization as described above. For the methanol samples, although the beta coefficient values are not significant, for both instruments they are negative. This raises the interesting possibility that the hydrophobic molecules have somewhat of a relative preference for droplet retention by the organic solvent compared with the aqueous droplets.

2.4 Continued studies: motivation and future work.

Admittedly, the potential explanations for the ionization results presented above are very cursory. One goal of the studies presented here was to begin to assess the differences in ionization efficiencies for the various techniques. A strong motivation for further study of the ionization process is that a number of fields stand to benefit from the elucidation of factors affecting

ionization by cVSSI. Here two fields are presented as they relate to recent advantages presented by cVSSI. The first area is that of native MS⁸⁸. The relatively recent experiments showing 10 to 100-fold improvement in ionization efficiency for proteins in negative ion mode using cVSSI⁵² could revitalize the study of many acidic proteins. Studies that utilize tandem MS and multistage tandem MS (MSⁿ) where high ion utilization is typically required would be impacted by higher ion signal levels. A second, but related, area is the analysis of small-molecule metabolites in negative ion mode. Studies have suggested a relatively limited sensitivity for compounds such as nucleosides and nucleotides analyzed by LC-MS techniques^{74,75}. Such limitations have led to the development of novel LC-MS approaches to provide high-sensitivity quantification and identification of such compounds⁷⁶. In addition to challenges associated with studying negatively-charged ions for ‘omics analyses, a largely underutilized regime for LC-MS studies is that employing microflow conditions⁸⁹. Such separations are highly robust and more amenable to high-throughput characterization than nanoflow experiments; however, such advantages come at a cost to overall sensitivity. Notably, the prior cVSSI experiments demonstrating enhanced ion signal levels were conducted in the microflow regime and offer the potential to obtain much higher sensitivity.

Although future investigations of factors affecting ionization by cVSSI will be guided by their potential to impact structural and comparative ‘omics fields of study, the first experiments will continue to focus on simple systems such as those presented here. First, a much more expansive group of molecules will be studied using the three different ionization techniques and the two mass spectrometers. This will not only provide higher confidence associations but also allow for the comparison of a greater number of physicochemical properties. The second area of research to be pursued is that of molecular dynamics (MD) simulations. There are three goals for

the initial MD simulations. These are: 1) to provide confirmatory support of the ionization processes proposed above, 2) to determine the effects different counter ions have on the ionization processes, and 3) to outline the role of the solvent in the ionization processes. To obtain confirmatory evidence, exhaustive MD simulations of water nanodroplets with the analyte ions and the appropriate amount of charge carriers and counterions (ionization technique dependent) will be conducted. For example, the number of ion evaporation events will be monitored for each molecule and for each type of modeled experiment (field-free cVSSI, field-enabled cVSSI, and ESI). To address issues of counterions, initial MD simulations will focus on acetate ions as ammonium acetate was used in these experiments to limit the amount of charge carriers (H_3O^+ and MeOH_2^+). Finally, MD simulations will also be conducted using methanol nanodroplets. This is important as the role the solvent plays in the overall ionization process is not well understood. For example, recent work has shown that solvent composition can be tailored to mitigate the effects of surface-active molecules⁸². More recently studies have shown differences in ionization efficiency for fixed-charge organic ions depending on their origin from protic or aprotic solvent systems⁹⁰. Thus a sound understanding of the effects of different solvent systems on the various ionization processes described here could allow the tailoring of cVSSI techniques for specific comparative and structural ‘omics analyses.

2.5 Conclusions

The ion intensities of various small-molecule compounds have been recorded for three different ionization techniques namely voltage-free capillary Vibrating Sharp-edge Spray Ionization (cVSSI), field-enabled cVSSI, and ESI. Experiments have been conducted for samples dissolved in methanol and water to examine ion intensities associated with the different solvent

systems. Multiple regression analysis has been used to determine the degree to which different physicochemical characteristics can be associated with the overall ionization of the small molecules. In general, the log of the base dissociation constant (pK_b) is observed to correlate the most significantly to ESI for both solvent systems. pK_b and gas-phase proton affinity (PA) are associated with the ion intensities of compounds using voltage-free cVSSI for both methanol and aqueous samples while log of the partition coefficient ($\log P$) exhibits the strongest correlation for the field-enabled cVSSI. Currently the data are too limited to fully elucidate ionization mechanism details; however, the differences lay the foundation for future studies as they demonstrate the very real possibility that different mechanisms or combinations of mechanisms exist for the various ionization processes. Additionally, a better understanding of the associations will help in the design of more efficient voltage-free and field-enabled cVSSI sources for mass spectrometry analyses.

2.6 Acknowledgments

Professor Li is grateful for partial support of this work from the National Institutes of Health (R01GM135432). Professor Valentine is grateful for partial support of this work from the National Science Foundation (CHE-1553021). We are grateful for the use of the WVU Shared Resources Facilities and the help of Dr. Callee Walsh and Ms. Sandra Majuta for help running experiments on the orbitrap mass spectrometer.

2.7 References

- (1) Fenn, J. B.; Mann, M.; Meng, C. K.; Wong, S. F.; Whitehouse, C. M. ELECTROSPRAY IONIZATION FOR MASS-SPECTROMETRY OF LARGE BIOMOLECULES. *Science* **1989**, 246 (4926), 64-71. DOI: 10.1126/science.2675315.
- (2) Tanaka, K.; Waki, H.; Ido, Y.; Akita, S.; Yoshida, Y.; Yoshida, T.; Matsuo, T. Protein and polymer analyses up to m/z 100 000 by laser ionization time-of-flight mass spectrometry. *Rapid Communications in Mass Spectrometry* **1988**, 2 (8), 151-153. DOI: 10.1002/rcm.1290020802.
- (3) Karas, M.; Bachmann, D.; Hillenkamp, F. Influence of the Wavelength in High-Irradiance Ultraviolet-Laser Desorption Mass-Spectrometry of Organic-Molecules. *Analytical Chemistry* **1985**, 57 (14), 2935-2939. DOI: DOI 10.1021/ac00291a042.
- (4) Mann, M. Electrospray - Its Potential and Limitations as an Ionization Method for Biomolecules. *Org Mass Spectrom* **1990**, 25 (11), 575-587. DOI: DOI 10.1002/oms.1210251104.
- (5) Smith, R. D.; Loo, J. A.; Loo, R. R. O.; Busman, M.; Udseth, H. R. Principles and practice of electrospray ionization—mass spectrometry for large polypeptides and proteins. *Mass Spectrometry Reviews* **1991**, 10 (5), 359-452. DOI: 10.1002/mas.1280100504.
- (6) Smith, R. D.; Loo, J. A.; Edmonds, C. G.; Barinaga, C. J.; Udseth, H. R. New developments in biochemical mass spectrometry: electrospray ionization. *Anal Chem* **1990**, 62 (9), 882-899. DOI: 10.1021/ac00208a002.
- (7) Covey, T. R.; Bonner, R. F.; Shushan, B. I.; Henion, J. The determination of protein, oligonucleotide and peptide molecular weights by ion-spray mass spectrometry. *Rapid Commun Mass Spectrom* **1988**, 2 (11), 249-256. DOI: 10.1002/rcm.1290021111.
- (8) Laiko, V. V.; Baldwin, M. A.; Burlingame, A. L. Atmospheric pressure matrix-assisted laser desorption/ionization mass spectrometry. *Anal Chem* **2000**, 72 (4), 652-657. DOI: 10.1021/ac990998k.
- (9) Emmett, M. R.; Caprioli, R. M. Micro-electrospray mass spectrometry: Ultra-high-sensitivity analysis of peptides and proteins. *J Am Soc Mass Spectrom* **1994**, 5 (7), 605-613. DOI: 10.1016/1044-0305(94)85001-1.
- (10) Wilm, M.; Mann, M. Analytical properties of the nanoelectrospray ion source. *Anal Chem* **1996**, 68 (1), 1-8. DOI: 10.1021/ac9509519.
- (11) Takats, Z.; Wiseman, J. M.; Gologan, B.; Cooks, R. G. Mass spectrometry sampling under ambient conditions with desorption electrospray ionization. *Science* **2004**, 306 (5695), 471-473. DOI: 10.1126/science.1104404.
- (12) Hirabayashi, A.; Sakairi, M.; Koizumi, H. Sonic spray mass spectrometry. *Anal Chem* **1995**, 67 (17), 2878-2882. DOI: 10.1021/ac00113a023.
- (13) Takats, Z.; Wiseman, J. M.; Gologan, B.; Cooks, R. G. Electrosonic spray ionization. A gentle technique for generating folded proteins and protein complexes in the gas phase and for studying ion-molecule reactions at atmospheric pressure. *Anal Chem* **2004**, 76 (14), 4050-4058. DOI: 10.1021/ac049848m.
- (14) Wang, H.; Liu, J.; Cooks, R. G.; Ouyang, Z. Paper spray for direct analysis of complex mixtures using mass spectrometry. *Angew Chem Int Ed Engl* **2010**, 49 (5), 877-880. DOI: 10.1002/anie.200906314.
- (15) Shiea, J.; Huang, M. Z.; Hsu, H. J.; Lee, C. Y.; Yuan, C. H.; Beech, I.; Sunner, J. Electrospray-assisted laser desorption/ionization mass spectrometry for direct ambient analysis of solids. *Rapid Commun Mass Spectrom* **2005**, 19 (24), 3701-3704. DOI: 10.1002/rcm.2243.

- (16) Sampson, J. S.; Hawkrigde, A. M.; Muddiman, D. C. Generation and detection of multiply-charged peptides and proteins by matrix-assisted laser desorption electrospray ionization (MALDESI) Fourier transform ion cyclotron resonance mass spectrometry. *J Am Soc Mass Spectrom* **2006**, *17* (12), 1712-1716. DOI: 10.1016/j.jasms.2006.08.003.
- (17) Nemes, P.; Vertes, A. Laser ablation electrospray ionization for atmospheric pressure, in vivo, and imaging mass spectrometry. *Anal Chem* **2007**, *79* (21), 8098-8106. DOI: 10.1021/ac071181r.
- (18) Chait, B. T. Chemistry. Mass spectrometry: bottom-up or top-down? *Science* **2006**, *314* (5796), 65-66. DOI: 10.1126/science.1133987.
- (19) Washburn, M. P.; Wolters, D.; Yates, J. R., 3rd. Large-scale analysis of the yeast proteome by multidimensional protein identification technology. *Nat Biotechnol* **2001**, *19* (3), 242-247. DOI: 10.1038/85686.
- (20) Adkins, J. N.; Varnum, S. M.; Auberry, K. J.; Moore, R. J.; Angell, N. H.; Smith, R. D.; Springer, D. L.; Pounds, J. G. Toward a human blood serum proteome: analysis by multidimensional separation coupled with mass spectrometry. *Mol Cell Proteomics* **2002**, *1* (12), 947-955. DOI: 10.1074/mcp.m200066-mcp200.
- (21) Liu, X.; Valentine, S. J.; Plasencia, M. D.; Trimpin, S.; Naylor, S.; Clemmer, D. E. Mapping the human plasma proteome by SCX-LC-IMS-MS. *J Am Soc Mass Spectrom* **2007**, *18* (7), 1249-1264. DOI: 10.1016/j.jasms.2007.04.012.
- (22) Sze, S. K.; Ge, Y.; Oh, H.; McLafferty, F. W. Top-down mass spectrometry of a 29-kDa protein for characterization of any posttranslational modification to within one residue. *Proc Natl Acad Sci U S A* **2002**, *99* (4), 1774-1779. DOI: 10.1073/pnas.251691898.
- (23) Feng, R.; Konishi, Y. Collisionally-Activated Dissociation of Multiply Charged 150-Kda Antibody Ions. *Analytical Chemistry* **1993**, *65* (5), 645-649. DOI: DOI 10.1021/ac00053a027.
- (24) Loo, J. A.; Quinn, J. P.; Ryu, S. I.; Henry, K. D.; Senko, M. W.; McLafferty, F. W. High-resolution tandem mass spectrometry of large biomolecules. *Proc Natl Acad Sci U S A* **1992**, *89* (1), 286-289. DOI: 10.1073/pnas.89.1.286.
- (25) Reid, G. E.; McLuckey, S. A. 'Top down' protein characterization via tandem mass spectrometry. *J Mass Spectrom* **2002**, *37* (7), 663-675. DOI: 10.1002/jms.346.
- (26) Kelleher, N. L. Peer Reviewed: Top-Down Proteomics. *Analytical Chemistry* **2004**, *76* (11), 196 A-203 A. DOI: 10.1021/ac0415657.
- (27) Hyung, S. J.; Ruotolo, B. T. Integrating mass spectrometry of intact protein complexes into structural proteomics. *Proteomics* **2012**, *12* (10), 1547-1564. DOI: 10.1002/pmic.201100520.
- (28) Domon, B.; Broder, S. Implications of new proteomics strategies for biology and medicine. *J Proteome Res* **2004**, *3* (2), 253-260. DOI: 10.1021/pr034082c.
- (29) Petrotchenko, E. V.; Borchers, C. H. Crosslinking combined with mass spectrometry for structural proteomics. *Mass Spectrom Rev* **2010**, *29* (6), 862-876. DOI: 10.1002/mas.20293.
- (30) Hoaglund-Hyzer, C. S.; Counterman, A. E.; Clemmer, D. E. Anhydrous protein ions. *Chem Rev* **1999**, *99* (10), 3037-3080. DOI: 10.1021/cr980139g.
- (31) Zhong, Y.; Hyung, S. J.; Ruotolo, B. T. Ion mobility-mass spectrometry for structural proteomics. *Expert Rev Proteomics* **2012**, *9* (1), 47-58. DOI: 10.1586/epr.11.75.
- (32) Sinz, A. The advancement of chemical cross-linking and mass spectrometry for structural proteomics: from single proteins to protein interaction networks. *Expert Review of Proteomics* **2014**, *11* (6), 733-743. DOI: 10.1586/14789450.2014.960852.
- (33) Xu, G.; Chance, M. R. Hydroxyl radical-mediated modification of proteins as probes for structural proteomics. *Chem Rev* **2007**, *107* (8), 3514-3543. DOI: 10.1021/cr0682047.

- (34) Seeley, E. H.; Caprioli, R. M. Molecular imaging of proteins in tissues by mass spectrometry. *Proc Natl Acad Sci U S A* **2008**, *105* (47), 18126-18131. DOI: 10.1073/pnas.0801374105.
- (35) Ho, Y.-N.; Shu, L.-J.; Yang, Y.-L. Imaging mass spectrometry for metabolites: technical progress, multimodal imaging, and biological interactions. *WIREs Systems Biology and Medicine* **2017**, *9* (5), e1387. DOI: 10.1002/wsbm.1387 (accessed 2020/02/27).
- (36) McDonnell, L. A.; Heeren, R. M. Imaging mass spectrometry. *Mass Spectrom Rev* **2007**, *26* (4), 606-643. DOI: 10.1002/mas.20124.
- (37) Rzagalinski, I.; Volmer, D. A. Quantification of low molecular weight compounds by MALDI imaging mass spectrometry - A tutorial review. *Biochim Biophys Acta Proteins Proteom* **2017**, *1865* (7), 726-739. DOI: 10.1016/j.bbapap.2016.12.011.
- (38) Ellis, S. R.; Brown, S. H.; In Het Panhuis, M.; Blanksby, S. J.; Mitchell, T. W. Surface analysis of lipids by mass spectrometry: more than just imaging. *Prog Lipid Res* **2013**, *52* (4), 329-353. DOI: 10.1016/j.plipres.2013.04.005.
- (39) Seng, P.; Drancourt, M.; Gouriet, F.; La Scola, B.; Fournier, P. E.; Rolain, J. M.; Raoult, D. Ongoing revolution in bacteriology: routine identification of bacteria by matrix-assisted laser desorption ionization time-of-flight mass spectrometry. *Clin Infect Dis* **2009**, *49* (4), 543-551. DOI: 10.1086/600885.
- (40) Seng, P.; Rolain, J.-M.; Fournier, P. E.; La Scola, B.; Drancourt, M.; Raoult, D. MALDI-TOF-mass spectrometry applications in clinical microbiology. *Future Microbiology* **2010**, *5* (11), 1733-1754. DOI: 10.2217/fmb.10.127 (accessed 2020/02/27).
- (41) Carbonnelle, E.; Mesquita, C.; Bille, E.; Day, N.; Dauphin, B.; Beretti, J. L.; Ferroni, A.; Gutmann, L.; Nassif, X. MALDI-TOF mass spectrometry tools for bacterial identification in clinical microbiology laboratory. *Clin Biochem* **2011**, *44* (1), 104-109. DOI: 10.1016/j.clinbiochem.2010.06.017.
- (42) Croxatto, A.; Prod'hom, G.; Greub, G. Applications of MALDI-TOF mass spectrometry in clinical diagnostic microbiology. *FEMS Microbiol Rev* **2012**, *36* (2), 380-407. DOI: 10.1111/j.1574-6976.2011.00298.x.
- (43) McEwen, C. N.; Trimpin, S. An alternative ionization paradigm for atmospheric pressure mass spectrometry: Flying elephants from Trojan horses. *International Journal of Mass Spectrometry* **2011**, *300* (2-3), 167-172. DOI: 10.1016/j.ijms.2010.05.020.
- (44) Trimpin, S.; Inutan, E. D.; Herath, T. N.; McEwen, C. N. Laserspray ionization, a new atmospheric pressure MALDI method for producing highly charged gas-phase ions of peptides and proteins directly from solid solutions. *Mol Cell Proteomics* **2010**, *9* (2), 362-367. DOI: 10.1074/mcp.M900527-MCP200.
- (45) Trimpin, S.; Inutan, E. D. New ionization method for analysis on atmospheric pressure ionization mass spectrometers requiring only vacuum and matrix assistance. *Anal Chem* **2013**, *85* (4), 2005-2009. DOI: 10.1021/ac303717j.
- (46) Pagnotti, V. S.; Chubaty, N. D.; McEwen, C. N. Solvent assisted inlet ionization: an ultrasensitive new liquid introduction ionization method for mass spectrometry. *Anal Chem* **2011**, *83* (11), 3981-3985. DOI: 10.1021/ac200556z.
- (47) Wang, B.; Trimpin, S. High-throughput solvent assisted ionization inlet for use in mass spectrometry. *Anal Chem* **2014**, *86* (2), 1000-1006. DOI: 10.1021/ac400867b.
- (48) Pagnotti, V. S.; Chakrabarty, S.; Wang, B.; Trimpin, S.; McEwen, C. N. Gas-phase ions produced by freezing water or methanol for analysis using mass spectrometry. *Anal Chem* **2014**, *86* (15), 7343-7350. DOI: 10.1021/ac500132j.

- (49) Trimpin, S. Novel ionization processes for use in mass spectrometry: 'Squeezing' nonvolatile analyte ions from crystals and droplets. *Rapid Commun Mass Spectrom* **2019**, *33 Suppl 3*, 96-120. DOI: 10.1002/rcm.8269.
- (50) Li, X.; Attanayake, K.; Valentine, S. J.; Li, P. Vibrating Sharp-edge Spray Ionization (VSSI) for voltage-free direct analysis of samples using mass spectrometry. *Rapid Commun Mass Spectrom* **2018**. DOI: 10.1002/rcm.8232.
- (51) Ranganathan, N.; Li, C.; Suder, T.; Karanji, A. K.; Li, X.; He, Z.; Valentine, S. J.; Li, P. Capillary Vibrating Sharp-Edge Spray Ionization (cVSSI) for Voltage-Free Liquid Chromatography-Mass Spectrometry. *J Am Soc Mass Spectrom* **2019**, *30* (5), 824-831. DOI: 10.1007/s13361-019-02147-0.
- (52) Li, C.; Attanayake, K.; Valentine, S. J.; Li, P. Facile Improvement of Negative Ion Mode Electrospray Ionization Using Capillary Vibrating Sharp-Edge Spray Ionization. *Anal Chem* **2020**, *92* (3), 2492-2502. DOI: 10.1021/acs.analchem.9b03983.
- (53) Cody, R. B.; Laramée, J. A.; Durst, H. D. Versatile new ion source for the analysis of materials in open air under ambient conditions. *Anal Chem* **2005**, *77* (8), 2297-2302. DOI: 10.1021/ac050162j.
- (54) Kolakowski, B. A.; Grossert, J. S.; Ramaley, L. Studies on the positive-ion mass spectra from atmospheric pressure chemical ionization of gases and solvents used in liquid chromatography and direct liquid injection. *Journal of the American Society for Mass Spectrometry* **2004**, *15* (3), 311-324, Article. DOI: 10.1016/j.jasms.2003.10.019.
- (55) Song, L.; You, Y.; Evans-Nguyen, T. Surface Acoustic Wave Nebulization with Atmospheric-Pressure Chemical Ionization for Enhanced Ion Signal. *Anal Chem* **2019**, *91* (1), 912-918. DOI: 10.1021/acs.analchem.8b03927.
- (56) Pol, J.; Kauppila, T. J.; Haapala, M.; Saarela, V.; Franssila, S.; Ketola, R. A.; Kotiaho, T.; Kostianinen, R. Microchip sonic spray ionization. *Anal Chem* **2007**, *79* (9), 3519-3523. DOI: 10.1021/ac070003v.
- (57) Yu, C.; Qian, X.; Chen, Y.; Yu, Q.; Ni, K.; Wang, X. Microfluidic self-aspiration sonic-spray ionization chip with single and dual ionization channels for mass spectrometry. *RSC Advances* **2016**, *6* (55), 50180-50189. DOI: 10.1039/c6ra07959h.
- (58) Narayanan, R.; Sarkar, D.; Cooks, R. G.; Pradeep, T. Molecular ionization from carbon nanotube paper. *Angew Chem Int Ed Engl* **2014**, *53* (23), 5936-5940. DOI: 10.1002/anie.201311053.
- (59) Wlekinski, M.; Li, Y.; Bag, S.; Sarkar, D.; Narayanan, R.; Pradeep, T.; Cooks, R. G. Zero Volt Paper Spray Ionization and Its Mechanism. *Anal Chem* **2015**, *87* (13), 6786-6793. DOI: 10.1021/acs.analchem.5b01225.
- (60) Ehrmann, B. M.; Henriksen, T.; Cech, N. B. Relative importance of basicity in the gas phase and in solution for determining selectivity in electrospray ionization mass spectrometry. *J Am Soc Mass Spectrom* **2008**, *19* (5), 719-728. DOI: 10.1016/j.jasms.2008.01.003.
- (61) Oss, M.; Krueve, A.; Herodes, K.; Leito, I. Electrospray ionization efficiency scale of organic compounds. *Anal Chem* **2010**, *82* (7), 2865-2872. DOI: 10.1021/ac902856t.
- (62) Kiontke, A.; Oliveira-Birkmeier, A.; Opitz, A.; Birkemeyer, C. Electrospray Ionization Efficiency Is Dependent on Different Molecular Descriptors with Respect to Solvent pH and Instrumental Configuration. *PLoS One* **2016**, *11* (12), e0167502. DOI: 10.1371/journal.pone.0167502.
- (63) Liigand, J.; Laaniste, A.; Krueve, A. pH Effects on Electrospray Ionization Efficiency. *J Am Soc Mass Spectrom* **2017**, *28* (3), 461-469. DOI: 10.1007/s13361-016-1563-1.

- (64) *Gaussian 09, Revision E.01*; Gaussian, Inc.: Wallingford CT, 2009. (accessed).
- (65) Cech, N. B.; Enke, C. G. Relating electrospray ionization response to nonpolar character of small peptides. *Anal Chem* **2000**, 72 (13), 2717-2723. DOI: 10.1021/ac9914869.
- (66) Mandra, V. J.; Kouskoura, M. G.; Markopoulou, C. K. Using the partial least squares method to model the electrospray ionization response produced by small pharmaceutical molecules in positive mode. *Rapid Commun Mass Spectrom* **2015**, 29 (18), 1661-1675. DOI: 10.1002/rcm.7263.
- (67) Kiontke, A.; Billig, S.; Birkemeyer, C. Response in Ambient Low Temperature Plasma Ionization Compared to Electrospray and Atmospheric Pressure Chemical Ionization for Mass Spectrometry. *Int J Anal Chem* **2018**, 2018, 5647536. DOI: 10.1155/2018/5647536.
- (68) Gamero-Castaño, M.; Fernandez de la Mora, J. Mechanisms of Electrospray Ionization of Singly and Multiply Charged Salt Clusters. *Analytica Chimica Acta* **2000**, 406, 67-91. DOI: 10.1016/S0003-2670(99)00596-6.
- (69) Znamenskiy, V.; Marginean, I.; Vertes, A. Solvated Ion Evaporation from Charged Water Nanodroplets. *The Journal of Physical Chemistry A* **2003**, 107 (38), 7406-7412. DOI: 10.1021/jp034561z.
- (70) Kebarle, P.; Peschke, M. On the mechanisms by which the charged droplets produced by electrospray lead to gas phase ions. *Analytica Chimica Acta* **2000**, 406 (1), 11-35, Article. DOI: 10.1016/S0003-2670(99)00598-x.
- (71) Kebarle, P.; Verkerk, U. H. ELECTROSPRAY: FROM IONS IN SOLUTION TO IONS IN THE GAS PHASE, WHAT WE KNOW NOW. *Mass Spectrometry Reviews* **2009**, 28 (6), 898-917, Review. DOI: 10.1002/mas.20247.
- (72) Rohner, T. C.; Lion, N.; Girault, H. H. Electrochemical and theoretical aspects of electrospray ionisation. *Physical Chemistry Chemical Physics* **2004**, 6 (12), 3056-3068, Review. DOI: 10.1039/b316836k.
- (73) Iribarne, J. V.; Thomson, B. A. On the evaporation of small ions from charged droplets. *Journal of Chemical Physics* **1976**, 64 (6), 2287-2294, Article. DOI: 10.1063/1.432536.
- (74) Kim, D.; Wagner, N.; Wooding, K.; Clemmer, D. E.; Russell, D. H. Ions from Solution to the Gas Phase: A Molecular Dynamics Simulation of the Structural Evolution of Substance P during Desolvation of Charged Nanodroplets Generated by Electrospray Ionization. *Journal of the American Chemical Society* **2017**, 139 (8), 2981-2988, Article. DOI: 10.1021/jacs.6b10731.
- (75) Kondalaji, S. G.; Khakinejad, M.; Valentine, S. J. Comprehensive Peptide Ion Structure Studies Using Ion Mobility Techniques: Part 3. Relating Solution-Phase to Gas-Phase Structures. *Journal of the American Society for Mass Spectrometry* **2018**, 29 (8), 1665-1677, Article. DOI: 10.1007/s13361-018-1996-9.
- (76) Konermann, L.; Ahadi, E.; Rodriguez, A. D.; Vahidi, S. Unraveling the Mechanism of Electrospray Ionization. *Analytical Chemistry* **2013**, 85 (1), 2-9, Article. DOI: 10.1021/ac302789c.
- (77) Özdemir, A.; Lin, J.-L.; Wang, Y. S.; Chen, C.-H. A deeper look into sonic spray ionization. *RSC Adv.* **2014**, 4 (106), 61290-61297. DOI: 10.1039/c4ra06409g.
- (78) Touboul, D.; Jecklin, M. C.; Zenobi, R. Ion internal energy distributions validate the charge residue model for small molecule ion formation by spray methods. *Rapid Commun Mass Spectrom* **2008**, 22 (7), 1062-1068. DOI: 10.1002/rcm.3469.
- (79) Takats, Z.; Nanita, S. C.; Cooks, R. G.; Schlosser, G.; Vekey, K. Amino acid clusters formed by sonic spray ionization. *Anal Chem* **2003**, 75 (6), 1514-1523. DOI: 10.1021/ac0260793.

- (80) Dole, M.; Mack, L. L.; Hines, R. L. MOLECULAR BEAMS OF MACROIONS. *Journal of Chemical Physics* **1968**, 49 (5), 2240-&, Article. DOI: 10.1063/1.1670391.
- (81) Gross, D. S.; Williams, E. R. EXPERIMENTAL-MEASUREMENT OF COULOMB ENERGY AND INTRINSIC DIELECTRIC POLARIZABILITY OF A MULTIPLY PROTONATED PEPTIDE ION USING ELECTROSPRAY-IONIZATION FOURIER-TRANSFORM MASS-SPECTROMETRY. *Journal of the American Chemical Society* **1995**, 117 (3), 883-890, Article. DOI: 10.1021/ja00108a004.
- (82) Pape, J.; Vikse, K. L.; Janusson, E.; Taylor, N.; McIndoe, J. S. Solvent effects on surface activity of aggregate ions in electrospray ionization. *International Journal of Mass Spectrometry* **2014**, 373, 66-71, Article. DOI: 10.1016/j.ijms.2014.09.009.
- (83) Cech, N. B.; Enke, C. G. Practical implications of some recent studies in electrospray ionization fundamentals. *Mass Spectrometry Reviews* **2001**, 20 (6), 362-387, Review. DOI: 10.1002/mas.10008.
- (84) Kebarle, P. A brief overview of the present status of the mechanisms involved in electrospray mass spectrometry. *Journal of Mass Spectrometry* **2000**, 35 (7), 804-817, Article. DOI: 10.1002/1096-9888(200007)35:7<804::aid-jms22>3.0.co;2-q.
- (85) Zhou, S. L.; Cook, K. D. A mechanistic study of electrospray mass spectrometry: Charge gradients within electrospray droplets and their influence on ion response. *Journal of the American Society for Mass Spectrometry* **2001**, 12 (2), 206-214, Article. DOI: 10.1016/s1044-0305(00)00213-0.
- (86) Tang, L.; Kebarle, P. DEPENDENCE OF ION INTENSITY IN ELECTROSPRAY MASS-SPECTROMETRY ON THE CONCENTRATION OF THE ANALYTES IN THE ELECTROSPRAYED SOLUTION. *Analytical Chemistry* **1993**, 65 (24), 3654-3668, Article. DOI: 10.1021/ac00072a020.
- (87) Enke, C. G. A predictive model for matrix and analyte effects in electrospray ionization of singly-charged ionic analytes. *Analytical Chemistry* **1997**, 69 (23), 4885-4893, Article. DOI: 10.1021/ac970095w.
- (88) van den Heuvel, R. H.; Heck, A. J. R. Native protein mass spectrometry: from intact oligomers to functional machineries. *Current Opinion in Chemical Biology* **2004**, 8 (5), 519-526, Review. DOI: 10.1016/j.cbpa.2004.08.006.
- (89) Bian, Y. Y.; Zheng, R. S.; Bayer, F. P.; Wong, C.; Chang, Y. C.; Meng, C.; Zolg, D. P.; Reinecke, M.; Zecha, J.; Wiechmann, S.; et al. Robust, reproducible and quantitative analysis of thousands of proteomes by micro-flow LC-MS/MS. *Nature Communications* **2020**, 11 (1), 12, Article. DOI: 10.1038/s41467-019-13973-x.
- (90) Omari, I.; Randhawa, P.; Randhawa, J.; Yu, J.; McIndoe, J. S. Structure, Anion, and Solvent Effects on Cation Response in ESI-MS. *J. Am. Soc. Mass Spectrom.* **2019**, 30 (9), 1750-1757, Article. DOI: 10.1007/s13361-019-02252-0.

3 Associating Molecular Physicochemical Properties with Ionization Efficiency for Compounds in Aprotic, Polar Solvent Using Field-free and Field-enabled cVSSI Techniques

3.1 Introduction

Mass spectrometry is one of the most versatile analytical techniques used for characterizing a broad range of samples, providing the mass-to-charge ratios (m/z) for gas-phase ions of various compounds. With the introduction of the soft ionization electrospray ionization (ESI)¹ and matrix-assisted laser desorption ionization (MALDI)² in the 1980s, there was a rapid proliferation of new ionization sources such as atmospheric pressure MALDI³, micro- and nanospray ionization^{4, 5}, desorption electrospray ionization (DESI)⁶, direct analysis in real time (DART)⁷, and atmospheric pressure chemical ionization (APCI)⁸. Due to the high utility of mass spectrometry applications in fields like chemical/biological warfare agent detection, forensic investigation, on-site metabolomics identification, and atmospheric toxic particle detection, the need for miniaturized and field-portable mass spectrometers has arisen^{9, 10, 11, 12, 13}. The need for in-situ and field analyses by MS has coincided with the development of various field-free ionization techniques such as sonic spray ionization (SSI)¹⁴, zero-voltage paper spray ionization (PSI)¹⁵, surface acoustic wave nebulization (SAWN)¹⁶, solvent assisted inlet ionization (SAII)¹⁷ and ultrasonication-assisted spray ionization¹⁸.

Recently, Li and coworkers introduced a new, field-free spray-based ionization technique called vibrating sharp-edge spray ionization (VSSI)¹⁹. This unique ion source only requires a vibrating substrate containing a sharp edge. When a liquid sample is placed at the edge of a vibrating microscope slide and a RF voltage is applied to an attached piezoelectric transducer, the

vibrating (~100 kHz) substrate produces a plume of micrometer-sized droplets emanating from the sharp tip of the slide. In the initial work, it VSSI has been shown to produce ESI-like ions even though no external electric field was utilized. The later addition of a capillary segment/tip to the glass slide presented another form for a sharp edge for efficient introduction of a sample-infused plume to a mass spectrometer inlet; this has been termed capillary vibrating sharp-edge spray ionization (cVSSI)²⁰. Finally, the application of a DC voltage to the solution infused through a cVSSI device (field-enabled cVSSI) provided an enhanced means of ion production. Remarkably, a ~10 to 100-fold ion signal enhancement in MS analyses in negative ion mode compared to ESI has been demonstrated²¹. Modest improvements (typically 5-fold) have also been observed for positive ion mode experiments. That said, because cVSSI can be conducted without the application of a voltage to the solution, the generated plume may exhibit some similarities to droplets produced by SSI, SAIL, SAWN, and Zv-PSI. That said, it is here stressed that the plume generated by VSSI and cVSSI results from a unique, mechanical vibration process that provides advantages with regard to ease of on-line coupling, robust function over a wide range of infused flow rates, and reduced footprint due to very low power requirements. The very fact that such differences exist could suggest that the droplet plume produced by VSSI and cVSSI has unique characteristics that can be exploited/tailored for MS analyses.

Over the years, much research effort has been expended to improve the ionization efficiency of new spray-based ionization techniques for MS analyses. For example, the use of heated transfer tubes and bath gas facilitated ion desolvation in SAIL and droplet-assisted inlet ionization^{7 22}. The advantages of using a carbon nanotube (CNT)-impregnated paper surface in field-free PSI²³ and incorporating microchips and microfluidics chips in sonic spray ionization to enhance ionization efficiency have also been shown^{24 25}. One area of research that has lagged in

field-free ion source studies has been the determination of the roles of analyte physicochemical properties on the overall ionization efficiency as well as ionization effects resulting from different solvent systems. Because of the potential for field-free ionization sources in the various fields mentioned above, the research gap should be filled with robust studies seeking to elucidate such roles for these techniques.

Over the years, several large-scale studies have sought to correlate specific physicochemical properties with ionization efficiency by ESI^{26 27 28 29 30 31}. Here, studies show that the log of the base dissociation constant (pK_b) significantly correlated with the ionization efficiency in small molecule analysis.^{27 29} Other studies have shown that different solvent conditions such as pH, polarity, and volatility influence ion signal levels in ESI.^{30 31} In an early study, Kebarle and coworkers reported that the high methanol content in a mixture of water and methanol gave rise to an enhancement in signal intensity of cocaine ions produced by ESI.³² In separate studies it was shown that by increasing the volume ratio of organic solvent in methanol/water and acetonitrile/water systems incremental changes in ion intensities of organic compounds could be achieved; as a general comparison, the optimum ion intensities for acetonitrile/water solvents were observed at lower proportions of organic component than for the methanol solvent system.³³ A similar observation was observed by Schneider *et al.* where it was found that the ion current was suppressed when 100% acetonitrile was used as the mobile phase in condensed-phase separations.³⁴ In contrast, Takayama and coworkers showed that when amino acids were examined in negative ion mode under different solvent compositions of methanol and acetonitrile, higher ion signals were obtained with higher acetonitrile content.³⁵ They proposed this may be due to a lower vaporization enthalpy for acetonitrile compared to methanol. In summary, these studies suggest that increased ion signal intensity is due to an increase in the

production efficiency of small droplets during the ESI process accomplished by a decrease in the surface tension and vaporization enthalpy of the solution system.

Another novel, voltage-free ionization technique employing a vibration tip has shown that increasing the methanol content to 100% in a water/methanol buffer system resulted in a significant ion signal enhancement compared to lower methanol content solutions.³⁶ Thus, the solvent effect on ionization efficiency differ between high voltage ionization techniques like ESI and voltage-free techniques. Such differences are also altered based on the voltage polarity (positive or negative) utilized in experiments. It is therefore important to compare the solvent effects for small molecules for different ionization techniques (high voltage and field-free) are in both positive and negative mode. To highlight the importance of such studies, consider that the new knowledge will be beneficial for LC/MS studies allowing the selection of the optimum solvent conditions when coupling to different ionization techniques.

The facile manner with which a DC voltage can be coupled with cVSSI make it an ideal source to perform studies seeking to understand the effects of solvent composition and molecular properties on ionization efficiency. Here, the same emitter tip can be used for voltage-free cVSSI, field-enabled cVSSI, and capillary ESI without introducing confounding factors such as a nebulization gas as is associated with current state-of-the-art ESI sources. Indeed, prior work explored the association of three molecular properties (proton affinity, solution base dissociation constant, and polarity) with ion intensities for compounds analyzed by field-free and field-enabled cVSSI.³⁷ The results were compared with ESI using the same flow rates and emitter tips.

The work reported here extends the study of ion formation by cVSSI techniques to include the new solvent systems of acetonitrile as well as acetonitrile:water (95:5). The work focuses on the influence of the aprotic environment on ionization efficiency in both positive and negative ion

mode. A motivation for this study is the fact that acetonitrile is used extensively in condensed-phase separations (e.g., HILIC and reversed-phase LC) employed in metabolomics analyses. Correlation studies involving the physiochemical properties $\log pK_b$, $\log P$, and proton affinity (PA) and ion intensity have been conducted in both positive and negative ion mode. These experiments were conducted using voltage-free cVSSI, field-enabled cVSSI, and ESI. Notable differences are observed compared to the prior work examining protic solvent systems (water and methanol). Here, pK_b less frequently correlates with ionization efficiency even when employing a DC voltage. Additionally, differences are observed in positive ion mode compared to negative ion mode; for example, for the former, both $\log P$ and PA appear to be most associated with ionization efficiency while for negative ion mode, the primary association is PA. The results are discussed with regard operational ionization mechanisms under different solvent compositions and electric field conditions.

3.2 Experimental

3.2.1 Ionization device fabrication.

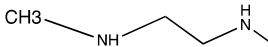
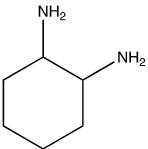
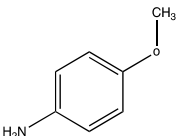
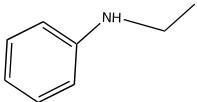
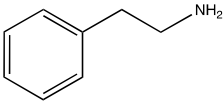
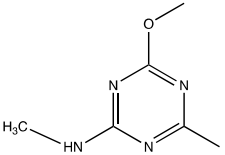
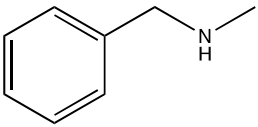
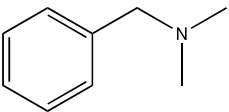
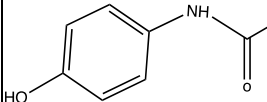
Pulled-tip capillary emitters were obtained using a laser puller (Sutter Instrument Co, Model P-2000, Novato CA, USA) and fused silica (100 μm ID \times 360 μm ID). Emitter tip diameters were examined by microscope to ensure that the tip sizes were ~ 25 to $30 \mu\text{m}$. Previous work demonstrated that droplet size distribution under field-free cVSSI for aqueous solutions is $17.5 \pm 5.6 \mu\text{m}^{20}$. cVSSI and ESI devices were fabricated as described previously³⁷. The VSSI devices were constructed by attaching a piezoelectric transducer (Murata) to a microscope glass slide using epoxy-based superglue (Devcon). Pulled emitter tips were glued to each microscope slide at the distal end using an angle of $\sim 60^\circ$. The sample solutions were infused through a syringe

connected to PTFE tubing. The opposite end of the PTFE tubing was slip fit over the cVSSI emitter. In field-enabled cVSSI and ESI, high voltage was supplied to the solvent by connecting to a Pt wire that punctured into the PTFE tubing near the emitter tip connection.

3.2.2 Reagents and Sample Preparation

For the experiments described here, 18 compounds for positive ion mode and 14 compounds for negative ion mode studies were used. Many of the compounds overlapped with those used in the previous study examining the physiochemical properties correlation in the polar, protic solvents of methanol and water. The compounds N-ethylaniline, cimetidine, phenylethylamine, acetaminophen, N-N dimethylethyldiamine, 4-methoxyaniline, N-N dimethylbenzylamine, atropine, methyltriazinamine c, 4-aminobenzoic acid, metronidazole, DADLE, N-methylbenzylamine, 3-aminopyridine, tetracine, trans 1,2 diaminocyclohexane, alpha-ketoglutaric acid, 2-4 dimethylphenol, phenol, p-cresol, benzoic acid, pentachlorophenol, MCPA, dichloropropanol, captopril, acetylsalicylic acid, and 4-nitrophenol were purchased from Thermo Fisher Scientific (Pittsburgh, PA, USA) and used without further purification. Tables 3-1 and 3-2 in show the structures of the compounds and their molecular weights, $\log P$, pK_b , and PA values. The majority of the PA values were obtained from the NIST Chemistry WebBook; for the compounds not included on the NIST website, PA values were calculated using the Gaussian 09 software suite. pK_a values in acetonitrile were computed using the empirical conversion proposed previously.³⁸ Stock solutions of each compound were prepared by dissolving 1 mg of each compound in 1 ml of solvent. Two different solvent systems were investigated, neat acetonitrile and a solvent mixture of acetonitrile and water in a 95:5 ratio (95% acetonitrile).

Table 3- 1 Structures and physicochemical property values for the compounds used in the positive mode ionization experiment.

#	Compound	Structure	pKa		pKb (CH ₃ CN)	logP	PA (kJ/mol)	MW
			Water	CH ₃ CN				
1	N,N dimethylethyldiamine		9.48	11.71	20.49	-0.60	937.4	88.15
2	Trans-1,2-Diaminocyclohexane		9.9	17.69	14.51	-0.008	973.5	114.19
3	4-methoxyaniline		5.36	12.16	20.04	0.74	900.3	123.15
4	N-ethylaniline		4.91	11.71	20.49	2.13	924.8	121.14
5	Phenylethylamine		9.79	17.49	14.71	1.49	936.2	121.18
6	Methyltriazinamine c		4.87	12.57	19.63	-1.34	882.7	154.17
7	N-methylbenzylamine		9.41	17.31	14.89	1.6	980.4	121.80
8	N-N-dimethylbenzylamine		8.9	17.75	14.45	1.98	968.4	135.17
9	Acetaminophen		-4.4	2.4	29.8	0.907	824.1	151.17

. Table 3- 1 To continued

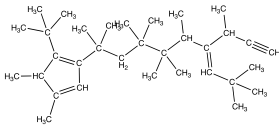
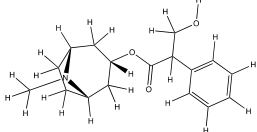
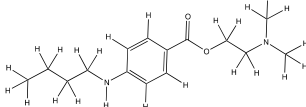
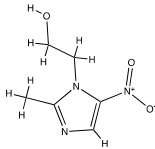
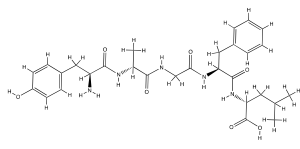
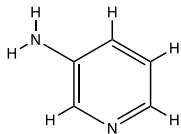
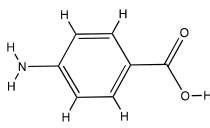
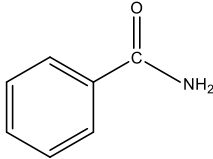
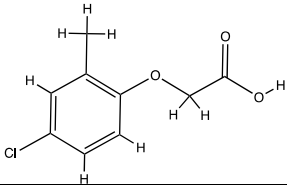
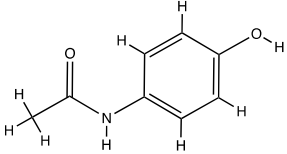
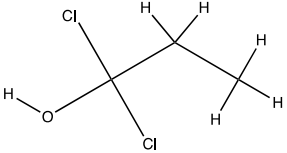
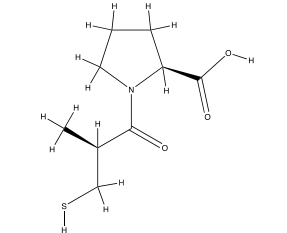
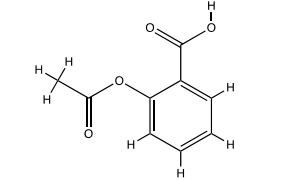
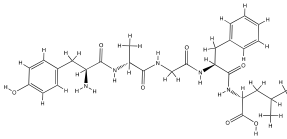
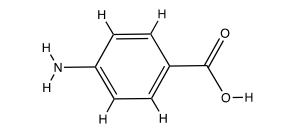
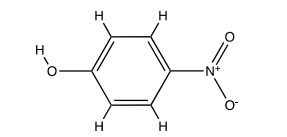
#	Compound	Structure	pKa Water	pKa CH ₃ CN	pKb (CH ₃ CN)	logP	PA (kJ/mol)
10	Cimetidine		6.91	13.51	18.69	- 0.109	992.5
11	Atropine		9.39	17.69	14.51	1.57	1002.1
12	Tetracaine		8.42	16.72	15.48	2.80	1024.4
13	Metronidazole		3.03	17.23	14.97	-0.46	886.9
14	DADLE		7.73	15.43	16.77	-1.30	1008.6
15	3-aminopyridine		5.75	13.45	18.75	-0.07	957.6
16	4-aminobenzoic acid		2.69	9.49	22.71	0.80	834.5
17	Benzamide		-1.2	-	-	0.74	892.1

Table 3- 2 Structures and physicochemical property values for the compounds used in the negative mode ionization experiment.

#	Compound	Structure	pKa		logP	PA (kJ/mol)
			Water	CH ₃ CN		
1	alpha-ketoglutaric		2.66	18.16	-0.10	1355.78
2	2,4-dimethylphenol		10.71	27.01	2.4	1448.24
3	Pentachlorophenol		4.98	21.38	4.69	1316.37
4	phenol		10.02	26.32	1.48	1432.65
5	p-cresol		10.36	26.66	1.94	1439.48
6	benzoic acid		4.08	19.58	1.89	1411.05

#	Compound	Structure	pKa		logP	PA (kJ/mol)
			Water	CH ₃ CN		
7	MCPA		3.36	18.86	2.49	1373.64
8	acetaminophen		9.46	25.76	0.90	1400.93
9	Dichloropropanol		2.95	18.45	3.07	1376.90
10	captopril		4.02	19.52	0.72	1373.18
11	acetylsalicylic acid		3.41	18.91	1.23	1372.95
12	DADLE		3.70	19.2	-1.3	1342.43
13	4-aminobenzoic acid		4.77	20.27	0.80	1431.87
14	4-nitrophenol		7.07	23.37	1.61	1341.69

3.2.3 Mass Spectrometry Data Collection.

The experiments were carried out on an Orbitrap mass spectrometer (Q Exactive, ThermoFisher). The commercial ionization source was removed from the mass spectrometer, and the system software was externally triggered. The cVSSI device was placed directly in front of the MS inlet at a distance of ~1 cm throughout the data collection. Data were collected under field-free cVSSI, field-enabled cVSSI, and ESI conditions. For the two cVSSI conditions, the glass slide was vibrated using an RF voltage of ~10 V_{pp} at a frequency of ~92 to 94 kHz (square wave). In both field-enabled cVSSI and ESI, a DC voltage of ±2 kV was utilized. Separate experiments were carried out with different sets of molecules for positive ion mode and negative ion mode experiments on the mass spectrometer. The temperature of the ion transfer tube was maintained at 275 °C for all experiments. Data were collected for 30 s over a mass-to-charge ratio (*m/z*) range of 50-750.

3.2.4 Data Analysis.

For all comparisons, ion signal intensities were obtained for each compound using the Xcalibur software suite (ThermoFisher). Linear regression was performed using the Excel software suite (Microsoft, Redmond, CA) for single parameter correlations of peak intensity versus physiochemical property of the molecules. The *R*² values of each separate analysis were compared. Multiple regression analysis was performed using the regression IBM SPSS Statistics 25 software suite using each analyte's peak intensity and physicochemical properties. In multiple regression analysis, the three physicochemical properties mentioned above were designated as independent variables and peak intensities were designated as the dependent variables. Each property's relative association with the degree of ionization (ion intensity) was compared using the beta coefficient

values from the multiple regression analysis. The coefficients and their associated significances are listed in Table 3-3 and 3-4 for each ionization mode and solvent system.

Table 3- 3 Beta coefficients and the associated significance values for the positive mode.

Property ^a	Neat acetonitrile (positive mode)			95% acetonitrile (positive mode)		
	cVSSI ^b	cVSSI+2KV	ESI	cVSSI	cVSSI+2KV	ESI
pk _b	-0.175(0.235) ^c	0.166 (0.395)	0.235 (0.235)	-0.163 (0.340)	0.107(0.582)	0.264(0.146)
logP	0.235 (< 0.001)	-0.319 (0.024)	-0.387(0.004)	0.434(< 0.001)	-0.215(0.117)	-0.278(0.031)
PA	0.269 (0.073)	0.519 (0.011)	0.639 (< 0.001)	0.257(0.257)	0.539(0.008)	0.721(< 0.001)

Table 3- 4 Beta coefficients and the associated significance values for the negative mode.

Properties	Neat acetonitrile (negative mode)			95% acetonitrile (negative mode)		
	cVSSI	cVSSI+2KV	ESI	cVSSI	cVSSI+2KV	ESI
pk _b	0.525(0.001)	0.352(0.031)	0.243(0.161)	0.070(0.630)	-0.295(0.082)	-0.388(0.021)
logP	-0.066(0.605)	0.071(0.585)	0.128(0.364)	0.587(< 0.001)	0.317(0.025)	0.230(0.060)
PA	-0.791(< 0.001)	-0.759(< 0.001)	-0.625(< 0.001)	-0.527(< 0.001)	-0.388(0.019)	-0.766(< 0.001)

^aPhysicochemical property for the different compounds. The compound-specific values are listed in Table 3-1 and 3-2

^bIonization mode. cVSSI, cVSSI+2kV, and ESI correspond to the Field-free cVSSI, Field-enabled cVSSI, and ESI experiments, respectively. See the Experimental section for more details.

^cBeta coefficients and associated significance values (given parenthetically) for the separate regression analyses. Bolded values represent the most significant results for each experiment. The sign of the coefficient indicates the nature of the correlation (positive versus negative correlation).

3.3 Results and Discussion

3.3.1 Relative ion intensities for compounds in neat acetonitrile using positive ion mode.

A total of 18 compounds have been examined for ion production from acetonitrile solutions. Here, field-free cVSSI as described previously³⁷ has been used initially to examine the relative ion signal levels produced in this operational mode. Figure 3-1 and Table 3-5 show the ion intensity levels for the different compounds. Overall, when voltage-free cVSSI is employed in positive ion mode, the ion signal intensity values span a relatively wide range ($\sim 10^6$ to 10^8). Notably, the minimum and maximum value of this range is significantly greater than that obtained ($\sim 10^4$ to 10^5) in the prior studies for compounds in water solutions examined by field-free cVSSI. Additionally, the magnitude of the range is also moderately greater than that obtained for methanol studies ($\sim 10^5$ to 10^7). For the prior studies, the same solution flow rates, pulled-tip emitter sizes, distance to the mass spectrometer inlet, and instrumentation settings were used as described in the Materials and Methods section above. Admittedly, not all of the compounds are the same as those examined by water and methanol; however, there are 7 compounds that are the same and a similar diversity in terms of pK_b , $\log P$, and PA is captured in the 18 compounds studied here.

Upon applying a voltage to the infused acetonitrile samples while vibrating the cVSSI device (field-enabled cVSSI), the average ion signal intensities decreased slightly for most compounds (Figure 3-1). Exceptions to this observation are N-Ndimethylethyldiamine, benzamide, and metronidazole. When the vibration of the emitter tip is subsequently stopped (ESI only), a total of seven compounds show significantly decreased ion intensity levels while four exhibit increased ion signal levels (Figure 3-1). The six remaining compounds exhibit similar levels (field-enabled cVSSI versus ESI) of ion production. From the previous work, when methanol and water solutions were used under applied voltage conditions (field-enabled cVSSI

and ESI), the same analyte compounds (4-methoxyaniline, N-ethylaniline, phenylethylamine, Methyltriazinamine c, N-methylbenzylamine, N-N-dimethylbenzylamine) have shown greater ion signal levels ($\sim 10^2$ on average) compared to the neat acetonitrile solvent system.

In summary, for positive ion mode analyses by field-free cVSSI of compounds in the polar, aprotic solvent acetonitrile, significant enhancements in ionization are observed when compared with results from polar protic solvents. Additionally, with the application of a DC voltage to the solution, notable changes in ion intensities are observed depending upon whether or not the emitter tip undergoes vibration. In comparison to the polar, protic solvents examined in the prior work, the ion intensity levels here are relatively depressed for both field-enabled cVSSI and ESI.

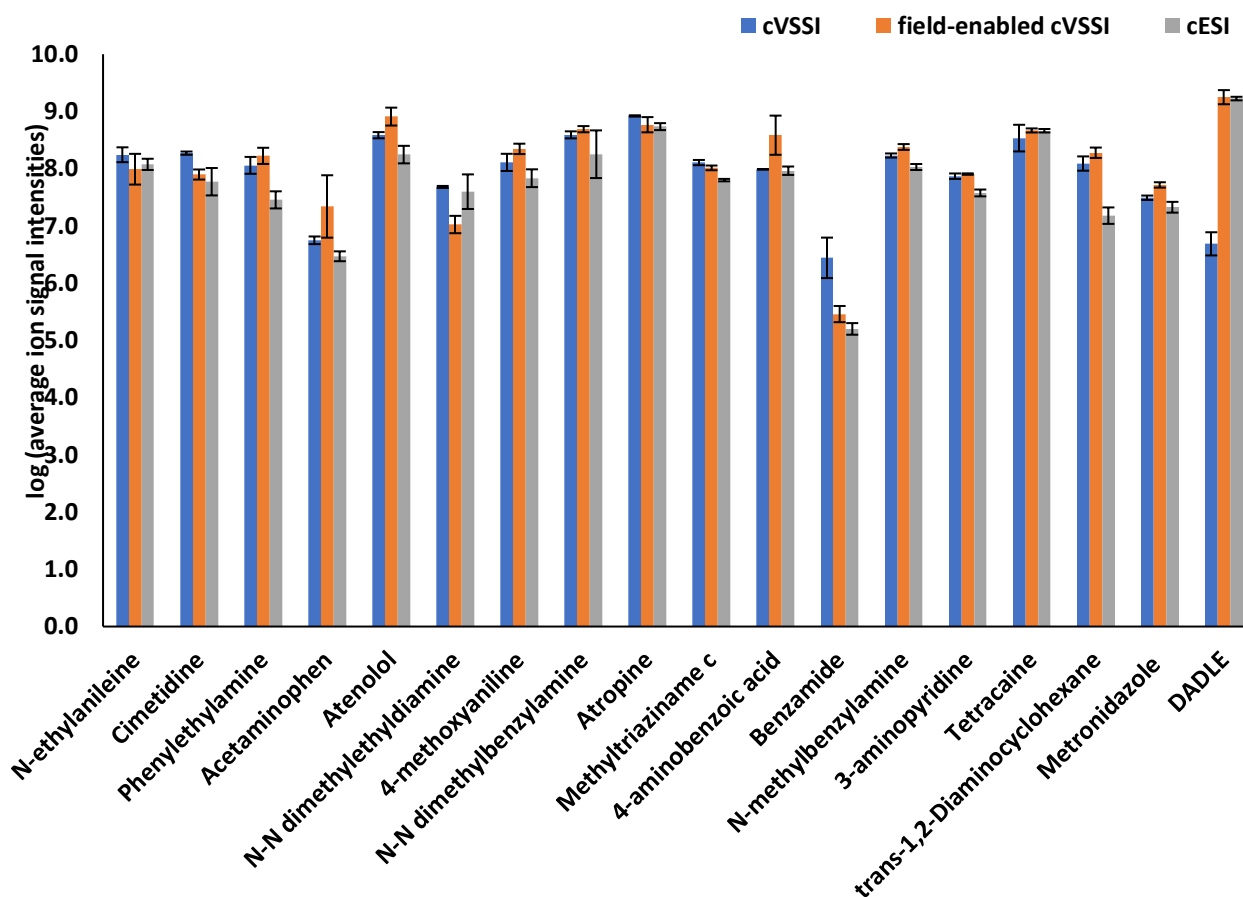


Figure 3- 1 Bar diagram log of the ion signal intensities of each analyte molecule in 95% acetonitrile under positive mode Field-free cVSSI, Field-enabled cVSSI, ESI.

Bar diagram log of the ion signal intensities of each analyte molecule in 95% acetonitrile under positive mode Field-free cVSSI, Field-enabled cVSSI, ESI.

Table 3- 5 Molecule-specific ion intensities for the neat acetonitrile in positive mode analysis

#	Compound	Neat acetonitrile solvent system					
		cVSSI		cVSSI+2KV		ESI	
		[M+H] ⁺	S.D.	[M+H] ⁺	S.D.	[M+H] ⁺	S.D.
1	N,N dimethylethyldiamine	1.53E+06	2.62E+05	2.05E+06	5.26E+05	4.65E+05	1.42E+05
2	Trans-1,2-Diaminocyclohexane	8.11E+07	5.20E+06	6.23E+07	2.81E+06	6.09E+07	7.09E+05
3	4-methoxyaniline	4.74E+07	2.36E+07	3.35E+07	3.96E+07	1.46E+07	3.69E+06
4	N-ethylaniline	1.22E+08	1.59E+07	3.48E+07	1.19E+07	1.11E+07	1.78E+06
5	Phenylethylamine	9.55E+07	5.61E+06	1.23E+07	3.08E+06	1.61E+07	1.22E+06
6	Methyltriazinamine c	8.64E+07	3.48E+07	3.66E+07	2.31E+07	3.19E+07	1.65E+07
7	N-methylbenzylamine	1.38E+08	7.57E+06	2.91E+07	1.93E+07	8.21E+07	3.90E+07
8	N-N-dimethylbenzylamine	4.33E+08	2.62E+05	2.05E+06	5.26E+05	4.65E+05	1.42E+05
9	Benzamide	4.32E+06	2.15E+06	6.40E+06	5.44E+06	2.22E+06	1.91E+06
10	Acetaminophen	5.68E+06	7.73E+05	1.09E+06	4.48E+07	1.18E+06	2.33E+05
11	Cimetidine	1.48E+08	3.92E+07	6.11E+07	7.04E+07	1.88E+07	3.38E+06
12	Atropine	4.91E+08	2.15E+08	1.79E+08	7.66E+07	1.82E+08	4.66E+07
13	Tetracaine	4.60E+08	1.31E+08	2.71E+08	1.36E+08	3.26E+08	1.50E+07
14	Metronidazole	4.86E+07	1.16E+07	8.75E+07	7.59E+08	4.92E+07	3.60E+06
15	DADLE	5.49E+06	1.09E+06	1.16E+09	1.01E+09	1.89E+09	1.76E+08
16	3-aminopyridine	4.77E+07	1.01E+07	2.63E+07	5.85E+07	2.80E+07	2.92E+06
17	4-aminobenzoic acid	1.48E+08	5.12E+07	8.89E+07	2.25E+07	7.40E+07	1.85E+06
18	Atenolol	5.46E+08	2.20E+07	3.39E+08	6.58E+07	1.23E+08	7.64E+06

3.3.2 Relative ion intensities for compounds in acetonitrile (ACN):water (95:5) solutions using positive ion mode.

Having noted that ion production is enhanced for polar protic solvent systems upon the application of voltage, experiments have been designed to examine the effect of a small addition of such solvent to the acetonitrile solution. To investigate the effect of increased protic solvent content on the ion signal levels, the same set of analyte compounds have been examined using an ACN:water (95:5) solvent system. All other instrumentation and data collection parameters are identical to those described for the neat acetonitrile experiments. Figure 3-2 and Table 3-6 shows the different ion intensity values obtained for the various compounds that are sprayed from this solution composition. In general, for field-free cVSSI, the ion intensity values do not change significantly (compared with neat ACN) ranging between 10^6 and 10^8 . Notable exceptions are N-N dimethylethyldiamine and benzamide where a significant increase and a decrease, respectively, are observed. Remarkably, the general ordering of ion intensities is preserved between the two different sample solution sets for field-free cVSSI.

The application of voltage to the ACN:water solution (Figure 3-2) generally results in increased ion intensity levels (compared with neat ACN in Figure 3-1) for many compounds. This is consistent with the increased ionization observed for identical compounds in water solution that occurs with the application of voltage³⁷. A notable exception is benzamide where the ion intensity levels decrease significantly for both field-enabled cVSSI and ESI.

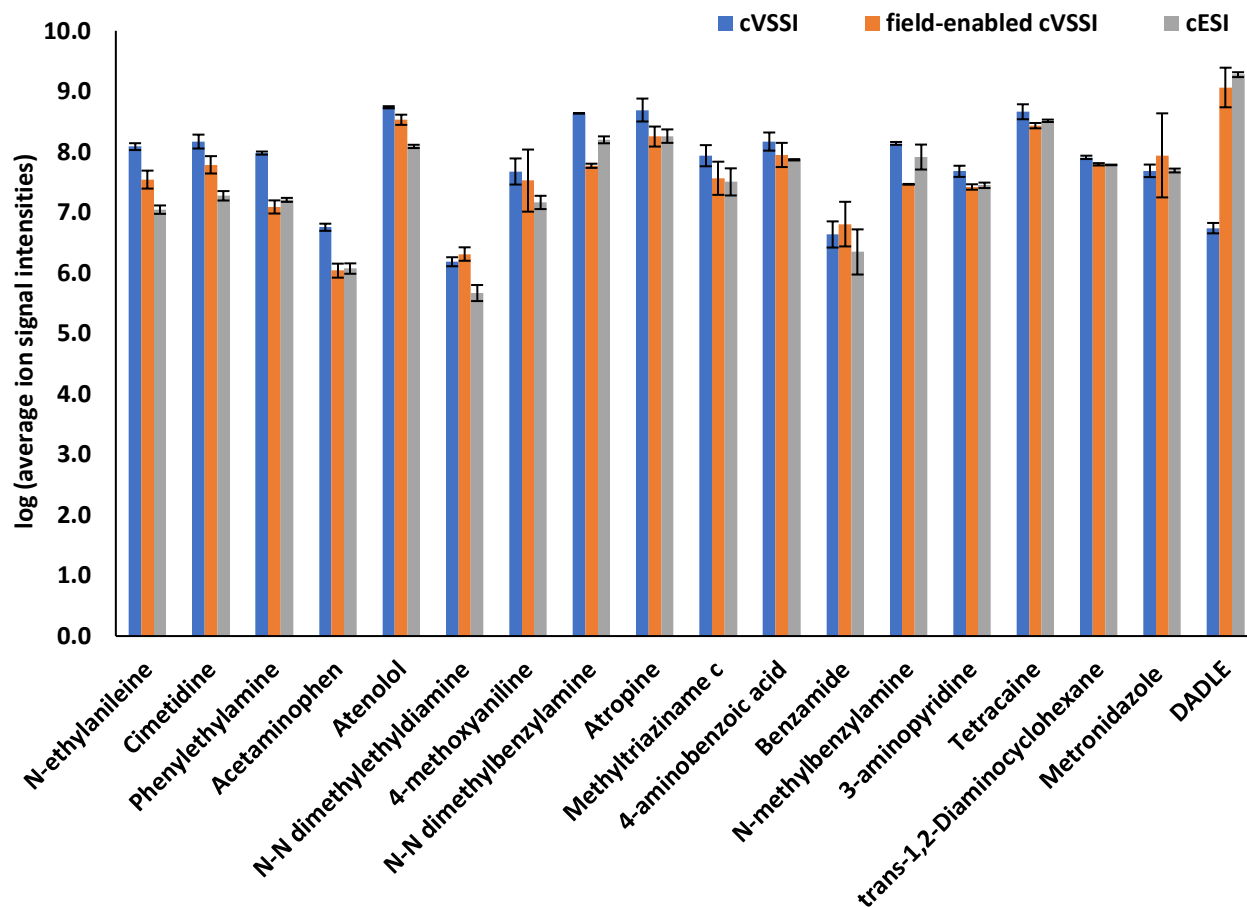


Figure 3- 2 Bar diagram log of the ion signal intensities of each analyte molecule in 95% acetonitrile under positive mode Field-free cVSSI, Field-enabled cVSSI,ESI.

Blue bars represent Field-free cVSSI, orange bars represent Field-enabled cVSSI and grey bars re represent Field-enabled cVSSI and grey bars represents cESI. Error bars represent relative error of one standard deviation about the mean.

Table 3- 6.Molecule-specific ion intensities for the 95% acetonitrile in positive mode analysis.

#	Compound	95% acetonitrile solvent system					
		cVSSI		cVSSI+2KV		ESI	
		[M+H] ⁺	S.D.	[M+H] ⁺	S.D.	[M+H] ⁺	S.D.
1	N,N dimethylethyldiamine	4.80E+07	1.93E+06	1.06E+07	3.70E+06	3.97E+07	2.76E+07
2	Trans-1,2-Diaminocyclohexane	1.23E+08	3.54E+07	1.90E+08	3.96E+07	1.51E+07	5.00E+06
3	4-methoxyaniline	1.29E+08	4.46E+07	2.22E+08	4.63E+07	6.82E+07	2.44E+07
4	N-ethylaniline	1.75E+08	5.24E+07	9.79E+07	6.06E+07	1.19E+08	2.69E+07
5	Phenylethylamine	1.14E+08	3.89E+07	1.68E+08	5.46E+07	2.85E+07	9.83E+06
6	Methyltriazinamine c	1.28E+08	1.35E+07	1.03E+08	9.81E+06	6.32E+07	3.11E+06
7	N-methylbenzylamine	1.70E+08	1.40E+07	2.40E+08	2.77E+07	1.07E+08	1.29E+07
8	N-N-dimethylbenzylamine	3.90E+08	5.52E+07	4.90E+08	6.10E+07	1.79E+08	1.72E+08
9	Benzamide	2.77E+06	2.25E+06	2.88E+05	9.40E+04	1.59E+05	3.71E+04
10	Acteaminophen	5.61E+06	8.64E+05	2.19E+07	2.75E+07	2.95E+06	5.86E+05
11	Cimetidine	1.87E+08	1.22E+07	7.91E+07	1.60E+07	5.92E+07	3.27E+07
12	Atropine	8.36E+08	2.15E+07	5.87E+08	1.80E+08	5.43E+08	7.63E+07
13	Tetracaine	3.42E+08	1.84E+08	4.66E+08	3.82E+07	4.60E+08	3.25E+07
14	Metronidazole	3.11E+07	2.75E+06	5.20E+07	5.61E+06	2.12E+07	4.60E+06
15	DADLE	4.86E+06	2.27E+06	1.78E+09	5.05E+08	1.68E+09	1.20E+08
16	3-aminopyridine	7.40E+07	8.16E+06	8.05E+07	2.29E+06	3.77E+07	5.16E+06
17	4-aminobenzoic acid	9.74E+07	4.95E+05	3.85E+08	3.04E+08	9.22E+07	1.56E+07
18	Atenolol	3.85E+08	4.82E+07	8.14E+08	2.93E+08	1.76E+08	6.22E+07

3.3.3 Relative ion intensities for compounds in neat acetonitrile using negative ion mode.

A total of 15 compounds have been examined for ion production from ACN solution in the negative ion mode studies. When field-free cVSSI is used to ionize the analyte molecules dissolved in neat ACN, the ion signal intensity values ranged between $\sim 10^{2.5}$ and $\sim 10^6$ as shown in Figure 3-3 and Table 3-7. These values represent the lowest ionization efficiency recorded for the acetonitrile studies presented here. In short, these varied compounds do not efficiently produce negatively charged ions from ACN solutions.

Upon utilizing the field-enabled conditions, ion signals are increased significantly (within the range of $\sim 10^6$ to 10^{10}) for both field-enabled cVSSI and ESI. Here it is noted that this behavior is exactly opposed to that observed in positive ion mode (Figure 3-1). In the positive ion mode studies, the field-free cVSSI generally provided the greatest ion production. In this case, the difference is more pronounced as multiple compounds exhibit $>10^3$ fold difference in ion intensity with the application of the DC voltage. Additionally, the ion intensities for field-enabled cVSSI and ESI are similar for most compounds and thus the same general ordering of ionization efficiency is preserved between the two methods (Figure 3-3). Notably, greater variability in ionization efficiency was observed for these two ionization methods in positive ion mode (Figure 3-1).

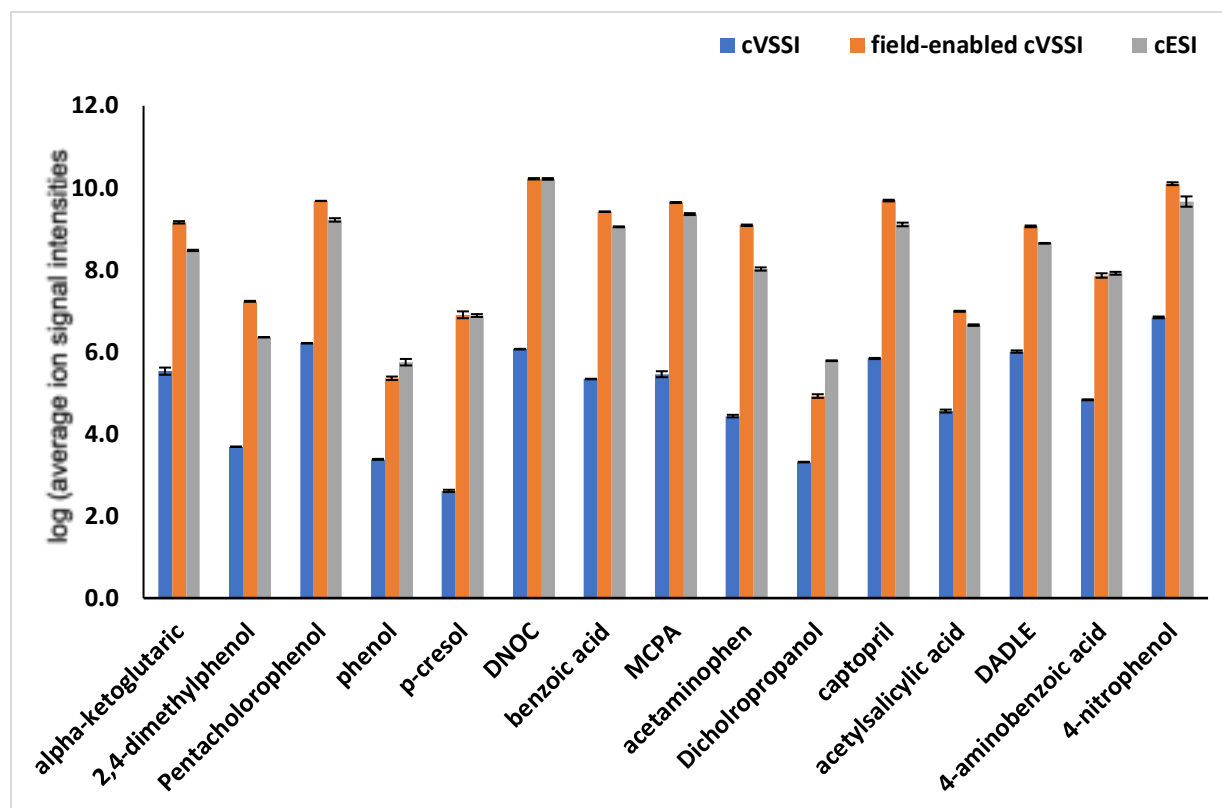


Figure 3- 3. Bar diagram log of the ion signal intensities of each analyte molecule in 95% acetonitrile under positive mode Field-free cVSSI, Field-enabled cVSSI, ESI. Blue bars represent Field-free cVSSI, orange bars represent Field-enabled cVSSI and grey bars represent relative error of one standard deviation about the mean.

Table 3- 7 Molecule-specific ion intensities for the neat acetonitrile in negative mode analysis.

#	Compound	Neat acetonitrile solvent system					
		cVSSI		cVSSI+2KV		ESI	
		[M-H] ⁻	S.D.	[M-H] ⁻	S.D.	[M-H] ⁻	S.D.
1	alpha-ketoglutaric	3.40E+05	1.18E+05	1.44E+09	1.63E+08	2.98E+08	1.91E+07
2	2,4-dimethylphenol	4.89E+03	3.54E+01	1.71E+07	8.08E+05	2.28E+06	1.53E+04
3	Pentachlorophenol	1.63E+06	4.73E+04	4.79E+09	5.77E+07	1.65E+09	2.80E+08
4	phenol	2.41E+03	1.08E+02	2.28E+05	3.87E+04	5.62E+05	1.79E+05
5	p-cresol	4.10E+02	4.58E+01	8.04E+06	2.67E+06	7.71E+06	1.06E+06
6	DNOC	1.17E+06	7.27E+08	1.66E+10	1.08E+09	1.65E+10	1.31E+09
7	benzoic acid	2.19E+05	5.51E+03	2.62E+09	7.57E+07	1.12E+09	4.93E+07
8	MCPA	2.86E+05	8.34E+04	4.38E+09	2.11E+08	2.29E+09	2.15E+08
9	acetaminophen	2.73E+04	3.46E+03	1.22E+09	8.74E+07	1.05E+08	1.65E+07
10	Dichloropropanol	2.07E+03	6.43E+01	8.41E+04	1.48E+04	6.10E+05	2.31E+04
11	captopril	6.92E+05	3.91E+04	4.89E+09	3.91E+08	1.28E+09	2.29E+08
12	acetylsalicylic acid	3.62E+04	5.23E+03	9.79E+06	4.64E+05	4.51E+06	3.30E+05
13	DADLE	1.02E+06	1.17E+05	1.15E+09	9.54E+07	4.44E+08	1.63E+07
14	4-aminobenzoic acid	6.81E+04	3.23E+03	7.29E+07	1.57E+07	8.26E+07	1.16E+07
15	4-nitrophenol	6.95E+06	5.98E+05	1.26E+10	1.74E+09	4.62E+09	2.32E+09

3.3.4 Relative ion intensities for compounds in acetonitrile (ACN): water (95:5) solutionnegative ion mode.

When the 15 compounds used for negative ion mode studies are examined in an ACN solution containing 5% water, ionization efficiency for field-free cVSSI remains the lowest of the three techniques as shown in Figure 3-4 and Table 3-8. That is, the two methods employing a DC voltage provide the greatest ion signal levels. Notably, for field-free cVSSI only one compound shows a truly significant change; pentachlorophenol ion signal increases by nearly 3 decades. With the application of voltage, the ion signal levels are also similar to those observed for the neat ACN studies. One exception is the ion signal level obtained for acetylsalicylic acid where an increase of at least 2 decades is obtained for the 5% water solution (Figure 3-4).

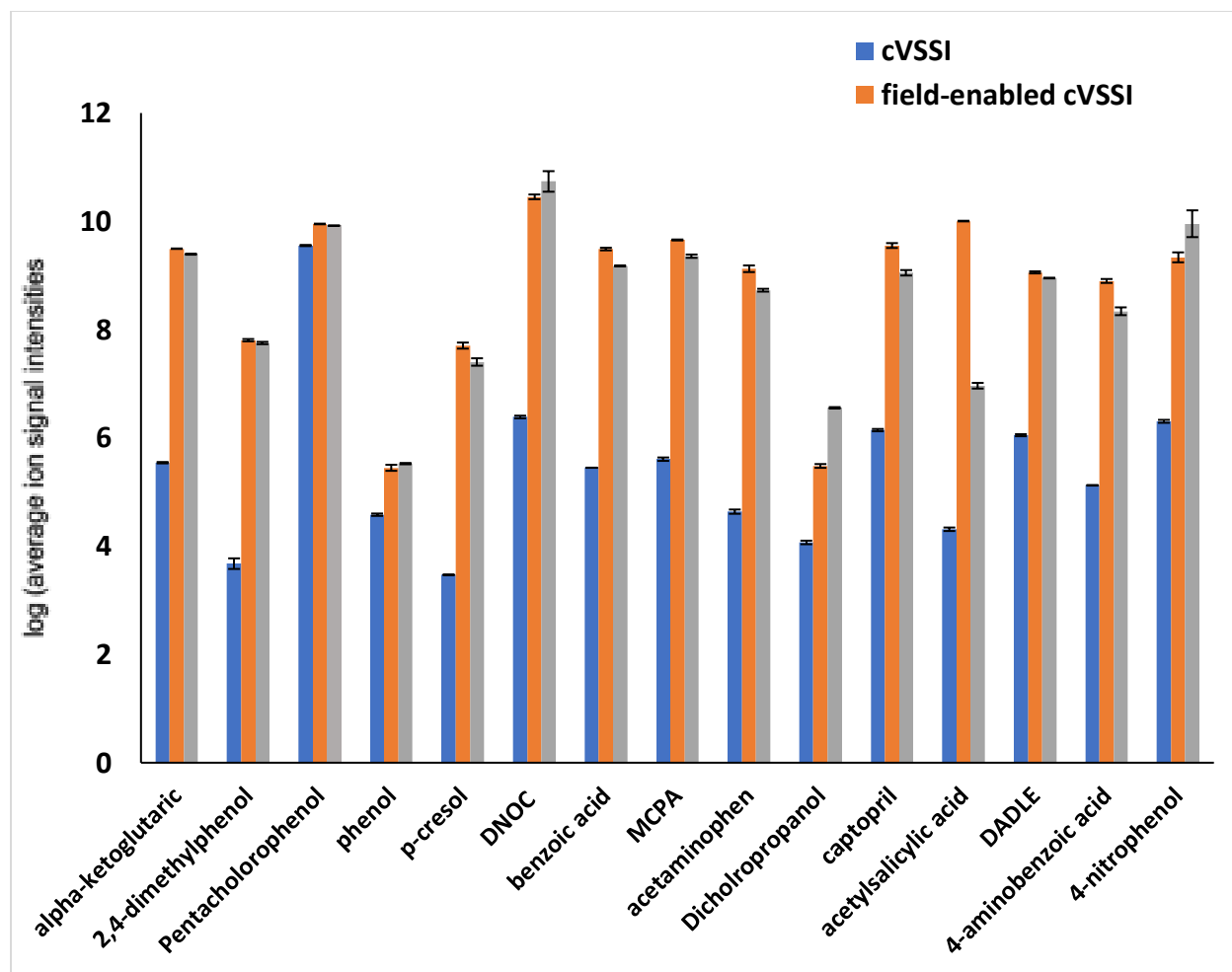


Figure 3- 4. Bar diagram log of the ion signal intensities of each analyte molecule in 95% acetonitrile under positive mode Field-free cVSSI, Field-enabled cVSSI, ESI. Blue bars represent Field-free cVSSI, orange bars represent Field-enabled cVSSI and grey bars represent Field-enabled cVSSI and grey bars represent relative error of one standard deviation about the mean.

Table 3- 8 Molecule-specific ion intensities for the 95% acetonitrile in negative mode analysis.

#	Compound	95% acetonitrile solvent system					
		cVSSI		cVSSI+2KV		ESI	
		[M-H] ⁻	S.D.	[M-H] ⁻	S.D.	[M-H] ⁻	S.D.
1	alpha-ketoglutaric	3.48E+05	1.75E+04	3.12E+09	5.20E+07	2.47E+09	9.02E+07
2	2,4-dimethylphenol	4.75E+03	1.86E+03	6.37E+07	5.51E+06	5.65E+07	4.90E+06
3	Pentachlorophenol	3.57E+09	1.51E+08	8.93E+09	2.19E+08	8.31E+09	8.62E+07
4	phenol	3.81E+04	3.30E+03	2.80E+05	6.27E+04	3.34E+05	1.61E+04
5	p-cresol	2.95E+03	6.36E+01	5.06E+07	1.13E+07	2.52E+07	6.88E+06
6	DNOC	2.43E+06	2.35E+05	2.83E+10	4.95E+09	5.45E+10	4.13E+10
7	benzoic acid	2.81E+05	1.73E+03	3.07E+09	2.95E+08	1.50E+09	5.77E+07
8	MCPA	4.04E+05	5.06E+04	4.52E+09	1.63E+08	2.27E+09	2.77E+08
10	acetaminophen	4.34E+04	6.83E+03	1.33E+09	3.27E+08	5.34E+08	5.53E+07
11	Dichloropropanol	1.17E+04	1.54E+03	3.03E+05	4.22E+04	3.59E+06	1.83E+05
12	captopril	1.39E+06	1.19E+05	3.57E+09	6.40E+08	1.12E+09	2.23E+08
13	acetylsalicylic acid	2.05E+04	2.64E+03	1.01E+10	2.38E+08	9.19E+06	1.93E+06
14	DADLE	1.12E+06	8.50E+04	1.14E+09	8.72E+07	8.95E+08	2.34E+07
15	4-aminobenzoic acid	1.33E+05	2.65E+03	7.91E+08	1.14E+08	2.18E+08	6.26E+07
16	4-nitrophenol	2.02E+06	2.19E+05	2.16E+09	7.94E+08	9.02E+09	8.90E+09

3.3.5 Associating molecular physicochemical property with ion intensity in positive ion mode studies.

It is instructive to consider the relationship of different physicochemical properties of analyte molecules and ion signal levels. Such efforts may be useful to obtain information about operative ionization mechanisms for the various techniques. Multiple regression analysis examines the correlations between ion signal levels (e.g., Figures 3-1 to 3-4) and the three distinct physiochemical molecular properties, pK_b , $\log p$, and PA . Table 3-3 and Table 3-4 show the beta coefficient values for each of the properties and their corresponding significance from the multiple regression analysis for data obtained from the samples in neat and 95% ACN, respectively.

For the experiments in which neat ACN solutions were used, no significant ($p < 0.05$) associations are observed with compound pK_b . This stands in stark contrast to the prior work in which pK_b correlated the most frequently for water and methanol solutions³⁷. For neat ACN, $\log P$ exhibits a significant correlation for all three ion source types. However, it is directly and indirectly correlated for field-free and applied voltage conditions, respectively. For the same solution, the largest significant correlation exists for PA for the experiments in which an electric field is utilized; for field-free cVSSI, this correlation is just outside the confidence interval ($p = 0.073$, Table 3-3). This is also very different than the prior results for methanol and water where the pulled-tip emitter studies showed no significant correlation with PA for all three ionization sources.

3.3.6 Associating molecular physicochemical property with ion intensity in negative ion mode studies.

Having noted the differences between molecular property correlations with intensity between the protic and aprotic solvent systems, it is useful to determine whether or not unusual behavior is observed when producing negatively-charged droplets. As indicated above, expanding the knowledge of factors contributing to negative ion production of different molecules by the various techniques could hold tremendous value for many different experiments. For example, consider ‘omics experiments in which quantitative determinations of nucleotides, carbohydrates, and fatty acids are desired. That is, the new knowledge from molecular property correlations could help to tailor ion source type (e.g., field-free cVSS) and solvent system to targeted compound analyses.

When the solvent is neat ACN, the largest correlating factor of significance is PA for all three ionization sources. In every case (field-free and field-enabled), PA is inversely correlated with ion intensity. In contrast to positive ion mode studies, no significant correlation is obtained for $\log P$. Another deviation from the positive ion mode data is the observation of significant correlations with pK_b for both field-free and field-enabled cVSSI. These are both direct correlations.

When the solvent is ACN:water (95:5), the largest correlations of significance are also observed for PA . Also, as observed for neat ACN, these are inverse correlations. One difference when compared to the neat ACN is that $\log P$ is observed to provide significant correlation for field-free and field-enabled cVSSI but not for ESI. Finally, pK_b is observed to correlate in an inverse manner for ESI.

3.3.7 Ionization process considerations.

Field-induced ionization processes like ESI have long shown strong correlations between pK_b and ion intensity for small molecules examined from polar, protic solvents like water and methanol.^{29 26, 39} Several extensive studies have shown that other molecular properties such as log P and volatility of the analyte molecules can also correlate with ionization efficiency.^{30 40} Because so little is known about ionization from aprotic polar solvents, the studies reported here were pursued with the goal of determining the operative ionization processes for different source types. Above, the molecular property correlations with ionization efficiency for analytes in a polar, aprotic solvent were reported as well as the determination of how those correlations are subject to change upon adding an incremental amount of a polar, protic solvent (water) to the solutions. A question arises as to whether or not such correlations shed light on the type of ionization processes occurring for the different combinations of solvent system and ion source type. This is examined below.

It is widely accepted that the ionization of small molecules by ESI occurs via the ion evaporation mechanism (IEM) proposed by Iribarne and Thomson.^{41 42 43 44 45} In IEM, when the field created by surface charge density on a droplet is sufficient to overcome forces associated with ion solvation, an analyte ion will be released to the gas phase environment.⁴⁶ Work performed by various research groups shows that the field-induced emission process is more efficient for the ionization of molecules having low pK_b (preformed ions in solution).^{27 47} This occurs as columbic interactions within the droplet cause the protonated species to locate near the droplet's surface. As further solvent evaporation events occur, a sufficiently strong field is formed to eject such preformed ions into the gas phase. So, this process is considered to be the primary method for ESI ion production of small molecules in protic solvent media. Additionally, it has been proposed that

field-free ionization sources such as SSI produce ions via the charge residue model (CRM)⁴⁸ of ion production;¹⁴ here, molecules are retained in the droplets until the last vestiges of solvent desorb and charge is transferred to the analyte. Hence, in the absence of a protic solvent medium, analyte molecules may undergo different protonation processes and/or different methods of release into the gas phase.

Apart from pK_b , the influence of surface activity or hydrophobicity of the molecules has been shown to correlate with small-molecule ion signal intensities in ESI when analytes were sprayed from aqueous media.^{39 49 47 50} That said, Cech and coworkers reported that when the small molecules are sprayed from organic solvent like methanol there is no direct correlation between $\log P$ and ion signal intensity.²⁷ Consistent with this work was the prior cVSSI studies in which no significant association of $\log P$ and ion signal level was obtained for ESI of methanol solutions³⁷. Hence, the influence of molecule surface activity can be different depending on the solvent properties.

A remarkable feature of the work reported here is that even in the absence of a protic agent (neat ACN) both protonated and deprotonated ions are readily formed even in the absence of an applied voltage. One explanation could be that the residual (~0.05%) water in neat ACN may serve directly to produce H_3O^+ protonating reagent within the droplet. Another explanation can be extracted from the results of previous studies where the protonation of different molecules under ESI was not expected. Fenselau and coworkers detected protonated proteins upon being electrosprayed from highly basic (pH=10) solutions; there the solution basicity was adjusted using ammonia.⁵¹ Wang and Cole reported protonation of peptides and small proteins in very basic solvent conditions and named this phenomenon as the “wrong-way-round” method.⁵² Boyd and co-workers have shown strong protonation incidents for smaller analytes like amino acids similar

to that reported for the “wrong-way-round” method⁵³ Zhou and Cook observed protonated caffeine from strong basic (ammonia) solutions and suggested this might result from an electric discharge-induced ionization process emanating from the ESI tip similar to atmospheric pressure chemical ionization (APCI). They suggested that this processes could account for much of the established “wrong-way-round” processes.⁵⁴

Having established that ionization processes can lead to ion formation that is not intuitive, it is instructive to consider the correlations in Tables 3-3 and 3-4 to consider this unusual ion formation by cVSSI. For positive ion production by field-free cVSSI (Table 3-3), the strongest correlating factor is $\log P$. Here it may be argued that, in the absence of high charge density at the droplet surface, the more surface-active molecules will locate at the interface with the apolar gas-phase environment and are thus released from the droplet more readily. Comparatively, with the addition of voltage, the increased droplet surface charge would favor more polar species (or at least be less discriminating against). This may account for the inverse correlation with $\log P$ for field-enabled cVSSI and ESI (Table 3-3). Additionally, PA becomes the greatest correlating factor.

To consider why PA could be a factor in field-free ionization, it is instructive to further consider ion production using a “wrong-way-round” protonation process as proposed by Kobarle and Ho.^{55 56} It was suggested that, because the basic solutions were made with ammonia and NH_4^+ ions, the latter must be the major charge carriers on the droplet surface. They also suggest that multiple NH_4^+ ions could protonate the protein in a manner similar to proton transfer reaction in the gas phase. In this scenario, when analyte molecules such as proteins undergo the CRM, protonation may be expected to happen at the end stage as the last solvent components leave the protein-containing droplet. Similarly, protonation may occur for ions that go through the IEM

when the analyte desorbs from the surface and represents a stronger base in the gas phase than NH_3 .

Although the above explanation, is consistent with the observation that *PA* correlates strongly with ion signal level for field-free cVSSI (Table 3-3), there exists an alternate scenario for gas-phase proton transfer. Boyd and co-workers have presented somewhat contradictory results. When basic amino acids like histidine were electrosprayed in a non-protic (tetramethylammonium hydroxide) basic solution, protonated amino acids, although unexpected, were observed.⁵³ For these types of scenarios, when there is not an abundant proton source in the solution phase, a discharged-induced ionization process may be possible as a result of the high voltage applied to the ESI tip.⁵⁴ Here, protonated solvent clusters would be generated in the gas phase similar to that described in the mechanism for atmospheric pressure chemical ionization (APCI) initiating from ambient species such as N_2 and O_2 . These protonated solvent clusters would then serve as reagent ions and undergo proton transfer reaction in the gas phase as explained by Kebarle and Ho. Notably, the introduction of the droplet plume produced by cVSSI into an electrical discharge region termed cVSSI-APCI, shows remarkable ionization efficiency⁵⁷. In the absence of a high electric field, alpha-particle irradiation of moist air can occur⁵⁸. Additionally, gamma irradiation can account for the production of ions which initiate the cascade responsible for production of protonated solvent clusters. Therefore, the above-mentioned discharged-induced ionization can be operative even with the field-free cVSSI technique.

When the water solvent is added to the ACN, the correlating factors remain relatively the same for positive ion mode (Table 3-3). A direct correlation between $\log P$ and ion intensity is observed with field-free cVSSI. This shifts to an inverse correlation for $\log P$ and the largest correlation for *PA* when a DC voltage is used for the other two ionization sources. Thus, it can be

argued that molecule/ion release from the droplet and protonation is similar to that observed for positive ion production from neat ACN. That is, 5% water is not sufficient to shift the ion process to the solution (pre-formed ions) as was observed in the prior cVSSI studies³⁷.

It should be noted that the strongest association of ion intensity with log *P* for field-free cVSSI does not necessarily indicate that ions are produced via IEM. The earlier cVSSI work employing polar, protic solvent systems found that when there is not a sufficient electric field at the droplet surface to overcome the activation barrier, molecules will undergo ionization by the CRM similar to that proposed for sonic spray ionization³⁷. In end stages of CRM, the evaporating droplet will experience several fission events upon reaching the Rayleigh limit and will end with complete solvent evaporation and charge transfer to the analyte ion. It has been argued that even when CRM is the operative mechanism, under certain conditions, surface-active ions will be more favorably transferred to the smaller fission droplets, which will eventually allow their release to the gas-phase environment after complete solvent evaporation. So, a positive correlation with log *P* does not necessarily suggest that molecules in high organic content solvents and examined by field-free cVSSI cannot undergo CRM. Said differently, unlike in polar protic solvents (water and methanol), a correlation of log *P* with ion intensity might be more readily expected for field-free cVSSI even as the CRM is the operative process of ion production. Here the vicinity of the analyte to “protic agents” like H₃O⁺ (generated from residual water) at the surface would facilitate ionization in the end stages of the droplet. For field-enabled conditions (field-enabled cVSSI and ESI) the shift in correlation with log *P* (direct to inverse) and *PA* provide some evidence for the IEM under wrong-way-round conditions as being the operative process.

In negative ion mode, the first correlations with pK_b are observed for the field-free cVSSI studies of neat ACN solutions (Table 3-4). Notably, these correlations are direct suggesting

increased ionization for more acidic species as may be expected for negatively-charged ions. Thus it may be possible that there is sufficient residual water in neat ACN to produce some pre-formed ions. Admittedly, this is a relatively limited sample (15 compounds) and if only a few of these showed the ability to exist as pre-formed ions, this could shift the correlation as shown in Table 3-4. The strongest correlating factor for the neat ACN solutions for all three ionization sources is *PA*. Here, in contrast to positive ion mode studies, the correlations are inverse relationships. This is consistent with gas-phase deprotonation events as being the operative process. That said, as indicated in the discussion for the positive ion mode studies, such proton-transfer events could occur at the droplet surface or via reaction with gas-phase reagent ions. In negative ion mode, basic gas-phase species like OH^- or methoxide ion are possible as a result of electric discharge.⁵⁹
⁶⁰ ⁵⁴ Additionally, it is noted that electrical breakdown is more readily observed at lower voltages for negative voltages and thus could argue for an APCI-like process being the primary mode upon application of voltage (field-enabled cVSSI and ESI).

When the solvent system became more protic (5% water) in nature an observed shift in the dominant correlations was observed (Table 3-4). For example, the ionization efficiency of all three ion modes shifted towards $\log P$ and *PA*. For ESI the $\log P$ correlation did not quite reach the confidence limits ($p = 0.06$). That said, it is essential to point out that the $\log P$ correlation for all three ionization techniques is positive, unlike that observed for the positive ion mode. Takayama and coworkers also reported a positive hydrophobicity correlation of amino acids dissolved in acetonitrile solvent systems under negative ion mode analysis.³⁵ This disparity between negative and positive mode $\log P$ correlation shows there could be an influence resulting from dielectric nature of the solvent with regard to positively- or negatively-charged analyte ions. Additionally, according to the IEM model proposed by Iribiane and Thomson, the rate of ion evaporation from

the droplet depends on the solvation-free energy of the analyte and the surface electric field around the charged droplet.^{46 61} Therefore, the lower dielectric nature of ACN versus water could influence the free energy of solvation of anionic/ or cationic analytes differently.

3.3.8 Ion signal enhancement in field-free cVSSI in positive ion mode.

A remarkable finding of the present work is the increase in average ion signal level obtained for 12 of the 17 compounds in positive ion mode when field-free cVSSI is employed compared to voltage-enabled techniques (Figure 3-1). Indeed, prior experimental and interpretive theoretical work suggests that solvents with lower surface tension and lower enthalpy of vaporization (surface tension; acetonitrile = 30 N/m water = 72 N/m, vaporization enthalpy; acetonitrile = 33 kJ/mol water = 44 kJ/mol) should more readily produce ions via the CRM.^{62 ,61} The positive ion studies presented here support this idea of highly efficient droplet drying for ACN.

A question then arises as to why the production of ions in negative ion mode is so suppressed for field-free cVSSI (Figure 3-3). That is, if droplet drying is so efficient for compounds in ACN, why are so few ions produced in negative ion mode? A possible answer to this question can be formulated when considering the production of negatively-charged ions by the field-enabled sources. Here, ion production is remarkably efficient as the upper range in ion signal level is higher by nearly an order of magnitude compared to the generation of ions by field-enabled sources in positive ion mode. As it is largely indicated by the multiple regression analysis, ions are produced by gas-phase proton transfer either at the droplet surface or via reagent ions. Because, electrical breakdown occurs at a lower negative bias compared with positive voltage, it can be argued that a much greater number of reagent ions may be produced for gas-phase proton transfer reactions. As it is assumed that the CRM is operative for field-free cVSSI in both positive

and negative ion mode (see discussion above), it would also be argued that the final transfer of charge during the droplet drying process was more efficient for positive ion mode than for negative ion mode. Whether or not this resulted from the selection of compounds for the study presented here cannot be determined from such limited sample sets.

It is also noteworthy to consider that the significant ion signal enhancement observed here with neat acetonitrile and field-free cVSSI in positive ion mode to some degree contradicts earlier work examining the efficacy of inlet ionization.⁶³ In that study, a low abundance of ubiquitin ions was observed when analyzed with 100% acetonitrile compared to 20 % water content in the acetonitrile solvent. Admittedly, the studies here are for small compounds. However, it is remarkable that ionization enhancements are observed for even some of the more polar compounds.

3.4 Conclusions

The ion intensities of various small-molecule compounds have been reported for three different ionization techniques: field-free capillary vibrating sharp-edge ionization (cVSSI), field-enabled cVSSI, and ESI. Experiments have been conducted for samples dissolved in neat acetonitrile and 95% acetonitrile (5% water) under both positive and negative ion modes. Multiple regression analysis has been used to determine the degree to which different physicochemical characteristics of the molecule can be associated with the overall ionization efficiency in both positive and negative ion mode and to reveal how such associations can be different from aprotic to protic solvent conditions.

In general, for samples using an aprotic solvent having lower surface tension and low vaporization enthalpy, the log of the partition coefficient ($\log P$) is observed to correlate most significantly under field-free cVSSI conditions. This suggests ionization via the CRM as has been

proposed for other field-free ionization sources. For both field-enabled cVSSI and ESI, $\log P$ and proton affinity (PA) are strongly associated with the ion intensities. Comparatively, in prior experiments, the log of the base dissociation constant (pK_b) has shown a much more significant correlation with protic solvents like water and methanol. This suggests that for the aprotic, polar solvent ACN, when an electric field is employed (field-enabled cVSSI and ESI), pre-formed ions are not responsible for the observed ion signals. Rather, gas-phase proton transfer reactions either at the droplet surface or via collisions with reagent ions occurs.

The differences in ionization efficiency observed suggest an opportunity to tailor ion source mode with desired analyte detection. For example, it may be most beneficial to use an aprotic solvent under field-free cVSSI conditions for certain molecules in positive ion mode. Conversely, for other compounds, it may be most beneficial to use field-enabled cVSSI in negative ion mode to gain the signal advantage produced by the cVSSI-APCI-like process. In any case, the new ionization techniques offer a number of possible usages and will require many more studies to begin to pin down their optimal operation under various conditions.

3.5 References

- (1) Fenn, J. B.; Mann, M.; Meng, C. K.; Wong, S. F.; Whitehouse, C. M. Electrospray Ionization for Mass-Spectrometry of Large Biomolecules. *Science* **1989**, 246 (4926), 64-71. DOI: DOI 10.1126/science.2675315.
- (2) Tanaka, K.; Waki, H.; Ido, Y.; Akita, S.; Yoshida, Y.; Yoshida, T.; Matsuo, T. Protein and polymer analyses up to m/z 100 000 by laser ionization time-of-flight mass spectrometry. *Rapid Communications in Mass Spectrometry* **1988**, 2 (8), 151-153. DOI: 10.1002/rcm.1290020802.
- (3) Laiko, V. V.; Baldwin, M. A.; Burlingame, A. L. Atmospheric pressure matrix-assisted laser desorption/ionization mass spectrometry. *Anal Chem* **2000**, 72 (4), 652-657. DOI: 10.1021/ac990998k.
- (4) Emmett, M. R.; Caprioli, R. M. Micro-electrospray mass spectrometry: Ultra-high-sensitivity analysis of peptides and proteins. *J Am Soc Mass Spectrom* **1994**, 5 (7), 605-613. DOI: 10.1016/1044-0305(94)85001-1.
- (5) Wilm, M.; Mann, M. Analytical properties of the nanoelectrospray ion source. *Anal Chem* **1996**, 68 (1), 1-8. DOI: 10.1021/ac9509519.
- (6) Takats, Z.; Wiseman, J. M.; Gologan, B.; Cooks, R. G. Mass spectrometry sampling under ambient conditions with desorption electrospray ionization. *Science* **2004**, 306 (5695), 471-473. DOI: 10.1126/science.1104404.
- (7) Cody, R. B.; Laramée, J. A.; Durst, H. D. Versatile new ion source for the analysis of materials in open air under ambient conditions. *Anal Chem* **2005**, 77 (8), 2297-2302. DOI: 10.1021/ac050162j.
- (8) Horning, E.; Horning, M.; Carroll, D.; Dzidic, I.; Stillwell, R. New picogram detection system based on a mass spectrometer with an external ionization source at atmospheric pressure. *Analytical Chemistry* **1973**, 45 (6), 936-943.
- (9) Brown, H.; Oktem, B.; Windom, A.; Doroshenko, V.; Evans-Nguyen, K. Direct Analysis in Real Time (DART) and a portable mass spectrometer for rapid identification of common and designer drugs on-site. *Forensic Chemistry* **2016**, 1, 66-73. DOI: <https://doi.org/10.1016/j.forc.2016.07.002>.
- (10) Bruno, A. M.; Cleary, S. R.; O'Leary, A. E.; Gizzi, M. C.; Mulligan, C. C. Balancing the utility and legality of implementing portable mass spectrometers coupled with ambient ionization in routine law enforcement activities. *Analytical Methods* **2017**, 9 (34), 5015-5022, 10.1039/C7AY00972K. DOI: 10.1039/C7AY00972K.
- (11) Lawton, Z. E.; Traub, A.; Fatigante, W. L.; Mancias, J.; O'Leary, A. E.; Hall, S. E.; Wieland, J. R.; Oberacher, H.; Gizzi, M. C.; Mulligan, C. C. Analytical Validation of a Portable Mass Spectrometer Featuring Interchangeable, Ambient Ionization Sources for High Throughput Forensic Evidence Screening. *Journal of the American Society for Mass Spectrometry* **2017**, 28 (6), 1048-1059. DOI: 10.1007/s13361-016-1562-2.
- (12) Meier, R. W. A field portable mass spectrometer for monitoring organic vapors. *American Industrial Hygiene Association Journal* **1978**, 39 (3), 233-239. DOI: 10.1080/0002889778507747.
- (13) Verbeck, G. F.; Bierbaum, V. M. Focus on Harsh Environment and Field-Portable Mass Spectrometry: Editorial. *J. Am. Soc. Mass Spectrom.* **2015**, 26 (2), 199-200. DOI: 10.1007/s13361-014-1057-y.
- (14) Hirabayashi, A.; Sakairi, M.; Koizumi, H. Sonic spray mass spectrometry. *Anal Chem* **1995**, 67 (17), 2878-2882. DOI: 10.1021/ac00113a023.

- (15) Wlekinski, M.; Li, Y.; Bag, S.; Sarkar, D.; Narayanan, R.; Pradeep, T.; Cooks, R. G. Zero Volt Paper Spray Ionization and Its Mechanism. *Anal Chem* **2015**, *87* (13), 6786-6793. DOI: 10.1021/acs.analchem.5b01225.
- (16) Song, L.; You, Y.; Evans-Nguyen, T. Surface Acoustic Wave Nebulization with Atmospheric-Pressure Chemical Ionization for Enhanced Ion Signal. *Anal Chem* **2019**, *91* (1), 912-918. DOI: 10.1021/acs.analchem.8b03927.
- (17) Pagnotti, V. S.; Chubaty, N. D.; McEwen, C. N. Solvent assisted inlet ionization: an ultrasensitive new liquid introduction ionization method for mass spectrometry. *Anal Chem* **2011**, *83* (11), 3981-3985. DOI: 10.1021/ac200556z.
- (18) Chen, T.; Lin, J.; Chen, J.; Chen, Y. Ultrasonication-Assisted Spray Ionization Mass Spectrometry for the Analysis of Biomolecules in Solution. *Journal of the American Society For Mass Spectrometry* **2010**, *21* (9), 1547-1553, Article. DOI: 10.1016/j.jasms.2010.04.021.
- (19) Li, X.; Attanayake, K.; Valentine, S. J.; Li, P. Vibrating Sharp-edge Spray Ionization (VSSI) for voltage-free direct analysis of samples using mass spectrometry. *Rapid Commun Mass Spectrom* **2018**. DOI: 10.1002/rcm.8232.
- (20) Ranganathan, N.; Li, C.; Suder, T.; Karanji, A. K.; Li, X. J.; He, Z. Y.; Valentine, S. J.; Li, P. Capillary Vibrating Sharp-Edge Spray Ionization (cVSSI) for Voltage-Free Liquid Chromatography-Mass Spectrometry. *Journal of the American Society for Mass Spectrometry* **2019**, *30* (5), 824-831, Article. DOI: 10.1007/s13361-019-02147-0.
- (21) Li, C.; Attanayake, K.; Valentine, S. J.; Li, P. Facile Improvement of Negative Ion Mode Electrospray Ionization Using Capillary Vibrating Sharp-Edge Spray Ionization. *Anal Chem* **2020**, *92* (3), 2492-2502. DOI: 10.1021/acs.analchem.9b03983.
- (22) Kolakowski, B. A.; Grossert, J. S.; Ramaley, L. Studies on the positive-ion mass spectra from atmospheric pressure chemical ionization of gases and solvents used in liquid chromatography and direct liquid injection. *Journal of the American Society for Mass Spectrometry* **2004**, *15* (3), 311-324, Article. DOI: 10.1016/j.jasms.2003.10.019.
- (23) Narayanan, R.; Sarkar, D.; Cooks, R. G.; Pradeep, T. Molecular ionization from carbon nanotube paper. *Angew Chem Int Ed Engl* **2014**, *53* (23), 5936-5940. DOI: 10.1002/anie.201311053.
- (24) Pol, J.; Kauppila, T. J.; Haapala, M.; Saarela, V.; Franssila, S.; Ketola, R. A.; Kotiaho, T.; Kostianen, R. Microchip sonic spray ionization. *Anal Chem* **2007**, *79* (9), 3519-3523. DOI: 10.1021/ac070003v.
- (25) Yu, C.; Qian, X.; Chen, Y.; Yu, Q.; Ni, K.; Wang, X. Microfluidic self-aspiration sonic-spray ionization chip with single and dual ionization channels for mass spectrometry. *RSC Advances* **2016**, *6* (55), 50180-50189. DOI: 10.1039/c6ra07959h.
- (26) Mandra, V. J.; Kouskoura, M. G.; Markopoulou, C. K. Using the partial least squares method to model the electrospray ionization response produced by small pharmaceutical molecules in positive mode. *Rapid Commun Mass Spectrom* **2015**, *29* (18), 1661-1675. DOI: 10.1002/rcm.7263.
- (27) Ehrmann, B. M.; Henriksen, T.; Cech, N. B. Relative importance of basicity in the gas phase and in solution for determining selectivity in electrospray ionization mass spectrometry. *J Am Soc Mass Spectrom* **2008**, *19* (5), 719-728. DOI: 10.1016/j.jasms.2008.01.003.
- (28) Henriksen, T.; Juhler, R. K.; Svensmark, B.; Cech, N. B. The relative influences of acidity and polarity on responsiveness of small organic molecules to analysis with negative ion electrospray ionization mass spectrometry (ESI-MS). *J Am Soc Mass Spectrom* **2005**, *16* (4), 446-455. DOI: 10.1016/j.jasms.2004.11.021.

- (29) Oss, M.; Kruve, A.; Herodes, K.; Leito, I. Electrospray ionization efficiency scale of organic compounds. *Anal Chem* **2010**, 82 (7), 2865-2872. DOI: 10.1021/ac902856t.
- (30) Kiontke, A.; Oliveira-Birkmeier, A.; Opitz, A.; Birkemeyer, C. Electrospray Ionization Efficiency Is Dependent on Different Molecular Descriptors with Respect to Solvent pH and Instrumental Configuration. *PLoS One* **2016**, 11 (12), e0167502. DOI: 10.1371/journal.pone.0167502.
- (31) Liigand, J.; Laaniste, A.; Kruve, A. pH Effects on Electrospray Ionization Efficiency. *J Am Soc Mass Spectrom* **2017**, 28 (3), 461-469. DOI: 10.1007/s13361-016-1563-1.
- (32) Ikonomou, M. G.; Blades, A. T.; Kebarle, P. Electrospray-ion spray: a comparison of mechanisms and performance. *Analytical Chemistry* **1991**, 63 (18), 1989-1998. DOI: 10.1021/ac00018a017.
- (33) Zhou, S.; Hamburger, M. Effects of solvent composition on molecular ion response in electrospray mass spectrometry: Investigation of the ionization processes. *Rapid Communications in Mass Spectrometry* **1995**, 9 (15), 1516-1521, <https://doi.org/10.1002/rcm.1290091511>.
- (34) Schneider, R. P.; Lynch, M. J.; Ericson, J. F.; Fouda, H. G. Electrospray ionization mass spectrometry of semduramicin and other polyether ionophores. *Analytical Chemistry* **1991**, 63 (17), 1789-1794. DOI: 10.1021/ac00017a024.
- (35) Ami; Motoyama, A.; Takayama, M. Influence of Solvent Composition and Surface Tension on the Signal Intensity of Amino Acids in Electrospray Ionization Mass Spectrometry. *Mass Spectrometry* **2019**, 8. DOI: 10.5702/massspectrometry.A0077.
- (36) Yao, Y.-N.; Wu, L.; Di, D.; Yuan, Z.-C.; Hu, B. Vibrating tip spray ionization mass spectrometry for direct sample analysis. *Journal of Mass Spectrometry* **2019**, 54. DOI: 10.1002/jms.4429.
- (37) Jayasundara, K. U.; Li, C.; DeBastiani, A.; Sharif, D.; Li, P.; Valentine, S. J. Physicochemical Property Correlations with Ionization Efficiency in Capillary Vibrating Sharp-Edge Spray Ionization (cVSSI). *Journal of the American Society for Mass Spectrometry* **2021**, 32 (1), 84-94. DOI: 10.1021/jasms.0c00100.
- (38) Rossini, E.; Bochevarov, A. D.; Knapp, E. W. Empirical Conversion of pKa Values between Different Solvents and Interpretation of the Parameters: Application to Water, Acetonitrile, Dimethyl Sulfoxide, and Methanol. *ACS Omega* **2018**, 3 (2), 1653-1662. DOI: 10.1021/acsomega.7b01895.
- (39) Cech, N. B.; Enke, C. G. Relating electrospray ionization response to nonpolar character of small peptides. *Anal Chem* **2000**, 72 (13), 2717-2723. DOI: 10.1021/ac9914869.
- (40) Kiontke, A.; Billig, S.; Birkemeyer, C. Response in Ambient Low Temperature Plasma Ionization Compared to Electrospray and Atmospheric Pressure Chemical Ionization for Mass Spectrometry. *Int J Anal Chem* **2018**, 2018, 5647536. DOI: 10.1155/2018/5647536.
- (41) Gamero-Castaño, M.; Fernandez de la Mora, J. Mechanisms of Electrospray Ionization of Singly and Multiply Charged Salt Clusters. *Analytica Chimica Acta* **2000**, 406, 67-91. DOI: 10.1016/S0003-2670(99)00596-6.
- (42) Znamenskiy, V.; Marginean, I.; Vertes, A. Solvated Ion Evaporation from Charged Water Nanodroplets. *The Journal of Physical Chemistry A* **2003**, 107 (38), 7406-7412. DOI: 10.1021/jp034561z.
- (43) Kebarle, P.; Peschke, M. On the mechanisms by which the charged droplets produced by electrospray lead to gas phase ions. *Analytica Chimica Acta* **2000**, 406 (1), 11-35, Article. DOI: 10.1016/s0003-2670(99)00598-x.

- (44) Kebarle, P.; Verkerk, U. H. ELECTROSPRAY: FROM IONS IN SOLUTION TO IONS IN THE GAS PHASE, WHAT WE KNOW NOW. *Mass Spectrometry Reviews* **2009**, 28 (6), 898-917, Review. DOI: 10.1002/mas.20247.
- (45) Rohner, T. C.; Lion, N.; Girault, H. H. Electrochemical and theoretical aspects of electrospray ionisation. *Physical Chemistry Chemical Physics* **2004**, 6 (12), 3056-3068, Review. DOI: 10.1039/b316836k.
- (46) Iribarne, J. V. On the evaporation of small ions from charged droplets. *The Journal of Chemical Physics* **1976**, 64 (6). DOI: 10.1063/1.432536.
- (47) Tang, L.; Kebarle, P. DEPENDENCE OF ION INTENSITY IN ELECTROSPRAY MASS-SPECTROMETRY ON THE CONCENTRATION OF THE ANALYTES IN THE ELECTROSPRAYED SOLUTION. *Analytical Chemistry* **1993**, 65 (24), 3654-3668, Article. DOI: 10.1021/ac00072a020.
- (48) Dole, M.; Mack, L. L.; Hines, R. L. MOLECULAR BEAMS OF MACROIONS. *Journal of Chemical Physics* **1968**, 49 (5), 2240-&, Article. DOI: 10.1063/1.1670391.
- (49) Cech, N. B.; Krone, J. R.; Enke, C. G. Predicting Electrospray Response from Chromatographic Retention Time. *Analytical Chemistry* **2001**, 73 (2), 208-213. DOI: 10.1021/ac0006019.
- (50) Tang, L.; Kebarle, P. Effect of the conductivity of the electrosprayed solution on the electrospray current. Factors determining analyte sensitivity in electrospray mass spectrometry. *Analytical Chemistry* **1991**, 63 (23), 2709-2715. DOI: 10.1021/ac00023a009.
- (51) Kelly, M. A.; Vestling, M. M.; Fenselau, C. C.; Smith, P. B. Electrospray analysis of proteins. *A comparison of positive-ion and negative-ion mass spectra at high and low pH* **1992**, 27 (10), 1143-1147, Article. DOI: 10.1002/oms.1210271028.
- (52) Wang, G.; Cole, R. B. Disparity between solution-phase equilibria and charge state distributions in positive-ion electrospray mass spectrometry. *Org Mass Spectrom* **1994**, 29 (8), 419-427.
- (53) Mansoori, B. A.; Volmer, D. A.; Boyd, R. K. 'Wrong-way-round' Electrospray Ionization of Amino Acids. *Rapid Communications in Mass Spectrometry* **1997**, 11 (10), 1120-1130, [https://doi.org/10.1002/\(SICI\)1097-0231\(19970630\)11:10<1120::AID-RCM976>3.0.CO;2-Q](https://doi.org/10.1002/(SICI)1097-0231(19970630)11:10<1120::AID-RCM976>3.0.CO;2-Q).
- (54) Zhou, S.; Cook, K. D. Protonation in electrospray mass spectrometry: Wrong-way-round or right-way-round? *J. Am. Soc. Mass Spectrom.* **2000**, 11 (11), 961-966. DOI: 10.1016/S1044-0305(00)00174-4.
- (55) Cole, R. B. Electrospray ionization mass spectrometry : fundamentals, instrumentation, and applications. 1997.
- (56) Kebarle, P. A brief overview of the present status of the mechanisms involved in electrospray mass spectrometry. *Journal of Mass Spectrometry* **2000**, 35 (7), 804-817, Article. DOI: 10.1002/1096-9888(200007)35:7<804::aid-jms22>3.0.co;2-q.
- (57) Pursell, M. E.; Sharif, D.; DeBastiani, A.; Li, C.; Majuta, S.; Li, P.; Valentine, S. J. Development of cVSSI-APCI for the Improvement of Ion Suppression and Matrix Effects in Complex Mixtures. *Analytical Chemistry* **2022**. DOI: 10.1021/acs.analchem.1c05136.
- (58) Kebarle, P.; Godbole, E. W. Mass-Spectrometric Study of Ions from the α -Particle Irradiation of Gases at Near Atmospheric Pressures. *The Journal of Chemical Physics* **1963**, 39 (4), 1131-1132. DOI: 10.1063/1.1734371 .
- (59) Harrison, A. G. Chemical Ionization Mass Spectrometry. 2 ed.; Routledge: New York, 1992; pp 91-100.

- (60) Bruins, A. P. Mass spectrometry with ion sources operating at atmospheric pressure. *Mass Spectrometry Reviews* **1991**, *10* (1), 53-77, <https://doi.org/10.1002/mas.1280100104>.
- (61) Labowsky, M. A model for solvated ion emission from electrospray droplets. *Rapid Communications in Mass Spectrometry* **2010**, *24* (21), 3079-3091, <https://doi.org/10.1002/rcm.4738>.
- (62) Nguyen, S.; Fenn John, B. Gas-phase ions of solute species from charged droplets of solutions. *Proceedings of the National Academy of Sciences* **2007**, *104* (4), 1111-1117. DOI: 10.1073/pnas.0609969104 .
- (63) Trimpin, S.; Inutan, E. D.; Karki, S.; Elia, E. A.; Zhang, W.-J.; Weidner, S. M.; Marshall, D. D.; Hoang, K.; Lee, C.; Davis, E. T. J.; et al. Fundamental Studies of New Ionization Technologies and Insights from IMS-MS. *J. Am. Soc. Mass Spectrom.* **2019**, *30* (6), 1133-1147. DOI: 10.1007/s13361-019-02194-7.

4 Insights into Ion release from cVSSI droplets obtained with Molecular Dynamics Simulations

4.1 Introduction

Measuring the mass-to-charge ratios (m/z) for ions in the gas phase, mass spectrometry (MS) is one of the most versatile analytical techniques used for characterizing a broad range of compounds and samples. Due to its robust data information nature, the development of miniaturized and field-portable mass spectrometers is an ongoing endeavor. Such a mass spectrometer may find utility in a variety of settings including chemical/biological warfare agent detection, forensic investigations, on-site metabolite identification, and atmospheric toxicant detection.

With regard to developing field-portable analytical instruments, one of the most prized design attributes is size. Smaller-sized instruments functioning as bench-top instruments are highly desired as well instruments that can detect analytes of interest in the field when operated by non-scientists.^{1 2} All MS instrumentation development has at its core the goal of providing the greatest sensitivity with the highest resolving power. It is highly challenging to develop field-portable mass spectrometers with the aforementioned characteristics without a simple and compact yet robust ionization source. Numerous ambient ionization methods have been introduced as a result of ongoing development in modern mass spectrometry.³ However, the reported methods require dedicated and specialized instrumentation components, the application of a high-voltage, auxiliary gas, and additional solvents.^{4 5} These limitations introduce significant challenges when designing a field-portable mass spectrometer.

The 1980s witnessed early steps toward the development of a suitable ionization source when Vestal and coworkers introduced the first voltage-free spray ionization method, thermospray

ionization, as an interface for LC-MS.^{6 7} Shortly later, sonic spray ionization (SSI) was introduced; this technique uses pneumatic force from a high-speed solvent spray to charge plume droplets.⁸ During the last decade, a number of novel field-free ionization techniques like solvent-assisted inlet ionization (SAII)⁹, zero-voltage paper spray ionization (PSI),¹⁰ and surface acoustic wave nebulization were introduced.⁵

Recently, the new field-free ionization source called vibrating sharp-edge spray ionization (VSSI)¹¹ has been introduced. In this approach, a vibrating substrate such as a microscope slide that is placed in contact with a liquid solvent generates a droplet plume directly at the very sharp edge. After the first demonstrations of VSSI, a capillary segment (blunt-tip or pulled-tip) was glued directly to the vibrating substrate allowing the direct infusion of a sample and plume generation from the end of the capillary segment. This mode of operation is called capillary vibrating sharp-edge spray ionization (cVSSI)¹². Notably, the technique can be operated under different conditions. For example, experiments can utilize a cVSSI device for which only the vibration of the tip produces the droplet plume (field-free cVSSI) as well as a setup in which an applied voltage and tip vibration (field-enabled cVSSI) function to produce ions of interest¹³.

cVSSI has been shown to provide a number of distinct capabilities. First, the method can provide a robust droplet plume over a nearly 3 decade range in flow rates (500 nL/min to 500 μ L/min). The method ionizes a broad range of compounds including small molecules, carbohydrates, peptides, proteins, and nucleic acids, even under field-free cVSSI conditions^{13 12}¹⁴. Field-enabled cVSSI is shown to offer ionization increases over state-of-art ESI; this advantage is especially pronounced for negatively charged ions where an ~10 to 100-fold enhancement ion signal levels.¹³ Overall, this technique shows promising characteristics for the field of MS and because of its low power requirements may be of significant benefit to field-portable

instrumentation. Therefore, developing an understanding of the mechanism behind the release of the analyte ions into the gas phase by cVSSI is valuable as it will enable the optimization of cVSSI sources for various MS studies.

The exact process by which the vibrating sharp edge creates the solvent spray is still a subject of intense study. The droplet creation process which Cooks and co-workers propose for their zero-volt paper spray ionization may serve in initial discussions of field-free cVSSI.¹⁰ Cook's proposed mechanism is based on a statistical charge separation between cations and anions during droplet formation. It is assumed that this charge separation occurs during or shortly after the aerodynamic breakup of liquid sample, as explained by Jarrold and co-workers.¹⁵ After this initial process, the late progeny droplets undergo fission events due to Coulombic forces within the charged droplets. It can be argued that this process is the same phenomenon as that experienced by the last progeny droplets in electrospray ionization (ESI).¹⁶

Two mechanisms have been introduced to explain the final stages of ion production from these late-stage droplets. Explanations for these mechanisms have been developed based on theoretical and experimental studies. The two models are the ion evaporation model (IEM)¹⁷ and the charge residue model (CRM)¹⁸. Both the IEM and CRM processes involve solvent evaporation and Coulombic fission events, but eventually these two mechanisms diverge into distinct pathways.¹⁹ In the IEM, an analyte ion is released to the gaseous environment by overcoming the solvation activation barrier leaving behind a charged droplet. In the CRM, the droplet is evaporated to dryness and the remaining charge is transferred directly to the analyte to produce the ions. Since the mechanism for analyte ion transfer into the gas phase at the late stage of ESI remains a matter of debate, some new models have been proposed that are somewhat distinct from the IEM and CRM mechanisms. The combined charge residue-field emission model proposed by Gross and

coworkers is a mechanism that attempts to resolve the differences between the IEM and CRM.²⁰ The new mechanism of ion evaporation of macromolecules introduced by Consta and Malevanets differs from the conventional CRM and IEM.²¹ The Konermann group proposed a chain ejection model describing the effect of proton hopping to transfer from the surface of the late-stage droplet to unfolded proteins effectively expelling the expanding polypeptide chain into the gas phase.²² A recent theoretical observed that globular proteins like ubiquitin favor the IEM when released to the gas phase from a larger droplet field²³. Because of the ongoing debate of ion production in the field of mass spectrometry, it is important to study the droplets in as realistic a fashion as possible. One example is to include any counter ions that may be present in the last progeny droplets produced from cVSSI as well as to consider how field-free ionization conditions will differ from field-enabled conditions with regard to the release of solution-phase analyte ions into the gas phase.

Another factor that may introduce differences in the mechanism of ion release is the degree of droplet charging experienced in both positive and negative ion mode. For ESI, the positive or negative ions are primarily present because of the counter electrode utilized as the mass spectrometer inlet. It can be argued that the high voltage conditions in ESI result in larger overall surface charge in the progeny droplets while for the field-free ionization conditions, the droplets may contain less charge. So in addition to having a lower overall net charge, the droplets from the latter source may also contain a greater amount of counterions on average. Because it has been shown that the total charge in progeny droplets affects the efficiency of the analyte ion release into the gas phase from the solution phase,^{19 24 25} an understanding of factors affecting the mechanism of analyte ion release into the gas phase under-voltage and voltage-free conditions is an active area of research.

In recent years, Molecular dynamics (MD) simulations have become a powerful technique for studying the temporal evolution of charged nanodroplets at the atomic level. The approach has been utilized to gain insight into the ejection of small ions from ESI droplets (IEM)^{26 27 28 29}. In comparison, CRM behavior was observed in MD simulations performed for folded proteins^{27 30}, nucleic acid duplexes³¹, and peptides^{32 33}, while for unfolded proteins, CEM behavior has been observed²⁷. These mechanisms have been discussed in more detail in Chapter 1.

Here insight into small-molecule ion introduction into the gas phase from nano-sized droplets comprised of different constituent parts is obtained from MD simulations and used to describe cVSSI-MS experiments. One system contained acetaminophen and dopamine in pure water solvent where a lower droplet charge representing zero-voltage spray conditions was used. A second system contained the same analyte ions in pure water but a higher droplet charge was used. This represents higher voltage conditions associated with ESI. Using MD simulation data, several characteristics of the analytes have been determined. These included the ion's diffusion coefficient and free energy change of desorption for both droplet systems, and the data were compared with the experimental results obtained when acetaminophen and dopamine were sprayed at equimolar concentrations from the same aqueous solvent.

In the second part of the study, the association of the surface activity of the small molecules with their ion release into the gas phase was examined using MD simulations representing field-enabled cVSSI and ESI charged droplets. MD simulations were designed to mimic the experimental ammonium acetate buffer solvent system in both ionization conditions.

4.2 Experimental

4.2.1 Sample Preparation.

All the compounds analyzed in this study were purchased from Thermo Fisher Scientific (Pittsburgh, PA, USA). In the first study, 1 mg of acetaminophen and 1 mg of dopamine were dissolved in 1 ml of water and were diluted to 0.01mg/ml concentration. The structures of dopamine and acetaminophen show in Table 4-1. For the second study, 10 small molecules; N-Dimethylbenzylamine, triethanolamine, Triethylamine, Benzylamine, N-methylbenzylamine, Quinclidine, phenylethylamine, N-ethylaniline, Bipyridine, Methoxyaniline were selected and used without further purification. Table 4-2 shows the structures of the compounds and their molecular weights, logarithm of the partition coefficient ($\log P$), logarithm of the base dissociation constant (pK_b), and proton affinity (PA) values. pK_b values were obtained from chemicalize.org by ChemAxon, Budapest, Hungary [<https://chemicalize.com>]. The PA values were obtained from the NIST Chemistry WebBook [<http://webbook.nist.gov/chemistry>] Stock solutions of each compound were prepared by dissolving 1 mg of each compound in 1 ml of aqueous ammonium acetate (100 mM) buffer solution. The buffer solution was utilized to limit the amount of droplet protonating species (H_3O^+). Before analysis by MS, all samples were diluted to 0.01 mg / mL.

Table 4- 1 Chemical structures of Acetaminophen and Dopamine.

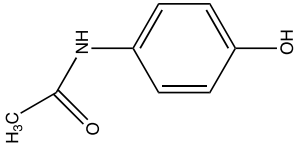
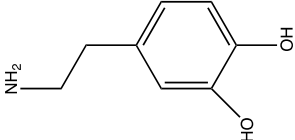
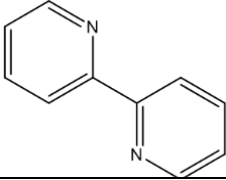
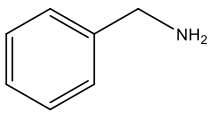
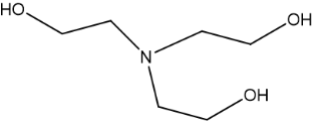
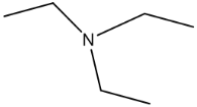
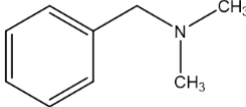
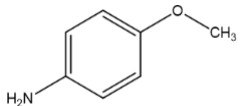
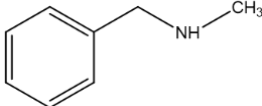
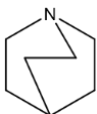
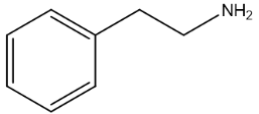
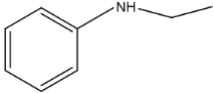
Molecule	Structure
Acetaminophen	
Dopamine	

Table 4- 2 Structures and physicochemical property values for the compounds used in the ionization event studies as examined by MD simulations.

#	Compound	Structure	pKa	logP	PA (KJ/mol)	MW
1	2-2 bipyridine		8.7	1.28	974.4	156.18
2	Benzylamine		4.7	1.09	922.7	107.15
3	Triethanolamine		5.6	-0.74	1000.4	149.19
4	Triethylamine		3.8	1.66	981.8	101.19
5	N,N-dimethylbenzylamine		5.1	1.98	968.4	135.21
6	4-Methoxyaniline		8.9	0.74	900.3	123.15
7	N-methylbenzylamine		4.6	1.60	980.4	121.18
8	Quinuclidine		3.1	1.38	983.3	111.18
9	Phenylethylamine		4.2	1.49	936.2	121.18
10	N-ethylaniline		9.1	2.13	924.8	123.15

4.2.2 cVSSI-Mass Spectrometry Data Collection.

cVSSI and capillary ESI (cESI) sources were constructed as described previously.³⁴ Briefly, 5-cm-long, blunt-tip capillary emitters were obtained using pre-cut fused silica (100 μm ID \times 360 μm OD) and were attached to the edge of a cVSSI device. The cVSSI devices consist of a piezoelectric transducer (Murata) attached to a microscope slide (VWR). This was accomplished with epoxy-based superglue (Devcon). For the field-free and field-enabled cVSSI experiments, an amplified (2 \times , Mini-Circuits) square waveform (Tektronix) was applied to the piezoelectric transducer in the range of ~94 to 95 kHz while infusing the sample at flow rates of 10 μL / min. For the first part of the study, field-enabled cVSSI experiments utilized 1 kV, 2 kV, 3 kV and 4 kV. In the second part of the study, under field-enabled cVSSI and cESI, only 2 kV voltage was utilized for all the sample analysis. In all the field-enabled experiments, the DC voltage was applied to the platinum wire just prior to the emitter tip. In both studies, the cVSSI source was coupled to a linear ion trap mass spectrometer (LTQ, Thermo Fisher, San Jose, CA). Experiments were conducted in positive ion mode. The ion transfer tube temperatures were maintained at 275 $^{\circ}\text{C}$ for all experiments. Data were collected in triplicate for 30 seconds over a mass-to-charge ratio (m/z) range of 50 to 300. Peak intensities were obtained using the Xcalibur software suite (ThermoFisher), for all comparisons, signal intensities were obtained from total ion signals for each compound.

4.2.3 Molecular Dynamics (MD) simulations.

For the first part of the study, singly-charged acetaminophen and dopamine ions were solvated in the center of a large octahedral TIP3P water box using the VMD 1.9.3 program. Figure 4-1 shows the snapshots from a MD simulation trajectory of a droplet containing an acetaminophen

ion and a dopamine ion. Singly-charged acetaminophen and dopamine ions were constructed using the Avagadro software and equilibrated before being solvated in a water box. Using the in-house script, the water box was carved into a spherical droplet with a 2.0 nm distance from the center of mass of the acetaminophen molecule. Using the Packmol software package, charge carrier ions were placed randomly within the droplet.³⁵ The Rayleigh limit for a droplet with a 2 nm radius is $z=10$, as calculated using the surface tension value for TIP3P water at 300 K. Hence, the upper limit of the total charge on the droplet is determined to be +10. The field-free cVSSI system contains 2 hydronium, two hydroxide, and 2 Na^+ ions, which yield a total charge of +4 with two analyte ions. In a field-enabled cVSSI system, 4 hydronium and two hydroxide, and 4Na^+ were added along with the analyte ions, which results in a net charge of +8, representing higher voltage (ESI) conditions.

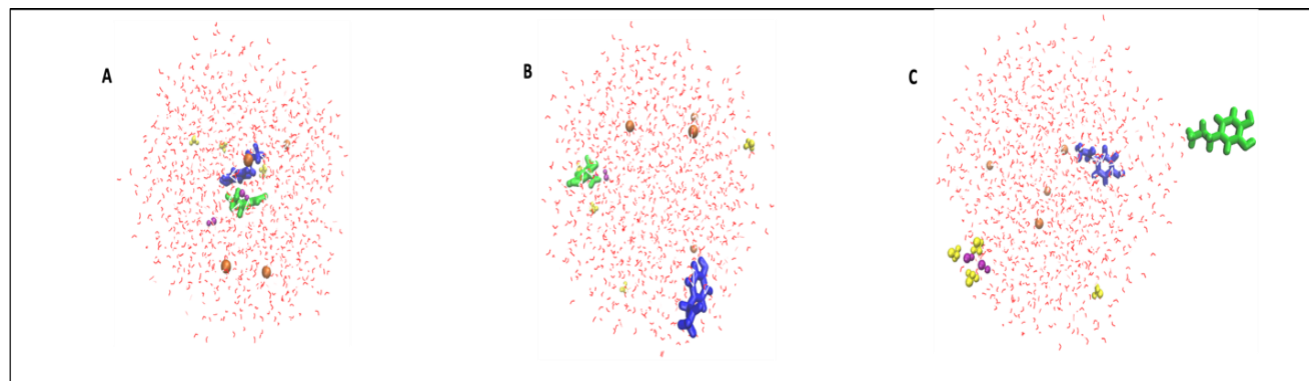


Figure 4- 1 Snapshots from a MD simulation trajectory of a droplet containing an acetaminophen ion (green) and a dopamine ion (blue) in $4\text{H}_3\text{O}^+$, 2OH^- , 4Na^+ (field-free cVSSI system). Water molecules are shown in red, H_3O^+ ions are yellow, OH^- ions are purple, and Na^+ ions are orange. The time points shown correspond to (A) $t=0$ ns, (B) $t=0.18$ ns (C) $t=4.67$ ns.

In the second study, equilibrated structures of 10 singly-charged analyte molecules (N-Dimethylbenzylamine, triethanolamine, Triethylamine, Benzylamine, N-methylbenzylamine, Quinclidine, phenylethylamine, N-ethylaniline, Bipyridine, Methoxyaniline) were obtained from Gaussian 09 software suite.³⁶ Each analyte ion was solvated similar to those in the first study with one exception. Instead of using the TIP3P, a TIP4P/2005 water model was used. Even though the TIP3P water model has a lower computational cost than other water models (TIP4P, SPC), it has a lower surface tension than the actual value for water³⁷. Hence, to obtain more accurate MD simulation data in this study, the TIP4P/2005 water model was used. Also, it is worth mentioning that the TIP3P model shows similar behavior to other water models. Using the same in-house script mentioned above, 2.5 nm water droplets were carved from the water box. The upper charge limit (Rayleigh) of a droplet of 2.5 nm is ~13. Then charge carriers were added using the Packmol by placing them in random positions mimicking field-enabled cVSSI and ESI droplets. The droplets system representing the field-enabled cVSSI has 10 hydronium ions, 5 acetic acid, and the analyte ion. The ESI type droplet contains 12 hydronium ions and the analyte ion. For both field-enabled cVSSI and ESI, five droplet systems were constructed for each analyte ion by placing charge carriers in random positions.

In both the first and second studies, the NAMD 2.13 molecular dynamic package and the CHARMM36 force field were used to run MD simulations. Since CHARMM does not contain parameters for the hydronium ion, the developed and tested hydronium ion parameter in the CHARMM force field was obtained from Shen *et al.*³⁸. In the second part of the study the CGenFF program was used to obtain CHARMM force field parameters for the analyte ions because they are not available in the CGenFF database.³⁹ The droplets were placed in a vacuum, and simulations were performed without Periodic Boundary Conditions (PBC), allowing non-equilibrium runs

which yield solvent and ion evaporation.^{40 41} Also, a large cutoff value (40 Å) was applied to experience the entire system with no cutoff effects for Coulomb or Lennard – Jones interactions.⁴¹ The temperature for each simulation was set to 300 K, which mimics the experimental temperature just prior to the MS inlet. Thus, the simulation system possesses a constant number of particles N, a constant temperature, and a constant volume, representing the NVT canonical ensemble corresponding to a system in thermal equilibrium with its surrounding environment. Simulations were carried out until the analyte ion was released to the gaseous phase. Every 20 ns, simulations were paused, and the evaporated water droplets were removed to accelerate the simulation time using an in-house TLC script. VMD 1.9.3 program was used to view the trajectories and analyze the data.

4.2.4 Data analysis.

In the first part of the study, the analyte molecule's dynamics (acetaminophen and dopamine) were analyzed by its diffusion coefficient and the free energy of desorption. To calculate the diffusion coefficient, we used the Einstein-Smoluchowski relation (Equation 1)

$$D = \frac{\langle \Delta r^2 \rangle}{6\Delta t} \quad \text{Equation (1)}$$

$\langle \Delta r^2 \rangle$ is the mean square displacement calculated for the trajectory of the acetaminophen molecule during the time interval Δt . The VMD distance TCL script was used to obtain the probability distribution of each ion and the distance between each ion and the center of the droplet.

⁴² Diffusion coefficients obtained from simulation runs are recorded in Table 4-3.

Table 4- 3 Diffusion coefficients for acetaminophen and dopamine ions in field-free and field-enabled cVSSI droplet systems.

Field-free cVSSI droplet system	acetaminophen	$0.1889 \times 10^{-7} \text{ cm}^2 \text{ s}^{-1}$
	dopamine	$0.1814 \times 10^{-7} \text{ cm}^2 \text{ s}^{-1}$
Field-enabled cVSSI droplet system	acetaminophen	$0.1599 \times 10^{-7} \text{ cm}^2 \text{ s}^{-1}$
	dopamine	$0.1783 \times 10^{-7} \text{ cm}^2 \text{ s}^{-1}$

To calculate the free energy of desorption of the analyte molecule, we used the Adaptive Biasing Force (ABF) methodology along with the Collective Variable-based Calculations Module (Colvars). Colvars calculations were used to define a transition coordinate, which is the distance between the center of mass of the acetaminophen or dopamine molecule and the droplet's surface along which sampling is enhanced. Then the Potential of Mean Force (PMF) was calculated and the free energy estimated.^{43 44} The obtained free energy of desorption values for acetaminophen and dopamine in field-free cVSSI and field-enabled cVSSI are shown in Table 4-4. The free energy profile of a dopamine ion in the droplet of a field-enabled cVSSI system is shown in Figure 4-2.

In the second study, the time required by each analyte ion to release into the gas phase was recorded for 10 analyte molecules under field-enabled cVSSI and ESI conditions (droplet systems, see above). Then the average release time for each analyte ion was calculated by the five trials performed for each ionization made. Linear regression analysis was performed using the Excel software suite (Microsoft, Redmond CA) for the data (the average time analyte ions require to release into the gas phase versus log P) from the MD simulation runs (Figure 4-3 and Figure 4-4). R-squared values were compared for the separate regression analyses in field-enabled cVSSI and ESI.

Table 4- 4 Free energy of desorption of acetaminophen and dopamine ions for field-free cVSSI and field-enabled cVSSI droplet systems.

Field-free cVSSI droplet system	acetaminophen	67.1 kcal/mol
	dopamine	69.1 kcal/mol
Field-enabled cVSSI droplet system	acetaminophen	27.3 kcal/mol
	dopamine	24.7 kcal/mol

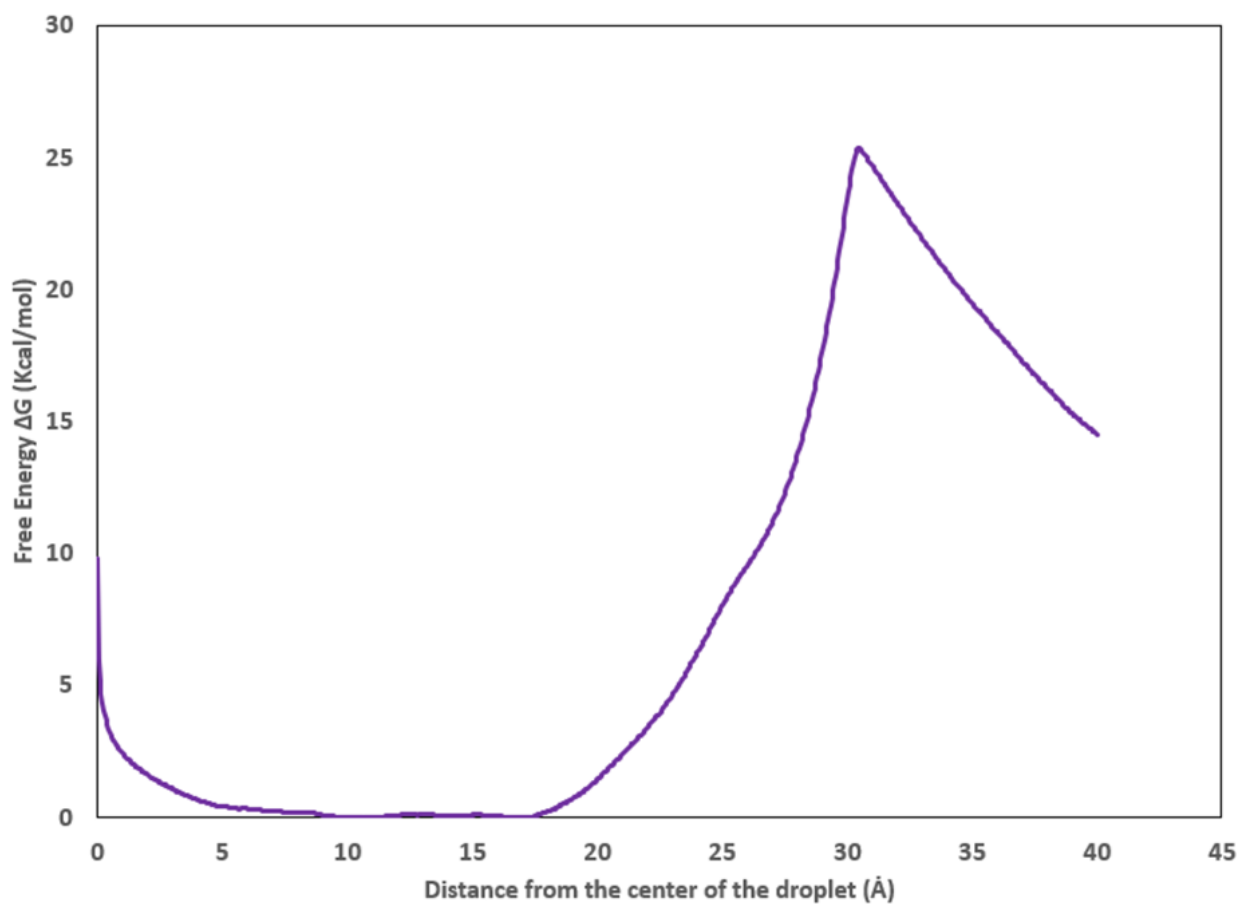


Figure 4- 2 Free energy profile of a dopamine ion obtained from the field-enabled cVSSI droplet system (see text for details).

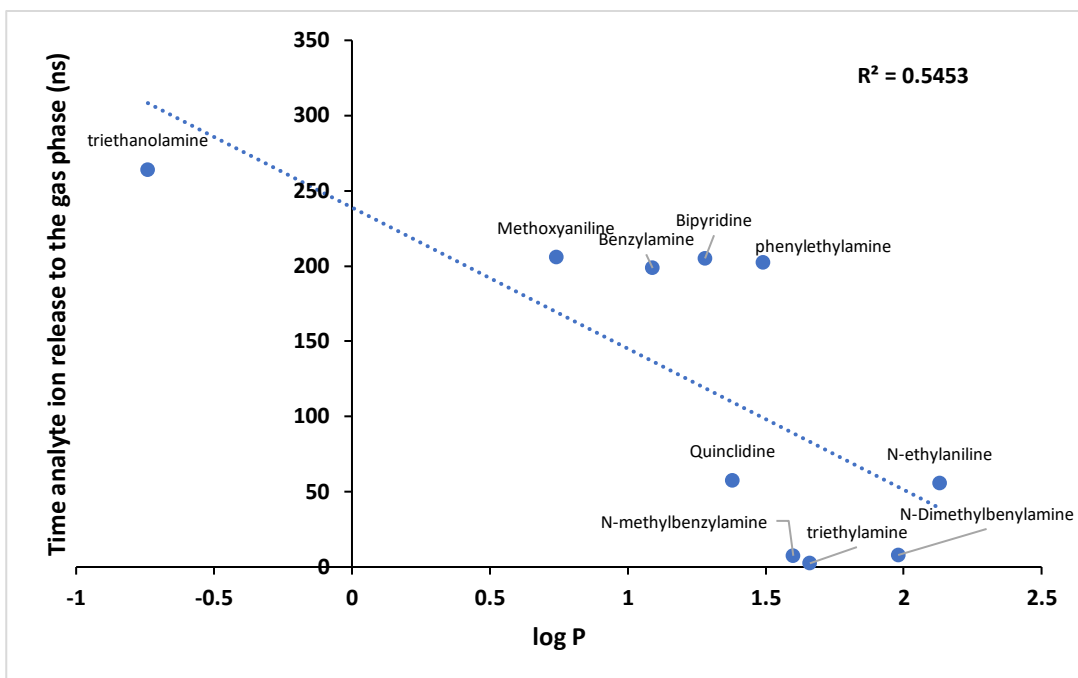


Figure 4- 3 Plot of the average time for analyte desorption into the gas phase from a field-enabled cVSSI type nanodroplet versus log P of the analyte molecule.

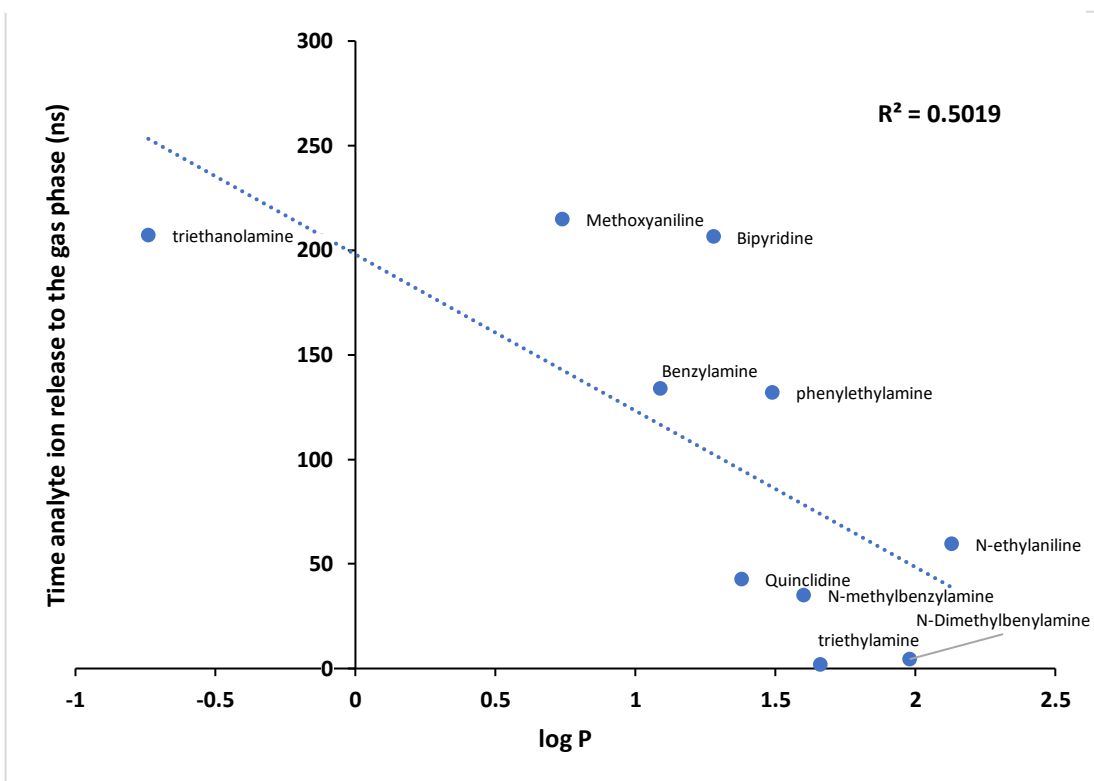


Figure 4- 4 Plot of the average time for analyte desorption into the gas phase from a cESI cVSSI type nanodroplet versus log P of the analyte molecule.

4.3 Results and Discussion

4.3.1 Comparing ion intensities for acetaminophen and dopamine.

Table 4-5 shows the ion intensities obtained for $[M+H]^+$ acetaminophen and dopamine ions. Notably for field-free cVSSI, the acetaminophen ions are suppressed relative to the dopamine ions by a factor of ~ 2 . With the addition of +1 kV voltage, the ionization efficiency of acetaminophen is still below that of dopamine (~ 1.7 fold). However, with the addition of +2 kV, the gap in ionization efficiencies is lowered to (~ 1.4 fold). When +3 kV is added to the solvents, the acetaminophen ions have a larger signal level (~ 1.02 fold). And, when +4 kV is added to the solvents, this advantage is maintained at ~ 1.04 fold. In summary, it appears that dopamine has a higher ionization efficiency under field-free and low voltage conditions. However, as the voltage is increased this advantage is erased.

Figure 4- 5 spectral intensities for $[M+H]^+$ acetaminophen and dopamine ions produced from water samples under field-free cVSSI conditions and different field-enabled cVSSI conditions.

Experimental Parameters (conditions)	[acetaminophen+H] ⁺ ion signal intensity	[dopamine+H] ⁺ ion signal intensity
Field-free cVSSI	7.40×10^6	1.46×10^7
1kV+cVSSI	1.75×10^6	2.91×10^6
2kV+cVSSI	6.17×10^6	8.41×10^6
3kV+cVSSI	6.39×10^7	6.29×10^7
4kV+cVSSI	1.94×10^8	1.87×10^8

One consideration that arises from the ionization study is whether or not the change in relative ion intensities could result from a change in ionization mechanism especially for acetaminophen. Multiple studies have shown that generally, the pK_b of the analyte ions has a strong linear correlation with the ion signal response in small molecule analysis by ESI.^{45 46} Thus ionization by ESI is thought to be very effective for species that can be observed as preformed ions in solution. The prior cVSSI source studies showed that the greatest correlation with ion intensity was pK_b for field-free cVSSI. This is also consistent with the results reported here in that the molecule with the lower pK_b (stronger base) exhibits the greater ion signal level. The primary amine in dopamine and the amide in acetaminophen are expected to have pK_b values in the 3 to 4 and 14 to 16, respectively (chemicalize.org by ChemAxon, Budapest, Hungary). Therefore, amides essentially exhibit no acid/base character in solution. Thus it is somewhat surprising that, under field free cVSSI conditions, the ionization level of acetaminophen is only ~2 fold lower than dopamine. Is it possible that another molecular property accounts for an increase in ionization efficiency of acetaminophen?

One consideration presented here is that of the effect of surface activity. Surface activity can be loosely defined as the probability of a molecule being at the surface or the droplet's interior, which can be calculated by the binomial distribution where the value falls between 1 and 0.1.¹³ Dopamine is significantly more polar than acetaminophen having respective log P values of 0.9 and 0.03. Could the difference in polarity account for the only slightly higher ionization efficiency for dopamine under field-free conditions as well as for the similarity in ionization efficiency under field enabled conditions where a large DC voltage is applied to the solution?

To begin to address these new questions, it is useful to consider which ionization mechanism (CRM or IEM) might be operative under the two different voltage conditions. It has

been proposed that low molecular weight analytes undergo ionization via the IEM in field-enabled ionization techniques similar to ESI ¹⁷. In contrast, it has been proposed that sonic spray ionization (SSI) undergoes the CRM ionization process because of the low charge density and the much larger size of the SSI droplets. ⁴⁷ Therefore, to explain the data in Table 4-5 with regard to these mechanisms, the surface activity of acetaminophen must provide an ionization boost for both the CRM and the IEM. Several researchers have suggested that this may occur. Cooks and co-workers reported in their zero-voltage work that the surface association of the small molecules they analyzed strongly influences ion signal response even though no claim as to whether or not the final stages of the progeny droplets undergo IEM or CRM is made. ¹⁰ For ESI, Fenn has described the direct influence of the surface activity on the ion evaporation from the charged droplet. ⁴⁸ Additionally, Cech and Enke have proposed a theoretical model to quantify the fraction of analyte ions that will be partitioned into the offspring droplet during fission events. ⁴⁹ Muddiman and coworkers later reported that translocating the analyte molecules to the surface allows the droplet to maximize enthalpically favorable water-water hydrogen bonds. ⁵⁰ In a remarkable study, Konermann and coworkers simulated a globular protein and showed that even such a large species could exhibit surface activity to the point of experiencing ionization by IEM from large aqueous droplets.²³ To begin to visualize the effect of surface activity on ionization efficiency for acetaminophen and dopamine, a number of MD simulation studies have been conducted.

4.3.2 Using estimated diffusion coefficient to assess ion surface activity.

From a first approximation, it can be argued that the least polar species will experience greater diffusion in the water droplet. That is, such a species will interact less with the water molecules. Because of the very large number of such interactions over time, it may be

expected that MD simulations will reveal such differences in the form of calculated diffusion coefficients. To accomplish this, it is necessary to establish a relatively short time frame over which the calculation is performed. That is, because of Coulomb repulsion, the ions will eventually reach the surface of the droplet. Therefore, the diffusion coefficients must be obtained using Equation 1 prior to reaching the droplet surface and being “frozen” in place to some degree by Coulombic force. Additionally, the diffusion coefficients must be computed after several ns to exclude any Coulomb repulsion between the two ions.

Table 4-3 shows the diffusion coefficients that have been obtained for the ions under droplet system 1 (field-free cVSSI conditions) and system 2 (field-enabled cVSSI or ESI). Under modeling parameters intended to represent field-free conditions, acetaminophen has a slightly larger (~4%) diffusion coefficient. However, when the parameters for the field-enabled conditions are employed, the diffusion coefficient for acetaminophen is smaller (~12%). Therefore, the question arises as to whether or not such a measurement accurately reflects a difference in analyte polarity.

Diffusion coefficient was selected as it is used in fluorescence studies to show decreased movement for proteins that interact with their direct environment such as lipid membrane components. That is, those proteins exhibiting greater interaction will show decreased displacement over time. Here, the concept is extended to include the “like dissolves like” idea. A much greater number of interactions of a polar compound with water molecules will essentially slow the motion of the analyte. It is noteworthy to indicate that the calculated diffusion coefficient values obtained here are $\sim 10^2 \times$ lower than those measured for Glucose (MW ~160 g/mol) in bulk, dilute solution.⁵¹ This difference likely occurs as a result of stronger ion-ion interactions that the acetaminophen and dopamine species experience in the confined nano droplet environment

containing H_3O^+ , Na^+ and OH^- ions. Additionally, the strong field charge at the surface of the droplet may limit the movement of the singly-charged analyte ions resulting in lower diffusion coefficient values. Upon further consideration, it is possible that the coefficients obtained in Table 4-3 are not realistic in that it is not possible to model the equilibrium species for the different compounds as well as the water molecules. That is, it is too computationally expensive to model the Grotthus mechanism.^{52 53 54} Thus the results obtained here should serve to aid in the development of new force fields and techniques for molecular modeling studies.

4.3.3 Modeling desorption energy for $[\text{M}+\text{H}]^+$ ions.

As mentioned above, the prior cVSSI studies suggested that for field-free cVSSI ionization efficiency primarily correlates with pK_b while the correlation shifts to $\log P$ for field-enabled cVSSI.³⁴ This could indicate that these techniques undergo ionization by different processes or a combination thereof (e.g., a combination of modes such as CRM following IEM).²⁰ Therefore, it may be useful to consider ion release efficiency from the droplet. Here, the desorption energy for $[\text{M}+\text{H}]^+$ ions of acetaminophen and dopamine is considered. Support for this consideration comes from Fenn's theoretical explanation, where it was shown that the ionization response of an analyte ion depends on (1) its surface activity and (2) the work required to remove the ion from the droplet / free energy of desorption.⁴⁸

Although desorption energy comparison should be most relevant for the IEM and thus field-enabled cVSSI, it is possible that it is still relevant for field-free cVSSI as well. Here, ions are produced via the CRM after release as a solvated ion cluster via the IEM. That is, the Rayleigh limit electric field resulting from the surface charge carriers on the nanodroplet after a degree of solvent evaporation is sufficient to cause the fission events of small, solvated ions from

the droplet surface. In short, the acetaminophen/dopamine ion may also undergo solvated ion evaporation. The analyte ion evaporation rate (k) can be explained using the transition state expression as shown in Equation 2;¹⁷

$$k = \frac{k_B T}{h} \exp\left(\frac{-\Delta G^*}{k_B T}\right) \quad (2)$$

In Equation 2, ΔG^* is the height of the activation energy barrier, h is Plank's constant, T is the temperature, and k_B is Boltzmann's constant. The free energy profile for the dynamics of small cations like NH_4^+ in the aqueous nanodroplet has been derived using the mathematical expression.⁵⁵ From the computational simulation, free energy profiles for both systems resembling field-free cVSSI and field-enabled cVSSI (Table 4-4) are obtained for both analytes. The energy profile nature is similar to a parabolic energy profile (Figure 4-2). From the calculations, it has been determined that the activation barrier for NH_4^+ ions ejected from the ESI droplet requires ~ 34 kJ/mol.⁵⁵ From the simulation data reported here, free energy estimates of ~ 24 and ~ 27 kcal/mol are obtained for the desorption of dopamine and acetaminophen ion, respectively, for the field-enabled conditions (droplet system 2) which is in close agreement with the values reported previously.⁵⁵ In the field-free cVSSI droplet system the desorption free energies for dopamine and acetaminophen are found to be ~ 69 and ~ 67 kcal/mol respectively. The free energy values obtained from our MD simulations show that the desorption energies of each analyte ion exhibit significant differences upon experiencing a significantly increased surface droplet charge.

Notably, the significant difference between field-free and field-enabled cVSSI simulations (~ 40 kcal/mole) could partially account for the ~ 10 to 20 fold difference in ionization

efficiency observed for the compounds examined with field-free cVSSI and the most efficient field-enabled cVSSI experiments (Table 4-5). It has been proposed that the activation energy barrier results from two competing factors: the role of the solvent polarization for an excess positive charge which creates an image charge tending to pull the ejected ion back toward the droplet and the inter-ionic forces due to the extra charge in the droplet which pushes the ejected ion further away from the droplet ^{56 26}. The change in free energy for the field-free and field-enabled cVSSI systems may be due to an increased image charge effect for the former system. That is, a decreased image charge may occur when the surface charge is strengthened significantly for the field-enabled cVSSI droplet system due to excess hydronium ions. Because of the higher image charge for the field free system, there are greater attractive forces towards the ejected analyte ion relative to the field-enabled system. Thus, it can be argued that the higher activation energy barrier leads to a lower ion evaporation rate and lower signal intensities in the mass spectrum.

Having described the differences for the field-free and field-enabled droplet system, it is instructive to consider the differences in free energy between the analytes from the same droplet system. Admittedly, these values for the separate compounds within individual droplet systems (Table 4-5) are essentially the same (similar to the strength of a single hydrogen bond). Thus, it would appear that the MD simulations cannot distinguish between the two compounds within each droplet system. Also, it should be mentioned that this first-approximation study may not well account for solvent cluster ion release.

4.3.4 Associating analyte log P with ion release for field-enabled cVSSI and cESI conditions.

In the prior cVSSI study, multiple regression analysis suggests that *log P* exhibits the greatest correlation with ion signal level for field-enabled cVSSI of aqueous samples.³⁴ This is not the case for ESI where *pK_b* was determined to provide the dominant association. Indeed, for field-enabled cVSSI, *log P* provided the largest R-squared (R^2) value of all single-component correlations from individual linear least-squares analyses. For ESI, no single-component correlation is observed with *log P*. That said, extensive studies performed under ESI conditions using a large number of diverse compounds have suggested that despite a strong correlation with *pK_b*, other factors such as *log P* can also correlate with ionization efficiency depending on factors as varied as solvent pH and the type of mass spectrometer employed for the analysis field^{57, 58}. Hence, in ESI, the surface activity of molecules has long been argued to benefit their ionization as more polar species are argued to prefer the core of the droplets, whereas more hydrophobic species would locate at the surface where they experience a high field^{24, 59-61}. Indeed, several models have been developed to account for surface activity in the ionization of different molecules.⁶²⁻⁶⁴ The increased ionization of surface-active molecules in ESI would arise from their localization in the droplet as the ions would be more prone to be ejected in the ion-producing progeny droplets as well as their overall decreased solvation energies^{24, 65}. Indeed, this was the purpose of the studies presented above. They represent an attempt to model the process whereby a preformed ion could be readily expelled from an ESI droplet due to rapid surface positioning by Coulomb forces and release by the same.

Overall, the modeling presented above provided only provided limited explanations for the observed ionization results for acetaminophen and dopamine. For example,

the diffusion coefficients do not correlate with $\log P$ values and the desorption free energy is essentially the same for the different compounds within individual droplet systems. So, a question arises as to whether or not any MD simulation strategy can truly capture $\log P$ ionization effects. Additionally, can such methods be further used to distinguish differences between field-enabled cVSSI and ESI. To consider $\log P$ ionization effects, a MD strategy was devised using 10 different compounds having varying $\log P$ characteristics. In these studies, MD simulations were performed until the release of the ion from the droplet was observed.

To compare the MD simulations intended to represent field-enabled cVSSI with those representing ESI, it is necessary to distinguish the systems. As mentioned above, this is accomplished using two different water droplet systems. For field-enabled cVSSI, experiments have shown that very efficient ionization occurs at voltages below the onset of a Taylor cone and microdroplet production by Coulomb forces¹³. Additionally, these experiments have shown that field-enabled cVSSI dissipates charge at the emitter tip and thus overcomes the corona discharge problem in negative ion mode analyses. Therefore, it can be argued that field-enabled cVSSI produces droplets of net charge that are higher than field-free cVSSI (because of increased ion signal level observations) and yet smaller than ESI (because of charge dissipation and voltage onset observations). Thus, ESI has been modeled using droplets of higher net charge. For these simulation studies, 2.5 nm-size water droplets containing each of the analyte ions with 11 hydronium ions and 8 hydronium ions representing ESI and field-enabled cVSSI conditions, respectively, were used.

Figure 4-3 and Figure 4-4 show the correlation obtained for the ion release time as a function of $\log P$ value for the 10 compounds. The R^2 value for this regression analysis is 0.55. This represents a reasonable correlation considering the single-component correlations

obtained from experimental values are all well below this value. When the droplet system is changed to that for ESI, the correlation drops to 0.50 as shown in Figure 4-4. These results are somewhat consistent with the prior study where multiple regression analysis performed on experimental results showed a primary association for $\log P$ with ionization efficiency for field-enabled cVSSI but not for ESI.³⁴ That is, these preliminary results seem to indicate that $\log P$ is not as definitive in forming ions by ESI for this theoretical treatment as well as for the prior experimental results.

To explain the results shown in Figures 4-3 and 4-4, the factors of ion translocation and expulsion are considered. The lower charge density associated with the field-enabled cVSSI conditions could decrease the effect of rapid positioning due to Coulomb repulsion of the preformed ion at the droplet surface (and thus enrichment to some degree). Additionally, the decreased surface field would affect field-induced ion evaporation events leading to longer droplet drying times. In this environment, the surface activity could provide more of an advantage to ionization leading to the $\log P$ associations obtained for field-enabled cVSSI experiments.

Furthermore, it is instructive to consider the sign of the $\log P$ association with ion signal intensities from the multiple regression analysis for the aqueous experiments. Besides being the dominant association for field-enabled cVSSI, the correlation is positive. This can be argued as being somewhat expected as the increased hydrophobicity of the molecules should result in more significant surface association and thus ionization. When the same analyte molecules are dissolved in and examined from methanol samples, the field-enabled cVSSI correlations are negative, although the beta coefficient values are not significant. In a more recent study where an acetonitrile solvent system was used (Chapter 3), the beta coefficient values for $\log P$ association are significant and negative in both field-enabled cVSSI and ESI. This raises the exciting

possibility that the hydrophobic molecules have somewhat of a relative preference for droplet retention by the organic solvent compared with the aqueous droplets. To better understand the underlying reasons for these observations, extensive MD simulation studies in different organic droplet systems will be helpful.

4.4 Conclusions

The effects of compound polarity on ionization by cVSSI techniques have been investigated by cVSSI-MS experiments and MD techniques. Overall, compound translocation to the droplet surface was not observed to correlate with compound log P values. It is suggested that this may occur in part due to the compound existing as the ion for the duration of the simulation. Because the amide group is a very weak base, it can be argued that future simulations should include it as a neutral compound. It would be very interesting to observe whether the neutral acetaminophen reaches the surface of a droplet faster than the dopamine ions considering that translocation of the latter is somewhat Coulombically driven. The calculation of free energy of desorption provides some insight into the suppression of ion signals in field-free cVSSI experiments; however, the calculation does not distinguish the two compounds within the separate water systems studied (representing field-free and field-enabled conditions). Finally, an association is observed for the release of preformed ions (10 compounds) and log P values using MD simulations of analytes in water droplets. This correlation is stronger for field-enabled cVSSI versus ESI models which is somewhat consistent with prior experimental results (Chapter 2). Overall, these studies provide some insight into the effect of log P and ionization efficiency and serve as the foundation for future studies. For example, because experimental significant associations are observed for log P and ionization efficiency for compounds in organic solvents (methanol and acetonitrile), more insight can be gained by modeling these systems. Such work is

important considering the variety of separation techniques and solvents used in LC-MS experiments of important molecular mixtures such as those encountered in metabolomics studies.

4.5 References

- (1) Wang, H.; Liu, J.; Cooks, R. G.; Ouyang, Z. Paper spray for direct analysis of complex mixtures using mass spectrometry. *Angew Chem Int Ed Engl* **2010**, *49* (5), 877-880. DOI: 10.1002/anie.200906314.
- (2) Li, A.; Wang, H.; Ouyang, Z.; Cooks, R. G. Paper spray ionization of polar analytes using non-polar solvents. *Chemical Communications* **2011**, *47* (10), 2811-2813, DOI: 10.1039/C0CC05513A. DOI: 10.1039/C0CC05513A.
- (3) Teunissen, S. F.; Eberlin, M. N. Transferring Ions from Solution to the Gas Phase: The Two Basic Principles. *J. Am. Soc. Mass Spectrom.* **2017**, *28*, 2255-2261.
- (4) Takats, Z.; Wiseman, J. M.; Gologan, B.; Cooks, R. G. Mass spectrometry sampling under ambient conditions with desorption electrospray ionization. *Science* **2004**, *306* (5695), 471-473. DOI: 10.1126/science.1104404.
- (5) Song, L.; You, Y.; Evans-Nguyen, T. Surface Acoustic Wave Nebulization with Atmospheric-Pressure Chemical Ionization for Enhanced Ion Signal. *Anal Chem* **2019**, *91* (1), 912-918. DOI: 10.1021/acs.analchem.8b03927.
- (6) Blakley, C. R.; Carmody, J. J.; Vestal, M. L. A new soft ionization technique for mass spectrometry of complex molecules. *Journal of the American Chemical Society* **1980**, *102* (18), 5931-5933. DOI: 10.1021/ja00538a050.
- (7) Blakley, C. R.; Vestal, M. L. Thermospray interface for liquid chromatography/mass spectrometry. *Analytical Chemistry* **1983**, *55* (4), 750-754. DOI: 10.1021/ac00255a036.
- (8) Hirabayashi, A.; Sakairi, M.; Koizumi, H. Sonic spray mass spectrometry. *Anal Chem* **1995**, *67* (17), 2878-2882. DOI: 10.1021/ac00113a023.
- (9) Pagnotti, V. S.; Chubaty, N. D.; McEwen, C. N. Solvent assisted inlet ionization: an ultrasensitive new liquid introduction ionization method for mass spectrometry. *Anal Chem* **2011**, *83* (11), 3981-3985. DOI: 10.1021/ac200556z.
- (10) Wlekinski, M.; Li, Y.; Bag, S.; Sarkar, D.; Narayanan, R.; Pradeep, T.; Cooks, R. G. Zero Volt Paper Spray Ionization and Its Mechanism. *Anal Chem* **2015**, *87* (13), 6786-6793. DOI: 10.1021/acs.analchem.5b01225.
- (11) Li, X.; Attanayake, K.; Valentine, S. J.; Li, P. Vibrating Sharp-edge Spray Ionization (VSSI) for voltage-free direct analysis of samples using mass spectrometry. *Rapid Commun Mass Spectrom* **2018**. DOI: 10.1002/rcm.8232.
- (12) Ranganathan, N.; Li, C.; Suder, T.; Karanji, A. K.; Li, X. J.; He, Z. Y.; Valentine, S. J.; Li, P. Capillary Vibrating Sharp-Edge Spray Ionization (cVSSI) for Voltage-Free Liquid Chromatography-Mass Spectrometry. *Journal of the American Society for Mass Spectrometry* **2019**, *30* (5), 824-831, Article. DOI: 10.1007/s13361-019-02147-0.
- (13) Li, C.; Attanayake, K.; Valentine, S. J.; Li, P. Facile Improvement of Negative Ion Mode Electrospray Ionization Using Capillary Vibrating Sharp-Edge Spray Ionization. *Anal Chem* **2020**, *92* (3), 2492-2502. DOI: 10.1021/acs.analchem.9b03983.

- (14) Majuta, S. N.; Li, C.; Jayasundara, K.; Kiani Karanji, A.; Attanayake, K.; Ranganathan, N.; Li, P.; Valentine, S. J. Rapid Solution-Phase Hydrogen/Deuterium Exchange for Metabolite Compound Identification. *Journal of the American Society for Mass Spectrometry* **2019**, *30* (6), 1102-1114. DOI: 10.1007/s13361-019-02163-0.
- (15) Zilch, L. W.; Maze, J. T.; Smith, J. W.; Ewing, G. E.; Jarrold, M. F. Charge separation in the aerodynamic breakup of micrometer-sized water droplets. *J Phys Chem A* **2008**, *112* (51), 13352-13363. DOI: 10.1021/jp806995h.
- (16) Kebarle, P.; Tang, L. From ions in solution to ions in the gas phase - the mechanism of electrospray mass spectrometry. *Analytical Chemistry* **1993**, *65* (22), 972A-986A. DOI: 10.1021/ac00070a001.
- (17) Iribarne, J. V. On the evaporation of small ions from charged droplets. *The Journal of Chemical Physics* **1976**, *64* (6). DOI: 10.1063/1.432536.
- (18) Dole, M.; Mack, L. L.; Hines, R. L. MOLECULAR BEAMS OF MACROIONS. *Journal of Chemical Physics* **1968**, *49* (5), 2240-&, Article. DOI: 10.1063/1.1670391.
- (19) Kebarle, P.; Peschke, M. On the mechanisms by which the charged droplets produced by electrospray lead to gas phase ions. *Analytica Chimica Acta* **2000**, *406* (1), 11-35, Article. DOI: 10.1016/s0003-2670(99)00598-x.
- (20) Hogan, C. J., Jr.; Carroll, J. A.; Rohrs, H. W.; Biswas, P.; Gross, M. L. Combined charged residue-field emission model of macromolecular electrospray ionization. *Anal Chem* **2009**, *81* (1), 369-377. DOI: 10.1021/ac8016532.
- (21) Consta, S.; Malevanets, A. Manifestations of Charge Induced Instability in Droplets Effected by Charged Macromolecules. *Physical Review Letters* **2012**, *109* (14), 148301. DOI: 10.1103/PhysRevLett.109.148301.
- (22) Konermann, L.; Rodriguez, A. D.; Liu, J. On the Formation of Highly Charged Gaseous Ions from Unfolded Proteins by Electrospray Ionization. *Analytical Chemistry* **2012**, *84* (15), 6798-6804. DOI: 10.1021/ac301298g.
- (23) Aliyari, E.; Konermann, L. Formation of Gaseous Proteins via the Ion Evaporation Model (IEM) in Electrospray Mass Spectrometry. *Analytical Chemistry* **2020**, *92* (15), 10807-10814. DOI: 10.1021/acs.analchem.0c02290.
- (24) Kebarle, P.; Verkerk, U. H. ELECTROSPRAY: FROM IONS IN SOLUTION TO IONS IN THE GAS PHASE, WHAT WE KNOW NOW. *Mass Spectrometry Reviews* **2009**, *28* (6), 898-917, Review. DOI: 10.1002/mas.20247.
- (25) Kwan, V.; O'Dwyer, R.; Laur, D.; Tan, J.; Consta, S. Relation between Ejection Mechanism and Ion Abundance in the Electric Double Layer of Droplets. *The Journal of Physical Chemistry A* **2021**, *125* (14), 2954-2966. DOI: 10.1021/acs.jpca.1c01522.
- (26) Consta, S. Fragmentation reactions of charged aqueous clusters. *Journal of Molecular Structure: THEOCHEM* **2002**, *591* (1-3), 131-140.
- (27) Konermann, L.; Metwally, H.; Duez, Q.; Peters, I. Charging and supercharging of proteins for mass spectrometry: recent insights into the mechanisms of electrospray ionization. *Analyst* **2019**, *144* (21), 6157-6171.
- (28) Znamenskiy, V.; Marginean, I.; Vertes, A. Solvated Ion Evaporation from Charged Water Nanodroplets. *The Journal of Physical Chemistry A* **2003**, *107* (38), 7406-7412. DOI: 10.1021/jp034561z.
- (29) Higashi, H.; Tokumi, T.; Hogan, C. J.; Suda, H.; Seto, T.; Otani, Y. Simultaneous ion and neutral evaporation in aqueous nanodrops: experiment, theory, and molecular dynamics simulations. *Phys. Chem. Chem. Phys.* **2015**, *17* (24), 15746-15755.

- (30) Beveridge, R.; Migas, L. G.; Das, R. K.; Pappu, R. V.; Kriwacki, R. W.; Barran, P. E. Ion mobility mass spectrometry uncovers the impact of the patterning of oppositely charged residues on the conformational distributions of intrinsically disordered proteins. *Journal of the American Chemical Society* **2019**, *141* (12), 4908-4918.
- (31) Porrini, M.; Rosu, F.; Rabin, C.; Darré, L.; Gómez, H.; Orozco, M.; Gabelica, V. Compaction of duplex nucleic acids upon native electrospray mass spectrometry. *ACS central science* **2017**, *3* (5), 454-461.
- (32) Kim, D.; Wagner, N.; Wooding, K.; Clemmer, D. E.; Russell, D. H. Ions from Solution to the Gas Phase: A Molecular Dynamics Simulation of the Structural Evolution of Substance P during Desolvation of Charged Nanodroplets Generated by Electrospray Ionization. *Journal of the American Chemical Society* **2017**, *139* (8), 2981-2988, Article. DOI: 10.1021/jacs.6b10731.
- (33) Kondalaji, S. G.; Khakinejad, M.; Valentine, S. J. Comprehensive Peptide Ion Structure Studies Using Ion Mobility Techniques: Part 3. Relating Solution-Phase to Gas-Phase Structures. *Journal of the American Society for Mass Spectrometry* **2018**, *29* (8), 1665-1677, Article. DOI: 10.1007/s13361-018-1996-9.
- (34) Jayasundara, K. U.; Li, C.; DeBastiani, A.; Sharif, D.; Li, P.; Valentine, S. J. Physicochemical Property Correlations with Ionization Efficiency in Capillary Vibrating Sharp-Edge Spray Ionization (cVSSI). *Journal of the American Society for Mass Spectrometry* **2021**, *32* (1), 84-94. DOI: 10.1021/jasms.0c00100.
- (35) Martínez, L.; Andrade, R.; Birgin, E.; Martínez, J. M. PACKMOL: A package for building initial configurations for molecular dynamics simulations. *Journal of Computational Chemistry* **2009**, *30*, 2157-2164. DOI: 10.1002/jcc.21224.
- (36) *Gaussian 09*; Gaussian, Inc.: Wallingford CT, 2009. (accessed).
- (37) Vega, C.; Miguel, E. d. Surface tension of the most popular models of water by using the test-area simulation method. *The Journal of Chemical Physics* **2007**, *126* (15), 154707. DOI: 10.1063/1.2715577.
- (38) Chen, W.; Wallace, J. A.; Yue, Z.; Shen, J. K. Introducing titratable water to all-atom molecular dynamics at constant pH. *Biophys J* **2013**, *105* (4), L15-L17. DOI: 10.1016/j.bpj.2013.06.036 PubMed.
- (39) Vanommeslaeghe, K.; MacKerell, A. D. Automation of the CHARMM General Force Field (CGenFF) I: Bond Perception and Atom Typing. *Journal of Chemical Information and Modeling* **2012**, *52* (12), 3144-3154. DOI: 10.1021/ci300363c.
- (40) Oh, M. I.; Consta, S. Charging and Release Mechanisms of Flexible Macromolecules in Droplets. *J. Am. Soc. Mass Spectrom.* **2017**, *28* (11), 2262-2279. DOI: 10.1007/s13361-017-1754-4.
- (41) Konermann, L.; Metwally, H.; McAllister, R. G.; Popa, V. How to run molecular dynamics simulations on electrospray droplets and gas phase proteins: Basic guidelines and selected applications. *Methods* **2018**, *144*, 104-112. DOI: <https://doi.org/10.1016/j.ymeth.2018.04.010>.
- (42) Hsin, J.; Arkhipov, A.; Yin, Y.; Stone, J.; Schulten, K. Using VMD: An introductory tutorial. *Current protocols in bioinformatics / editorial board, Andreas D. Baxevanis ... [et al.]* **2008**, Chapter 5, Unit 5.7. DOI: 10.1002/0471250953.bi0507s24.
- (43) Comer, J.; Gumbart, J. C.; Hénin, J.; Lelièvre, T.; Pohorille, A.; Chipot, C. The Adaptive Biasing Force Method: Everything You Always Wanted To Know but Were Afraid To Ask. *The Journal of Physical Chemistry B* **2015**, *119* (3), 1129-1151. DOI: 10.1021/jp506633n.

- (44) Comer, J.; Phillips, J.; Schulten, K.; Chipot, C. Multiple-Replica Strategies for Free-Energy Calculations in NAMD: Multiple-Walker Adaptive Biasing Force and Walker Selection Rules. *J. Chem. Theory Comput.* **2014**, *10*, 5276-5285. DOI: 10.1021/ct500874p.
- (45) Ehrmann, B. M.; Henriksen, T.; Cech, N. B. Relative importance of basicity in the gas phase and in solution for determining selectivity in electrospray ionization mass spectrometry. *J Am Soc Mass Spectrom* **2008**, *19* (5), 719-728. DOI: 10.1016/j.jasms.2008.01.003.
- (46) Oss, M.; Kruve, A.; Herodes, K.; Leito, I. Electrospray ionization efficiency scale of organic compounds. *Anal Chem* **2010**, *82* (7), 2865-2872. DOI: 10.1021/ac902856t.
- (47) Takats, Z.; Nanita, S. C.; Cooks, R. G.; Schlosser, G.; Vekey, K. Amino acid clusters formed by sonic spray ionization. *Anal Chem* **2003**, *75* (6), 1514-1523. DOI: 10.1021/ac0260793.
- (48) Fenn, J. B. Ion formation from charged droplets: roles of geometry, energy, and time. *J. Am. Soc. Mass Spectrom.* **1993**, *4* (7), 524-535. DOI: [https://doi.org/10.1016/1044-0305\(93\)85014-O](https://doi.org/10.1016/1044-0305(93)85014-O).
- (49) Cech, N. B.; Enke, C. G. Effect of affinity for droplet surfaces on the fraction of analyte molecules charged during electrospray droplet fission. *Analytical chemistry* **2001**, *73* (19), 4632-4639.
- (50) Null, A. P.; Nepomuceno, A. I.; Muddiman, D. C. Implications of Hydrophobicity and Free Energy of Solvation for Characterization of Nucleic Acids by Electrospray Ionization Mass Spectrometry. *Analytical Chemistry* **2003**, *75* (6), 1331-1339. DOI: 10.1021/ac026217o.
- (51) Höber, R. *Physical Chemistry of Cells and Tissues*; Blakiston, 1948.
- (52) Cukierman, S. Et tu, Grotthuss! and other unfinished stories. *Biochimica et Biophysica Acta (BBA) - Bioenergetics* **2006**, *1757* (8), 876-885. DOI: <https://doi.org/10.1016/j.bbabi.2005.12.001>.
- (53) Nagle, J. F.; Morowitz, H. J. Molecular mechanisms for proton transport in membranes. *Proc Natl Acad Sci U S A* **1978**, *75* (1), 298-302, Research Support, U.S. Gov't, Non-P.H.S. DOI: 10.1073/pnas.75.1.298 [doi].
- (54) Nagle, J. F.; Mille, M.; Morowitz, H. J. Theory of hydrogen bonded chains in bioenergetics. *J. Chem. Phys.* **1980**, *72*, 3959-3971. DOI: 10.1063/1.439674.
- (55) Ahadi, E.; Konermann, L. Ejection of Solvated Ions from Electrosprayed Methanol/Water Nanodroplets Studied by Molecular Dynamics Simulations. *Journal of the American Chemical Society* **2011**, *133* (24), 9354-9363. DOI: 10.1021/ja111492s.
- (56) Konermann, L.; Ahadi, E.; Rodriguez, A. D.; Vahidi, S. Unraveling the Mechanism of Electrospray Ionization. *Analytical Chemistry* **2013**, *85* (1), 2-9, Article. DOI: 10.1021/ac302789c.
- (57) Kiontke, A.; Oliveira-Birkmeier, A.; Opitz, A.; Birkemeyer, C. Electrospray Ionization Efficiency Is Dependent on Different Molecular Descriptors with Respect to Solvent pH and Instrumental Configuration. *PLoS One* **2016**, *11* (12), e0167502. DOI: 10.1371/journal.pone.0167502.
- (58) Kiontke, A.; Billig, S.; Birkemeyer, C. Response in Ambient Low Temperature Plasma Ionization Compared to Electrospray and Atmospheric Pressure Chemical Ionization for Mass Spectrometry. *Int J Anal Chem* **2018**, *2018*, 5647536. DOI: 10.1155/2018/5647536.
- (59) Pape, J.; Vikse, K. L.; Janusson, E.; Taylor, N.; McIndoe, J. S. Solvent effects on surface activity of aggregate ions in electrospray ionization. *International Journal of Mass Spectrometry* **2014**, *373*, 66-71, Article. DOI: 10.1016/j.ijms.2014.09.009.

- (60) Cech, N. B.; Enke, C. G. Practical implications of some recent studies in electrospray ionization fundamentals. *Mass Spectrometry Reviews* **2001**, *20* (6), 362-387, Review. DOI: 10.1002/mas.10008.
- (61) Kobarle, P. A brief overview of the present status of the mechanisms involved in electrospray mass spectrometry. *Journal of Mass Spectrometry* **2000**, *35* (7), 804-817, Article. DOI: 10.1002/1096-9888(200007)35:7<804::aid-jms22>3.0.co;2-q.
- (62) Zhou, S. L.; Cook, K. D. A mechanistic study of electrospray mass spectrometry: Charge gradients within electrospray droplets and their influence on ion response. *Journal of the American Society for Mass Spectrometry* **2001**, *12* (2), 206-214, Article. DOI: 10.1016/s1044-0305(00)00213-0.
- (63) Tang, L.; Kobarle, P. DEPENDENCE OF ION INTENSITY IN ELECTROSPRAY MASS-SPECTROMETRY ON THE CONCENTRATION OF THE ANALYTES IN THE ELECTROSPRAYED SOLUTION. *Analytical Chemistry* **1993**, *65* (24), 3654-3668, Article. DOI: 10.1021/ac00072a020.
- (64) Enke, C. G. A predictive model for matrix and analyte effects in electrospray ionization of singly-charged ionic analytes. *Analytical Chemistry* **1997**, *69* (23), 4885-4893, Article. DOI: 10.1021/ac970095w.
- (65) Rohner, T. C.; Lion, N.; Girault, H. H. Electrochemical and theoretical aspects of electrospray ionisation. *Physical Chemistry Chemical Physics* **2004**, *6* (12), 3056-3068, Review. DOI: 10.1039/b316836k.

5. Future Directions

5.1. Improving the ionization efficiency of cVSSI with nonpolar aprotic solvent compositions

The effects of protic versus aprotic solvent systems on ionization efficiency by field-free and field-enabled cVSSI along with the ESI has been described in Chapters 2 and 3. These proof-of-principle experiments were based on the polar solvents water, methanol, and acetonitrile. Notably, the latter system showed a remarkable ability to produce ions from without the aid of an applied voltage (Chapter 3). Indeed, for most of the compounds examined, an increased ionization efficiency was observed when operated without the voltage in positive ion mode. Additionally, the aprotic solvent system was markedly different in that no association of ionization efficiency was found with log of the base dissociation constant (pK_b) of the analyte; rather the strongest associations were observed for the log of the partition coefficient ($\log P$) proton affinity (PA). For the protic solvents, a unique association of $\log P$ with ionization efficiency was observed for field-enabled cVSSI. This association was further explored with molecular dynamics (MD) simulations where it was shown that such an approach can capture a relationship between ion release from a water droplet and compound polarity. This new information is important to continue to develop cVSSI as a powerful new ionization technique that may be tailored to individual analyses. To further flesh out the capabilities of cVSSI it would be helpful to study the effect of apolar solvents on cVSSI performance.

It has been shown that the electrical breakdown that occurs in negative ion mode can be diminished in the presence of chlorinated solvents because of their propensity for electron capture. Thus, for

some highly sensitive measurements, it is important to use such a solvent with electron capture capability to combat the instability created by the corona discharge in negative ion mode. The propensity for electron capture by chlorinated solvents increases with highly chlorinated species like chloroform compared to, for example, dichloromethane, 1,2-dichloroethane, and carbon tetrachloride ¹. Also, it has been shown that the solvents which have high solution dielectric constants greatly influence the stability of multiply-charged ions. Cole and Harrata suggested this may be due to the greater charge separation (cation and anion) occurring at the Taylor cone or the influence on the “electrophoretic” mechanism of droplet charging in ESI ¹. Thus, the dielectric constant of the solvent influences its ability to disperse the attractive forces between cations and anions. This can increase the degree of solution-phase charge separation and ion solvation in the charged-droplet formation which will eventually increase the droplet charging with either predominantly anions or cations. Even though the work performed by Cole and Harrata focused on negative ion mode studies and multiply-charged ions, it was suggested that if the solvent dielectric constant is low, even singly-charged species will be formed in low yield because of the minimal dissociation of ion pairs occurring in solution.

This minimal dissociation of ion pairs may occur more predominantly in field-free ionization conditions, unlike field-enabled conditions. This may be due to the absence of the counter electrode or the absence of electrophoretic processes at the capillary tip. As described in Chapter 1, in field-free ionization conditions, the generated charged droplet contains cations and anions, which may influence the total droplet charge. Also, according to the “bag mechanism” proposed by Jarrold and coworkers, when the aerodynamic breakup of a droplet occurs, most of the cations and anions are separated into the annulus and bag ². Thus, efficient charge separation in field-free ionization is vital to produce a greater yield of highly-charged positive or negative ions. Therefore,

as described by Cole and Harrata, solvents with higher dielectric constant like acetonitrile can be beneficial for field-free cVSSI. This was demonstrated for positive ion mode analyses in Chapter 3. However, for negative ion mode, the ion intensity signals were very diminished for field-free cVSSI. Incorporating highly chlorinated solvents like chloroform with acetonitrile may positively influence the charge buildup within droplets in field-free cVSSI for negative ion mode studies. Also, such a solvent system may significantly enhance the ionization efficiency of field-enabled cVSSI over that of ESI beyond that observed in work published by Li and coworkers.³ Utilizing this chlorinated mixture, an acetonitrile solvent system may be beneficial for small metabolite analysis as well as large molecules in negative ion mode.

5.2. Investigating the acetonitrile solvent effect on ionization efficiency with molecular dynamics (MD) simulations.

Our previous MD simulation studies described in Chapter 4 show that it is a powerful tool for studying the dynamics that occur for charged droplets. All the simulation studies reported in Chapter 4 were for water droplet systems. These studies demonstrated that MD simulations could capture some of the effects that were observed for cVSSI techniques. Therefore, it may be beneficial to perform MD simulations for acetonitrile droplets to better understand the experimental results reported in Chapter 3.

The MD simulations can be conducted similar to those described in Chapter 4. Here, droplet makeup would be approximated by increasing the number of surface charge carriers from field-free cVSSI, to field-enabled cVSSI, to ESI conditions. The same types of studies can be conducted. That is, tracking ion translocation to the surface of the droplet can be examined. One question that may be addressed by monitoring the motion of the ions is whether or not the MD

simulations can capture the switch from direct to inverse correlation of ionization efficiency with $\log P$ observed for positive ions in Chapter 4. That is, the MD simulations should show that the field-free conditions promote earlier release of non-polar compounds; the droplets with higher charge density should promote increased release of the polar compounds. Because nanodroplet modeling of acetonitrile is essentially non-existent, the work can be performed iteratively where the droplet composition is changed (e.g., charge density) to best match experimental results. This will lay the foundation for further MD simulations including those to be performed for other solvent systems.

One interesting area to consider is that of energy of desorption. Here experiments can be performed as described previously where the free energy profile is generated up to the transition state and ion release from the droplet. That said, because the major correlator with ionization efficiency from acetonitrile was found to be PA, it may be more useful to monitor the neutral compounds. Such a process suggests gas-phase reactions are responsible for ion production. Such reaction can occur at the surface of the droplet as the compound “steals” a proton from a charge carrier in the ion evaporation mechanism (IEM). The process can also occur via the CRM where the charge carrier and the analyte compete for the charge at the end stage of the drying droplet. Therefore, it may be useful to model the behavior of the neutral compounds within the droplet systems.

A treatment of preformed ions can also be considered. Acetonitrile being a polar aprotic solvent with the lone pair on the nitrogen atom offers the unique opportunity to consider the role of the solvent dipole in ion solvation. An intriguing result is that pK_b shows a significant correlation with ionization efficiency in negative ion mode for field-free and field-enabled cVSSI (Chapter 4)., MD simulations can provide information about how the solution phase solvation occurs via

the preferred orientation of the solvent dipole. Additionally, the simulations can test the theory of how such solvation affects the ionization efficiency as suggested Cole and Harrata.¹

5.3. Microwave-assisted heating for efficient droplet evaporation in field-free ionization

Mass Spectrometry

In field-free ionization, the mechanical disintegration of bulk liquid leads to a statistical ionization of the droplets as described by Dodd⁴. According to Dodd's mechanism, the droplets created are mostly of lower charge and are micrometer sized. Introducing precursor droplets to a heated environment is one approach to enhance droplet disintegration that is different from Coulombically driven fissioning. Such an approach can lead to nanometer-sized droplets which undergo an efficient droplet desolvation process. Field-free ionization techniques like solvent-assisted inlet ionization (SAII) and droplet assisted inlet ionization (DAII) have shown that the use of high temperature via a heated inlet capillary of a mass spectrometer enhances the formation of ions^{5 6} Moreover, a new field-free ionization technique called aerodynamic thermal breakup droplet ionization (ATBDI) has shown the importance of introducing a thermal environment to the spray plume⁷.

Thus, the desolvation or evaporation of spray-based droplets and the creation of smaller droplets significantly influences sample ionization efficiency by transmitting ions from the solution phase to the gas phase environment of a mass analyzer. Also, the greater solvent evaporation within the spray plume can be beneficial for reducing the formation of ion solvent clusters. All of the techniques mentioned above utilized a conductive heating process. But conductive heating has some limitations in terms of localized, controlled heating delivery, rapid contactless heating, and uniform heating. These limitations can be overcome by incorporating microwave (MW) heating

in a spray plume⁸. Also, utilizing microwaves will be beneficial for substrate-based field-free ionization techniques like paper spray ionization (PSI)⁹, surface acoustic nebulization ionization (SAWN)¹⁰ and capillary vibrating sharp-edge spray ionization (cVSSI)¹¹. One of the primary goals of developing field-free ionization sources is to potentially couple them with field-portable or miniaturized mass spectrometers. Thus, a low-power input microwave applicator that can supply localized radiation to the spray plume would enhance these field-free ion sources' potential for application in field portable or miniaturized mass spectrometers. A MW applicator that can operate with low input power and is smaller in size can be utilized to heat a droplet plume^{12 13}. The microwave-assisted heating methodology can easily be tested using field free cVSSI-MS. Here, ionization efficiencies can be monitored as a function of input power. Additionally, the unfolding transitions of proteins can be monitored with microwave -assisted heating to provide an estimate of droplet temperatures. One embodiment of the proposed microwave applicator as incorporated with a cVSSI-MS system is illustrated in Figure 1.

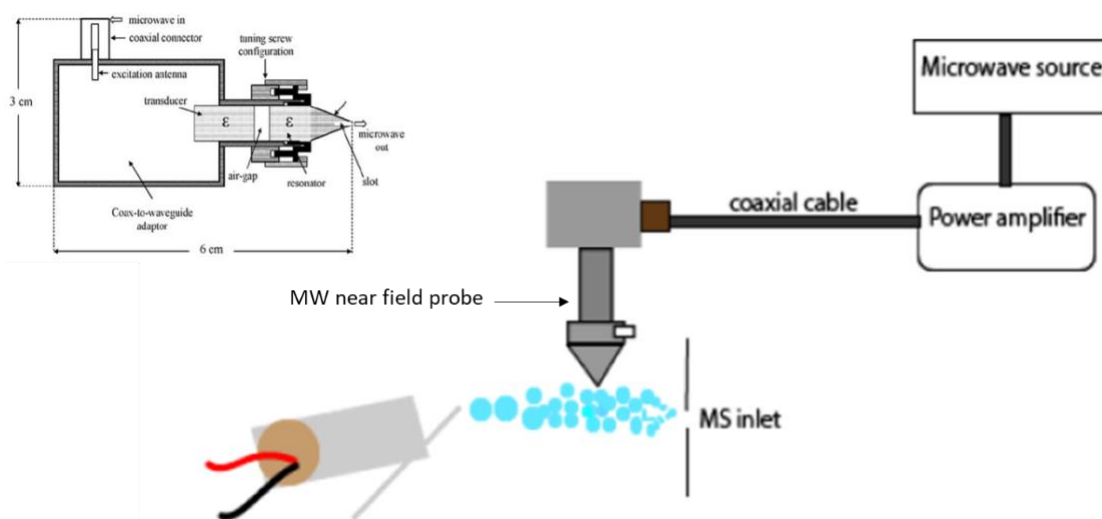


Figure 5- 1 Schematic diagram of the instrumental platform to apply microwave assisted heating into the spray plume

5.4 References

- (1) Cole, R. B.; Harrata, A. K. Solvent effect on analyte charge state, signal intensity, and stability in negative ion electrospray mass spectrometry; implications for the mechanism of negative ion formation. *J. Am. Soc. Mass Spectrom.* **1993**, *4* (7), 546-556. DOI: [https://doi.org/10.1016/1044-0305\(93\)85016-Q](https://doi.org/10.1016/1044-0305(93)85016-Q).
- (2) Zilch, L. W.; Maze, J. T.; Smith, J. W.; Ewing, G. E.; Jarrold, M. F. Charge separation in the aerodynamic breakup of micrometer-sized water droplets. *J Phys Chem A* **2008**, *112* (51), 13352-13363. DOI: 10.1021/jp806995h.
- (3) Li, C.; Attanayake, K.; Valentine, S. J.; Li, P. Facile Improvement of Negative Ion Mode Electrospray Ionization Using Capillary Vibrating Sharp-Edge Spray Ionization. *Anal Chem* **2020**, *92* (3), 2492-2502. DOI: 10.1021/acs.analchem.9b03983.
- (4) Dodd, E. E. The Statistics of Liquid Spray and Dust Electrification by the Hopper and Laby Method. *Journal of Applied Physics* **1953**, *24*, 73-80. DOI: 10.1063/1.1721137.
- (5) Apsokardu, M. J.; Kerecman, D. E. Ion formation in droplet-assisted ionization. **2021**, *35 Suppl 1*, e8227.
- (6) McEwen, C. N.; Pagnotti, V. S.; Inutan, E. D.; Trimpin, S. New paradigm in ionization: multiply charged ion formation from a solid matrix without a laser or voltage. *Anal Chem* **2010**, *82* (22), 9164-9168. DOI: 10.1021/ac102339y.
- (7) Pervukhin, V. V.; Sheven, D. G. Aerodynamic Thermal Breakup Droplet Ionization in Mass Spectrometric Drug Analysis. *Journal of the American Society for Mass Spectrometry* **2020**, *31* (5), 1074-1082. DOI: 10.1021/jasms.0c00016.
- (8) Palma, V.; Barba, D.; Cortese, M.; Martino, M.; Renda, S.; Meloni, E. Microwaves and Heterogeneous Catalysis: A Review on Selected Catalytic Processes. *Catalysts* **2020**, *10*, 246. DOI: 10.3390/catal10020246.
- (9) Wleklinski, M.; Li, Y.; Bag, S.; Sarkar, D.; Narayanan, R.; Pradeep, T.; Cooks, R. G. Zero Volt Paper Spray Ionization and Its Mechanism. *Anal Chem* **2015**, *87* (13), 6786-6793. DOI: 10.1021/acs.analchem.5b01225.
- (10) Kiontke, A.; Roudini, M.; Billig, S.; Fakhfour, A.; Winkler, A.; Birkemeyer, C. Surface acoustic wave nebulization improves compound selectivity of low-temperature plasma ionization for mass spectrometry. *Scientific Reports* **2021**, *11*. DOI: 10.1038/s41598-021-82423-w.
- (11) Ranganathan, N.; Li, C.; Suder, T.; Karanji, A. K.; Li, X. J.; He, Z. Y.; Valentine, S. J.; Li, P. Capillary Vibrating Sharp-Edge Spray Ionization (cVSSI) for Voltage-Free Liquid Chromatography-Mass Spectrometry. *Journal of the American Society for Mass Spectrometry* **2019**, *30* (5), 824-831, Article. DOI: 10.1007/s13361-019-02147-0.
- (12) Copt, A.; Golosovsky, M.; Davidov, D.; Frenkel, A. Localized heating of biological media using a 1-W microwave near-field probe. *Ieee Transactions on Microwave Theory and Techniques* **2004**, *52* (8), 1957-1963, Article. DOI: 10.1109/TMTT.2004.831986.
- (13) Golosovsky, M.; Copt, A.; Davidov, D.; Frenkel, A. *Localized heat processing of soft materials using a low-power microwave applicator*; 2004. DOI: 10.1109/IEEEI.2004.1361144.

